AN EXPERIMENTAL INVESTIGATION INTO THE MECHANICS OF DYNAMIC FRACTURE

Thesis by

K. Ravi Chandar

In partial fulfilment of the requirements
for the degree of
Doctor of Philosophy

California Institute of Technology

Pasadena, California

1982

(Submitted: February 1, 1982)

ACKNOWLEDGEMENTS

I would like to express my thanks and appreciation to Prof. Knauss for his guidance and encouragement throughout the course of this investigation. I would also like to thank Prof. Babcock for many valuable discussions over the past several years.

This research effort was funded primarily by the National Science Foundation. During the progress of this work, parallel research on the dynamic fracture of strongly viscoleastic materials was in progress. The present work has profited from the interaction with that program, which was supported by the Office of Naval Research.

I would like to thank Clarence Hemphill of the Electronics Shop for assistance in building the experimental apparatus. I would also like to thank the members of the Machine Shop for their assistance in the specimen preparation. The help of Harry Hamagouchi of the Photo lab in the preparation of this thesis is acknowledged.

I dedicate this thesis to my parents for their support, encouragement and understanding.

ABSTRACT

Current theories of dynamic fracture are based on elastodynamic analyses of mathematically sharp plane cracks and as such do not explain the observed terminal velocities or the phenomenon of crack branching satisfactorily. The present investigation addresses the above problems by using both microscopic and macroscopic interpretations. The experimental scheme that is used in this investigation is the configuration of a pressure loaded semi-infinite crack in an infinite medium. The loading is achieved through an electromagnetic device which provides highly repeatable loading. The method of caustics is used in conjunction with a high speed camera to obtain the time histories of the crack tip stress intensity factor and the crack position.

The problems of crack initiation and crack arrest are explored. The stress intensity factor at initiation is found to be independent of the rate of applied loading when the latter is below about 10^4MPa/sec, but the initiation stress intensity factor increases considerably when the loading rate is increased further. Crack arrest is obtained in large specimen by using very low energy loading pulses. It was found that the stress intensity factor at crack arrest was constant and also that, within the time resolution of the high speed camera (5 μsec), the crack comes to a stop abruptly.

The crack propagation and branching aspects were investigated first using post-mortem analysis of the fracture surfaces and high speed photomicrography to get an idea of the microscopic processes that occur in the fracure process. From this investigation, it was found that crack propagation involving high stress intensity factor and high velocity situations takes place by the growth and interaction of microcracks, due to the voids present in the material. A surprising result of this investigation was that cracks propagated at a constant

velocity, although the stress intensity factor varied. Current theories of dynamic fracture cannot explain such behaviour. The crack branching process was found to be a continuous process arising out of propagation along a straight line. High speed photomicrographs of the branching process indicated the presence of a number of part-through attempted branches that interact with one another and finally the successful emergence of a few full fledged branches.

The microscopic observations on the crack propagation and branching process leads to a new interpretation of dynamic fracture that attempts to qualitatively explain the constancy of the velocity of propagation, the terminal velocity and crack branching. The crack branching mechanism is a logical continuation of the mechanism for crack propagation.

Table of Contents

NOMENCLATURE

a	crack length
c, $c_{1,2}$	stress-optic coefficients.
d	plate thickness.
i	current.
n	index of refraction.
p, $p_{1,2}$	pressure.
v	velocity
t	time.
z_0	distance between specimen midplane and reference plane.
C_0	$\sqrt{\frac{E}{\rho}}$
C_1	longitudinal wave velocity in a plate.
C_2	distortional wave velocity.
C_r	Rayleigh surface wave velocity.
D	diameter of the caustic.
E	modulus of elasticity.
G	energy release rate.
K	stress intensity factor.
P	optical coefficient for birefringent materials.
ν	Poisson's ratio.
ρ	density.
σ, $\sigma_{1,2}$	stresses.
Γ	energy required to create new surface.
$\Delta S_{1,2}$	change in path length.

1. INTRODUCTION

The mechanics of fracture of materials was first investigated in a systematic way by Griffith.[1] Since this early development, the field of fracture mechanics has grown substantially. It can generally be divided into two broad categories: one dealing with the effect of the constitutive behaviour on fracture and the other dealing with the effect of the loading conditions on fracture. Under the first category in fracture mechanics we include linearly elastic, plastic and viscoelastic materials. In the second category we place quasi-static and dynamic fracture mechanics. Quasi-static fracture has received a great deal of attention since the work of Griffith and the mechanics of quasi-static fracture of linearly elastic, plastic and viscoelastic materials are quite well understood. On the other hand, dynamic fracture - that is fracture where the effect of inertia forces is important in determining the nature of crack propagation - has received relatively little attention, mainly due to the complex nature of the problem. There is, however, substantial interest in the dynamic fracture problem due to its importance in many engineering applications. The problem is encountered in impact damage to fan blades, automotive and aircraft windshields; in mining and oil recovery operations, one needs to increase the rock porosity by explosives. In these problems, an understanding of the physics of crack branching is required. There is considerable interest in the problem of arrest of a fast running crack, especially in large structures like pipelines, ships and nuclear reactors.

The objective of the present investigation is to identify the important physical processes that determine the nature of dynamic fracture and is achieved through a carefully designed experimental program. Before proceed-

1. Griffith, A.A., *Phil. Trans. Royal Soc. London: Series A*,**221**,(1920),p.163; Griffith, A.A., *Proceedings of the First International Congress of Applied Mechanics*,(1924),p.55.

ing to the results of the experimental investigation, the state of the art of dynamic fracture is reviewed from two standpoints in this chapter. First, the major problems with the current view of dynamic fracture are discussed. Secondly a comprehensive survey of the literature on dynamic fracture is presented. The results of this investigation are then presented in the following order: The experimental apparatus that was developed for this program and the detailed calibration procedure as well as the reliability of the experimental results are described in Chapter 2. The problem of crack initiation, under varying rates of loading and the problem of crack arrest are considered next in Chapter 3. Before the crack propagation behaviour and the branching phenomenon are discussed, we investigate in detail the microscopic aspects of the fracture process, using both post-mortem analysis and real time high speed photography. Finally, in Chapter 5, the problem of crack propagation and branching are analysed, using both the quantitative measurements and the qualitative observations in order to arrive at a unified view of the crack propagation process that ultimately leads over into crack branching in a logical way. Some of the macroscopic conditions that affect the crack branching behaviour, such as stress waves interacting with the crack tip and the global stress parallel to the propagating crack, are also examined.

1.1 The Dynamic Fracture Problem

Griffith[2] considered the problem of an isolated crack in an unbounded medium under external loads from the point of view of thermodynamic energy balance. Griffith postulated that at incipient motion of a crack, the total energy of the system was stationary. The total energy of the system can be written as the sum of the work done by the external forces W, the elastic energy stored in the system U, and the energy expended in creating new surfaces Γ, all of the

2. Griffith, A.A., *op. cit.*

above being functions of the crack length a. Thus the total energy in the system is

$$P = (-W+U) + \Gamma \tag{1}$$

For a body under constant applied stress, it can be shown that $W=2U$ and then equation (1) becomes

$$P = -U + \Gamma \tag{2}$$

The Griffith criterion for unstable equlibrium of a crack is then

$$\frac{dP}{da} = 0 \tag{3}$$

From the solution of Inglis,[3] the strain energy term U can be evaluated[4] and is given by $U=\pi a^2\sigma^2 / E$, for plane stress, where σ is the applied stress and E in the modulus of elasticity. If γ is the energy required to create a unit of new surface, then $\Gamma=4a\gamma$. Thus equations (2) and (3) yield,

$$\sigma = \left\{\frac{2E\gamma}{\pi a}\right\}^{1/2} \tag{4}$$

Then equation (4) gives the stress at which the crack is at equilibrium under the applied load. The stability of the crack motion is given by the second derivative of P with respect to a and in the case of constant applied loads, the crack is unstable. Thus Griffith provided the foundation of modern fracture mechanics, by investigating the failure load and describing the stability of the system all based on the thermodynamic concept energy balance. Since this pioneering work of Griffith, the field of fracture mechanics has undergone significant further development. The mechanics of quasi-static fracture of brittle as well as ductile, elastic and viscoelastic materials is quite well developed that the field is being gainfully applied in problems of engineering design.

3. Inglis, C.E., *Trans. Inst. Naval Archit.*, **55**, (1913), p.219.
4. Spencer, A.J.M., *Int. J. Engng. Sci.*, **3**, (1965), p.441.

It is important to note that the Griffith energy balance equation is valid only up to the point of initiation of crack growth and during the crack propagation phase, the kinetic energy of the system has to be included in the energy balance equation. The first effort to formulate the energy equation for propagating cracks was that of Mott[5] who suggested to simply add the kinetic energy term and calculated the kinetic energy through dimensional arguments. Although an unknown constant was left in the final equation, an important result of this analysis was the prediction of a terminal velocity for crack propagation. Schardin and Struth[6] had earlier found that cracks in glass would not travel above a certain maximum velocity which was independent of the applied stress. Since the dynamic stress field was unknown at the time of Mott's formulation, he was unable to determine the value of the terminal velocity. Roberts and Wells[7] calculated the terminal velocity by using the static stress distribution around the crack tip, but the neglect of the dynamic nature of the stress field is not justified and their analysis although closely agreeing with the experimental results is not valid in principle. Dulaney and Brace[8] and later Berry[9] derived the equation of motion of a crack using the same argument as that of Mott. But their final estimate of the terminal velocity turned out to be the same as that of Roberts and Wells. The problem with these analyses seems to be that in considering the kinetic energy term, the energy transported away from the crack tip by the elastic waves is not accounted for completely. This is due to the fact that the energy balance equation was applied in a form integrated over the whole body and therefore, the kinetic energy in the complete body has to be taken into account; however all the available solutions for propagating crack problems only

5. Mott, N.F., *Engineering*, **165**,(1948),p.16.
6. Schardin, H., and Struth, W., *Glastechnishe Berichte*, **16**,(1938),p.219.
7. Roberts D.K., and Wells, A.A., *Engineering*, **178**,(1954),p.820.
8. Dulaney E.N.,and Brace, W.F., *Journal of Applied Physics*, **31**,(1960),p.2233.
9. Berry, J.P., *Journal of the Mechanics and Physics of Solids*, **8**,(1962),p.194.

give the asymptotic stress field near the crack tip and thus the total kinetic energy cannot be calculated. On the other hand, if the energy balance equation is applied over a small region around the crack tip, then the flux of energy through this region can and needs to be considered. The first estimate of the terminal velocity based on the transient stress field around a central crack growing symmetrically was presented by Broberg,[10] who determined that the terminal velocity should be the Rayleigh surface wave velocity, C_r; this result was later confirmed by a number of other researchers. A rigorous analysis based on the flux of energy into a small zone around a running crack tip by Freund,[11] described the equation for crack motion in terms of the dynamic stress intensity factor, K by

$$g(V) = \frac{E\Gamma}{K^2} \approx \left\{1 - \frac{V}{C_r}\right\} \tag{5}$$

Assuming that the energy required to create a new surface is independent of the rate at which the surface is being created, equation (5) also leads to the conclusion that the limiting velocity is the Rayleigh surface wave velocity. The variation of the crack velocity versus the stress intensity factor for Homalite-100 is shown in figure 1. The value of Γ was taken to be equal to the quasi-static measurements. Also shown on this figure is the experimentally obtained relationship between the applied stress intensity factor and the observed crack velocity. Such measurements have been carried out for Homalite-100 by Irwin, *et. al.*[12] and A.S.Kobayashi, *et. al.*[13] *It is seen that the observed maximum velocity is significantly smaller than the predicted Rayleigh surface wave velocity*. One of the objectives of this investigation is to go into the reasons for the lower

10. Broberg,K.B., *Arkiv fur Fysik*,**18**,(1960),p.159.
11. Freund, L.B., *Journal of Elasticity*,**2**,(1972),p.341.
12. Irwin, G.R., *et.al.*, *Experimental Mechanics*,**19**,(1979),p.121.
13. Kobayashi,A.S., and Mall, S., *Experimental Mechanics*,**18**,(1978),p.11.

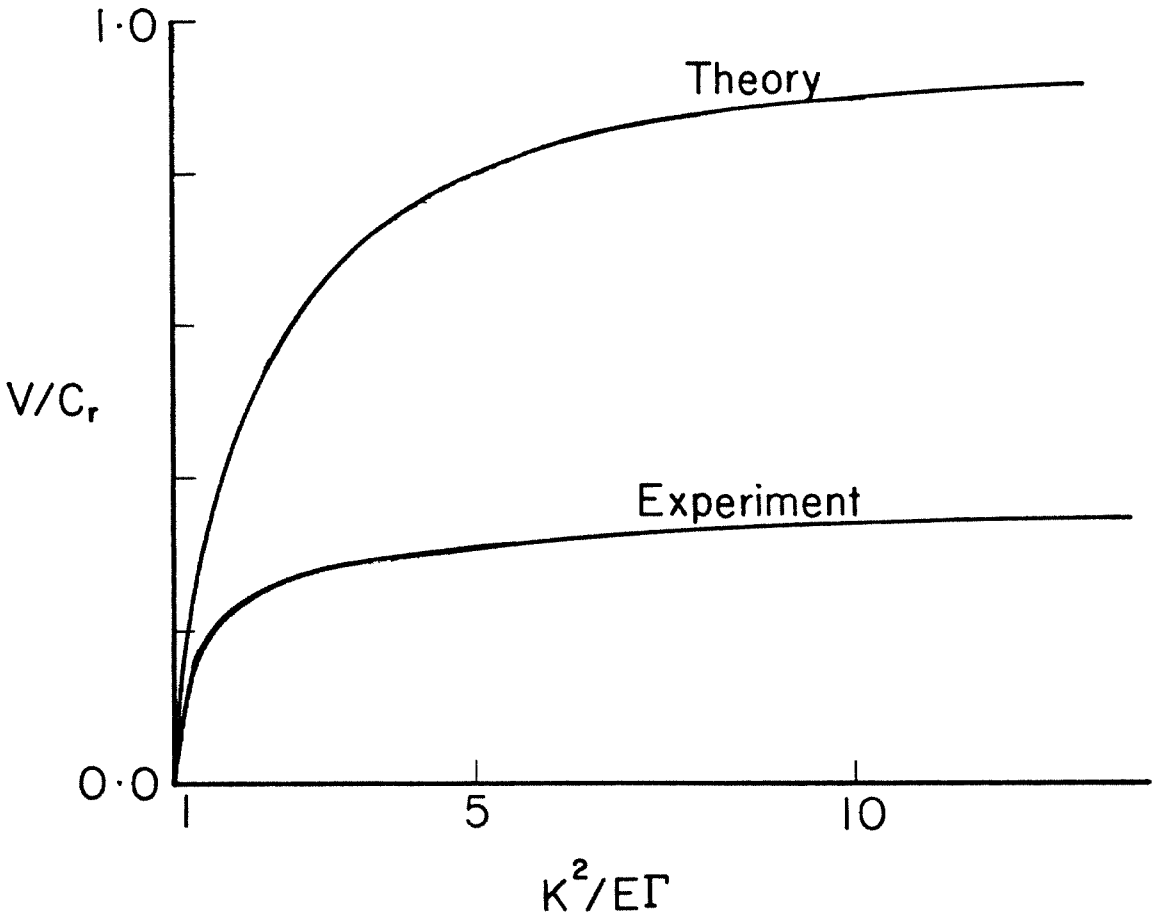

Figure 1. Stress intensity factor - crack velocity relationship.

observed terminal crack velocities. All of the above analyses assume that the material is linearly elastic and use the two-dimensional linearised theory of elasticity.

Anticipating a result of this investigation, there exists a second problem regarding the nature of the crack propagation, as currently viewed. The theoretical analyses described above and also the experimental results of Irwin *et. al.* indicate that there exists a one to one relationship between the instantaneous stress intensity factor and the crack velocity. Such a relationship is deemed to be a material property that can be characterised experimentally. Once such a relationship is established, the crack propagation behaviour of the material is presumed to be known completely. We find, in this work, that cracks tend to travel at a constant velocity, even though the stress intensity factor varies, indicating that such a unique relationship between the stress intensity factor and the crack velocity may not exist. This results in a loss of the one-to-one character of the relationship between the stress intensity factor and the crack velocity and this aspect of crack propagation is investigated in detail in Chapter 5.

When the stress intensity factor rises to sufficiently high levels, a propagating crack has the tendency to branch into multiple cracks, as shown in figure 2. Branching of cracks in glass was observed by Schardin[14] and other investigators have observed crack branching in crystalline as well as amorphous materials.[15] This bifurcation is totally unpredicted by analytical solutions to propagating cracks. This is due in part to the fact that in analysing the problem, the equations of elasticity are solved independently of the fracture criterion, by restricting the crack to travel along a straight line. If the equations

14. Schardin, H., in *Fracture*,(eds. Averbach *et. al.*),John Wiley,(1959),p.297.

15. Field, J., *Contemporary Physics*,**12**,(1971),p.1.; Beebe, W.M., Ph.D Thesis, California Institute of Technology, (1966); Finkel, V.M., *et. al.*, *Fiz. metal. metalloved.*,**15**,(1963),p.754.

Figure 2. Crack branching.

of elasticity could be solved together with the fracture criterion without any *a priori* assumption regarding the nature of crack motion, the solutions might reveal some additional or different features. Solutions of such general form are not in sight for the complicated two dimensional problems and the crack motion is usually prescribed to be along a straight line. The problem of branching and a review of the attempts at explaining the phenomenon are fully described in Chapter 5.

In view of the discrepancy between the theoretical and experimental results the following questions have to be answered: *Are there possibly non-linear phenomena occuring near the crack tip that have to be taken into account? Are there any three dimensional effects that have to be considered? If the limiting velocity of crack propagation is not the Rayleigh surface wave velocity as predicted by the analysis, what are the possible causes for the lower observed terminal velocity? Under what conditions, if any, would the theoretical limiting velocity be attained?* **The main goal of this investigation is to examine the dynamic fracture process in detail, both macroscopically and microscopically in order to better understand the fundamental processes that control the dynamic fracture behaviour in brittle solids.** This investigation is confined to the model material Homalite-100, a thermo-setting polyester which is commonly classified as being brittle.

The rest of this chapter is devoted to a survey of the field of dynamic fracture mechanics of linear elastic bodies. This review is presented in two sections: first the stress analysis of dynamic crack problems and second the experimental investigations in dynamic fracture.

1.2 Review of Status of Dynamic Fracture

1.2.1 Stress Analysis of Dynamic Crack Problems: The first analytical solution to the problem of a moving crack was the solution of Yoffe[16] who considered the problem of a crack of constant length moving along a straight line in an infinite two dimensional medium under remote tractions. From an examination of the asymptotic stress field, it was determined that the maximum $\sigma_{\theta\theta}$ stress at the crack tip acted at an angle of $60 degree$ to the crack propagation direction when the crack speed exceeded $0.6C_s$. Based on this finding Yoffe suggested that at such high velocities, this change in the angle at which the maximum $\sigma_{\theta\theta}$ acts could cause the crack to deviate from the straight path. We will discuss this suggestion in greater detail in Chapter 5. Craggs[17] provided the solution to the steady state problem of a semi-infinite crack in an infinite solid under crack face loading that moves along with the crack tip. A major feature of the above two solutions was that they were steady state solutions and hence the stress intensity factor was constant and equal to the appropriate static stress intensity factor. However the two solutions described the asymptotic stress distribution at the crack tip accurately.

The first solution to a truly transient problem of a center crack extending symmetrically at constant velocity from zero length under remotely applied loads was obtained by Broberg.[18] Whereas the earlier steady state solutions indicated that the stress intensity factor was equal to the appropriate quasi-static stress intensity factor, the Broberg solution showed that the dynamic stress intensity factor decreased with velocity, decreasing to zero at the Rayleigh wave velocity. The solution also showed that the deformed crack shape was elliptic, just as in the static case. Baker[19] considered a semi-infinite

16. Yoffe, E., *Philosophical Magazine*,**42**,(1951),p.739.
17. Craggs, J.W., *Journal of the Mechanics and Physics of Solids*,**8**,(1960),p.66.
18. Broberg, K.B., *Arkiv fur Fysik*,**18**,(1960),p.159.

crack in an infinite medium. At a certain instant, the crack faces were loaded by uniform pressure and the crack started to grow at a constant velocity. He pointed out that the $\sigma_{\theta\theta}$ stress at the crack tip is not the principal stress. Since in a brittle material, the maximum stress is the one believed to cause crack propagation perpendicular to it, Yoffe's interpretation of the change in the direction of the $\sigma_{\theta\theta}$ stress as the possible cause of crack branching should be examined more closely. The problem considered by Baker is equivalent to the growth of a semi- infinite crack due to a plane wave impinging on the stationary crack causing it to propagate at constant velocity. Nuismer and Achenbach[20] continued the analysis of Baker to determine the asymptotic nature of the displacements behind the crack tip and from this were able to formulate an energy balance equation for the propagating crack. Assuming that the surface energy Γ is a constant their analysis also led to the conclusion that the limiting velocity is the Rayleigh wave velocity.

All of the above analyses address problems for cracks propagating along a straight line and at a constant velocity. Kostrov[21] was the first to study the problem of non-uniform extension of a center crack, under Mode III loading, retaining the restriction of extension of the crack along a straight line. The stress intensity factor was found to be identical to the expression for the constant velocity case, with the velocity just replaced by the instantaneous velocity. In a series of four papers, Freund[22] analysed the problem of Mode I crack extension under plane wave loading. The most important result of these latter analyses was that the *dynamic stress intensity factor of a semi-infinite crack is the*

19. Baker, B.R.,*Journal of Applied Mechanics*,**29**,(1962),p.449.

20. Nuismer, R.D., Achenbach, J.D., *International Journal of Fracture*,**20** ,(1972),p.203.

21. Kostrov, B.V., *Applied Mathematics and Mechanics, (English translation of PMM)*,**30**,(1966),p.1241.

22. Freund, L.B., *Journal of the Mechanics and Physics of Solids*,**20**,(1972),p.129. Freund, L.B., *Journal of the Mechanics and Physics of Solids*,**20**,(1972),p.141. Freund, L.B., *Journal of the Mechanics and Physics of Solids*,**21**,(1973),p.47. Freund, L.B., *Journal of the Mechanics and Physics of Solids*,**22**,(1974),p.137.

product of a velocity dependent function and the stress intensity factor appropriate for a stationary crack of the instantaneous length subjected to the given time independent or time dependent loading. Kostrov[23] provided some improvements over this work of Freund by deriving the same result from a more direct approach, and considering a more general dependence. The above general solutions to non-uniform extension of cracks were all for semi-infinite crack configurations and as such are valid for short times for finite length cracks, until the two crack tips communicate with each other. For the case of a centre crack growing symmetrically, self-similar solutions can be applied as a reasonable approximation even during the initial stages of crack propagation as pointed out by Rose.[24]

A number of solutions have been obtained for the dynamic problem of crack propagation for special specimen configurations, like the Timoshenko beam type analysis for a double cantilever specimen by Kanninen,[25] and the solution to axial propagation of cracks in shells by Abou-Sayed and Freund[26] for example. We do not consider these in detail since they are not really relevant here.

The problem of crack arrest is a transient dynamic phenemenon and has to be treated as such. It is not likely to be treatable simply as a time reversal of the crack initiation process, for the following reason: Consider the dynamic crack propagation process initiated by a quasi-static loading process. The crack initiation occurs essentially in a quasi-static stress state, but the subsequent growth takes place in a dynamic stress field. On the other hand, the crack that comes to rest does so in a dynamic stress field both prior to and

23. Kostrov, B.V.,*International Journal of Fracture*,**11**,(1975),p.47.

24. Rose,L.R.F., *International Journal of Fracture*,**12**,(1976),p.799.

25. Kanninen, M.F.,*International Journal of Fracture*,**10**,(1974),p.415.

26. Abou-Sayed, I.S., and Freund,L.B., in *Developments in Theoretical and Applied Mechanics*,**8**,(ed.McNitt, R.P.), VPI & SU Press, (1976),p.161.

after the arrest process. The problem of crack arrest was studied by Mansinha[27] who considered the propagation of an elliptical crack with constant shape and came to the conclusion that the crack would arrest instantaneously. The problem of arrest was also treated by Freund[28] who considered a constant velocity crack in an infinite medium that was brought to rest instantaneously. The result was that a static stress field appropriate to the arrested crack configuration was radiated out from the crack tip. Both these analyses represent an idealization in that the crack comes to rest instantaneously. In practice, in all cases where crack arrest has been observed, the crack decelerates continuously and finally arrests. This topic will be discussed in greater detail in Section 3.2. Crack branching, although observed experimentally by Schardin[29] long ago, has equally long defied analytical modelling or explanation. We will review the work on crack branching, both analytical and experimental, later in Section 5.2.

1.2.2 Experimental Investigations in Dynamic Fracture: Experimental investigations into the dynamic behaviour of materials were started late in the 19th century by J.Hopkinson who tested the dynamic strength of steel wires under impact loading. B. Hopkinson[30] carried out similar experiments and also performed some experiments on the scabbing of plates. Kolsky and Christie[31] and Kolsky and Shearman[32] continued testing on scabbing using transparent blocks and were able to relate the fracture patterns to the wave interactions. The mechanism of scabbing was also investigated by Broberg,[33] who studied the

27. Mansinha, L., *Journal of Mechanics and Physics of Solids*, **12**,(1964),p.353.
28. Freund, L.B., *Journal of the Mechanics and Physics of Solids*,**20**,(1972),p.141.
29. Schardin, H., in *Fracture*,(eds. Averbach *et. al.*),John Wiley,(1959),p.297.
29. Hopkinson, J., *Collected Scientific Papers, Vol. ii*, (1872),p.316.
30. Hopkinson, B., *Proc. of the Royal Society, London: Series A*,**74**,(1905),p.498.
31. Kolsky, H., and Christie, D.G., *Trans. Soc. Glass Tech.*, **36T**,(1952),p.88.
32. Kolsky, H., and Shearman, A.C., *Research*,**2**,(1949),p.384.
33. Broberg, K.B., *International Symposium on the Propagation of Stress waves in Materials, (ed. Davids, N.)* Interscience Publishers, New York, (1960),p.229.

effect of the stress pulse duration on the formation of scabs in brittle and ductile materials. He also recognized the role played by microcracks in the formation of scabs. All of the above were tests in which there was no dominant crack to begin with and in this sense were not tests carried out from a fracture mechanics point of view. The first such test, where a dominant crack was identified and its subsequent behaviour followed, was that of Schardin.[34] He conducted experiments on glass and followed the crack propagation using a high speed camera. He obtained the remarkable result that the *cracks travelled with a constant maximum velocity* and that this maximum velocity was independent of the applied stress level. He also observed crack branching, which resulted always in only two branches. There was no attempt to determine the stress field in which the cracks propagated or branched due to the lack of suitable experimental techniques at that time.

Wells and Post[35] used a high speed camera in conjunction with photoelasticity set up to obtain the isochromatic fringe pattern around a moving crack. They noted that the dynamic isochromatics exhibited a remarkable similarity to the static isochromatics, but that the stress level at which the dynamic isochromatic resembled the static isochromatic was higher. Beebe[36] carried out extensive tests on Homalite-100 under both high and low rates of loading. He concluded that the velocity behaviour of the centre cracked specimen did not agree with the calculations of Berry.[37] Beebe used the Broberg solution to determine the dynamic isochromatics and compared them to the experimentally obtained isochromatics, and found that the experimental isochromatics agreed with the static isochromatics while the cracks were stationary, but for the run-

34. Schardin, H., in *Fracture*,(eds. Averbach *et. al.*),John Wiley,(1959),p.297.
35. Wells, A.A., and Post, D., *Proceedings, SESA*,**16**,(1958),p.69.
36. Beebe, W.M., Ph.D., Thesis, California Institute of Technology, (1966)
37. Berry, J.P., *Journal of the Mechanics and Physics of Solids*,**8**,(1962),p.194.

*ning cracks the observed isochromatics agreed with the isochromatics calcu*lated from the Broberg solution. Beebe also found that the maximum velocity at which the cracks propagated was around $0.31C_s$, somewhat lower than that observed by other investigators for this material. Cotterell[38] tested polymethylmethacrylate in the centre crack and edge crack configurations and found that the maximum velocity at which the cracks propagated was $0.54C_s$. By introducing guiding grooves, the maximum velocity was increased to about $0.75C_s$. Cotterell observed that the roughness of the newly created fracture surface increased with crack velocity. Clark and Irwin[39] suggested that a high crack velocity alone was not sufficient to cause crack branching but that a high stress level was also necessary. Congleton[40] suggested that flaws are nucleated ahead of the main crack and are a possible mechanism of crack branching. He also determined through experiments that the crack velocity at branching was not always equal to the maximum velocity in the material. Field[41] tested several materials, crystalline and amorphous, and concluded that the cracks in crystalline materials travelled with velocities closer to the Rayleigh wave velocity than in amorphous materials.

Kobayashi and co-workers performed extensive experimental work on dynamic fracture of Homalite-100 using photoelastic techniques and the dynamic stress field to determine the dynamic stress intensity factor from the isochromatics.[42] They studied the crack arrest capabilities of holes and pretensioned stiffeners in large plates.[43] They developed finite element codes to

38. Cotterell, B., *Applied Materials Research*, **4**,(1964),p.227.

39. Clark, A.B.J., and Irwin, G.R., *Experimental Mechanics*,**6**,(1966),p.321.

40. Congleton, P, *Philosophical Magazine*,**16**,(1967),p.749.

41. Field, J., *Contemporary Physics*,**12**,(1971),p.1.;

42. Bradley, W.B., and Kobayashi, A.S., *Experimental Mechanics*,**10**,(1970),p.106; Kobayashi, A.S., *et. al.*, in *Deformation and Fractur of High Polymers, (eds. Kausch et.al.)*, Plenum Press, (1973), p.487.

43. Kobayashi, A.S., *et. al.*, *Experimental Mechanics*,**12**,(1972),p.32. Kobayashi, A.S., *et. al.*, *Experimental Mechanics*,**15**,(1975),p.1.

study numerically, the problem of dynamic crack propagation.[44] Kobayashi *et.al.*,[45] have also suggested that the stress level at the crack tip might be the determining factor in crack branching. From an examination of the fracture surface roughness, they conclude that the surface roughness is related to the crack tip stress level and not the crack velocity.

Dally and co-workers also used the photoelastic techniques in studying the dynamic fracure of Homalite-100.[46] Through numerical computations of the isochromatic data, they determined not only the dynamic stress intensity factor, but also the higher order terms in the asymptotic stress field. They characterised the crack propagation behaviour in terms of the relationship between the crack velocity and the stress intensity factor.[47] This relationship was determined experimentally for Homalite-100, KTE epoxy and some steels. Their test data revealed, however, that this relationship between crack velocity and stress intensity factor was dependent on the specimen size and configuration. Although, under the usual testing conditions, their observed maximum velocity was $0.35C_s$, they were able to propagate cracks at velocities higher than this under some special conditions, but still far below the Rayleigh wave velocity.[48] With regard to crack branching Dally[49] restates the microcrack hypothesis of Congleton[50] and suggests an empirical relationship to determine the stress intensity factor at branching.

Kalthoff and co-workers[51] have investigated dynamic fracture of Araldite B, an epoxy, using the method of caustics. They derived the analysis for the

44. Kobayashi, A.S., *et. al.*, *Experimental Mechanics*,**20**,(1980),p.73.
45. Kobayashi, A.S., *et. al.*, *Eng. Fract. Mech.*,**6**,(1974),p.81.
46. Dally, J.W., *Experimental Mechanics*,**19**,(1979),p.349.
47. Irwin, G.R., *et.al.*, *Experimental Mechanics*,**19**,(1979),p.121.
48. Dally, J.W., *Experimental Mechanics*,**19**,(1979),p.349.
49. *Ibid.*
50. Congleton, P, *Philosophical Magazine*,**16**,(1967),p.749.
51. Kalthoff, J.F., *et. al.*,*Fast Fracture and Crack Arrest*, *ASTM STP 627*,(1977),p.161.

method of caustics including the effects of inertia in a propagating crack,[52] to study the arrest behaviour of cracks in wedge loaded and machine loaded double cantilever and compact tension specimen in Araldite B and steel.[53] They found that the stress intensity factor oscillates about the static crack arrest stress intensity factor and that the magnitude of this oscillation depends on the specimen type. The frequency of oscillation was found to be close to the vibrational modes in the specimen. They also found that while the crack started propagating with a constant velocity, *with no resolvable acceleration phase*, the cracks always arrested with a finite deceleration.

Curran *et.al.*,[54] approached the dynamic fracture process from a microstructural viewpoint. They impact tested small blocks of specimens, both brittle and ductile, with short duration high pressure level pulses. By a careful post-mortem examination of slices of the specimen, they detected small microcracks nucleated and grown by the impact induced stress waves. These microcracks varied in size and density depending on the stress level and the material properties. Also, the microcracks were oriented at various angles to the direction of the major stress field. Although these tests were conducted at very high pressure level and using short time pulses, the growth of microcracks that were observed point to a mechanism by which cracks may grow in general. This is a view point that we take in this investigation and we will substantiate this by visual observations on the crack propagation process.

52. Kalthoff, J.F., *VDI Berichte Nr. 313*,(1978),p.791.
53. Kalthoff, J.F., *Crack Arrest Methodology and Applications*, *ASTM STP 711*,(1980),p.109.
54. Curran *et. al.*, *Journal of Applied Physics*, **44**,(1973),p.4025.

2. EXPERIMENTAL PROCEDURE

2.1 Stress Wave Generator

Central to the goals delineated in the introduction is the capability to generate reproducibly stress waves that engulf the initially stationary or the moving crack tip. While several means are readily available, as for example, explosives, electro-magnetically or explosively driven flyer-plates, we place emphasis on a *high degree* of repeatability. Moreover, the just mentioned means generate compressive stresses which need to be converted to tensile stresses by reflection at a stress-free boundary. In a cracked plate this is virtually impossible to achieve because the crack will diffract the compressive wave. Note that the problem of a plane wave impinging on a crack parallel to its front is, from a crack initiation point of view, equivalent to the problem of a pressurized crack. While the generation of such a tensile wave propagating parallel to a crack turned out to pose some experimental difficulties the pressurization of the crack surface was indeed feasible with an electro-magnetic device.

2.1.1 Principle of the Loading Method: The electro-magnetic loading device consists of a doubled-up conductor (copper strip) which is inserted into a crack as shown in figure 3 and the space in between is filled with a mylar strip as a dielectric. When a current flows through the loop each leg generates a magnetic field surrounding it, the magnetic field vector being normal to the current vector. The current (vector) in each leg interacts with the magnetic field of the other leg to produce an electro-magnetic pressure that forces the conductors apart: for two (idealized) current sheets this electro-magnetic pressure is given by

$$P = \frac{1}{2}\mu\left(\frac{i}{w}\right)^2 \tag{6}$$

where

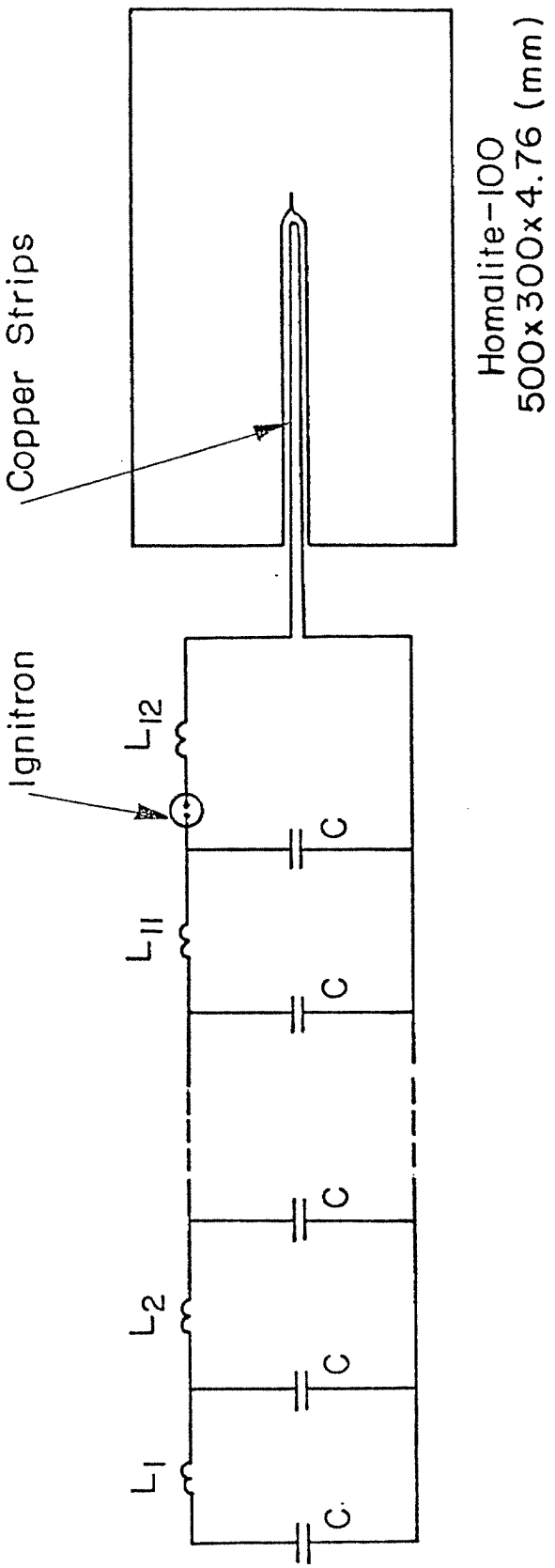

Figure 3. Electromagnetic loading scheme and specimen configuration.

μ = permeability of free space

i = current in the strips

w = width of strip

We discuss the details of the current generation and the related circuitry in the next section.

2.1.2 Current Shaping and Charge-Discharge Circuits: The current in the copper-strip is generated by a discharge from a capacitor bank. In order to control the time history of the current (i.e., to control the pressure pulse shape), several capacitors are arranged with inductors as shown in figure 3. The maximally stored energy in the capacitor bank is 60 kJ (at 20 kV) which is discharged in 160 μsec through an ignitron switch. Two such capacitor banks were built in order to be able to transmit compression waves from two sides to study wave interaction problems. The time history that is derived from this circuit is shown in figure 4. The rise time and the duration of the pulse could be altered by suitably changing the lab manufactured inductors. In the present tests a pulse was used that had a rise time of $\approx 25\mu$sec and a total duration of 160 μsec. The capacitors are charged to the desired voltage level by a standard high voltage power supply capable of charging at a rate of 200 J/sec. The discharging is achieved through a thyratron-ignitron firing system. The ignitron is a fast mercury switch that is capable of sustaining the high currents generated by the capacitor bank and the thyratron pulse primes the ignitron switch's pool of mercury. The advantage of this electrical discharge system is the ease with which time sequencing of the events can be effected. When mechanical loading devices are employed, the only feasible way of recording crack propagation events in a reproducible manner seems to be the breaking of a wire or conductive strip of paint across the crack path for triggering purposes. That method makes it virutally impossible to study the initial phases of the fracture process. With the electromagnetic loading device, where the start of load application is

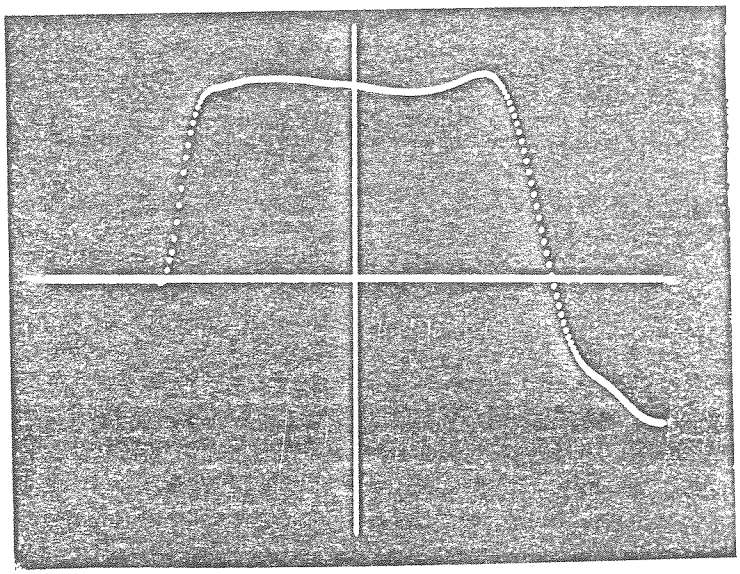

Figure 4. Time history of the current that is derived from the capacitor-inductor circuit

controlled by an electrical pulse, proper sequencing with the recording device is easily achieved. The high speed camera is triggered 30 μsec before the crack is loaded so that the crack tip is already recorded prior to initial growth.

2.1.3 Calibration of the Loading Device: The current flowing in the copper strip is measured by a Rogovski coil, which is a toroidal coil wrapped around a conductor loop: it measures the rate of change of current flux through the loop. This assembly surrounds the lead carrying the current to the copper strip. The signal from this coil is integrated by a passive RC integrator to yield the instantaneous current. In order to fix the relationship between the current in the copper strips and the integrated Rogovski coil output, a known current is applied to the copper strip and the corresponding integrated output recorded. This determines the calibration factor.

We have thus established one way of ascertaining the load applied to the crack - measuring the current by the Rogovski coil and using equation (6) to obtain the pressure. An alternate way to determine the load can be derived from network theory. The capacitor-inductor circuit of figure 3 can be analysed to yield the current which is used in equation (6). The two results were in agreement.

A third way to establish the pressure supplied by the device is by transmitting a (compressive) wave in an uncracked plate and measure the strains by strain gauges. In pursuing this additional avenue, the plate was chosen large enough so as not to provide any reflections arriving at the strain gauges before the loading pulse had passed. The stresses as measured by these gauges were in agreement with those calculated from the pressure-current relations. In figure 5, the results from the three independent calibration methods, namely, the Rogovski coil measurements, the network calculation and the strain

gauge calibration are shown plotted as a function of the charge voltage. These values all fell within the band shown in figure 5.

In addition to the calibration that was achieved by the strain gauge measurements, it was also possible to monitor the stress pulse as it travelled along the plate by mounting three strain gauges 3, 6 and 9 inches from the loading edge. The stress at any gauge location normalized by the stress at the three inch gauge is plotted in figure 6. It is seen that there exists very little attenuation in the stress pulse, a result that is at variance with earlier measurements by Smith.[1] One reason for this discrepancy could be the large scatter involved in the strain gauge data. The electromagnetic loading device sets up strong magnetic fields in the area around it that interfere with the strain gauges and their circuitry. An example of the kind of data obtained is illustrated in figure 7 where the strain gauge output is from the oscilloscope is shown. The first trace is the output that contains both the signal and the noise due to the electromagnetic interference. In the second trace, the output from a repeat test is shown, but this time the power supply to the strain gauge bridge circuit was turned off and thus this trace represents the noise that is picked up by the measuring system. Finally the last trace shows the result of subtracting the noise from the first trace. Although the noise was assiduously minimized the resulting scatter could not be reduced any further.

With this complete characterization of the pressure generator, we are now able to produce a well defined state of stress at the crack tip. We note that the reproducibility of the pressure generator is excellent as illustrated by figure 4. Here, the integrated Rogovski coil output from three different capacitor discharges is shown. The voltage level to which the capacitors are charged is dialed in through a potentiometer and hence the capacitors are charged to

1. G.C. Smith, Ph.D Thesis, California Institute of Technology, (1975).

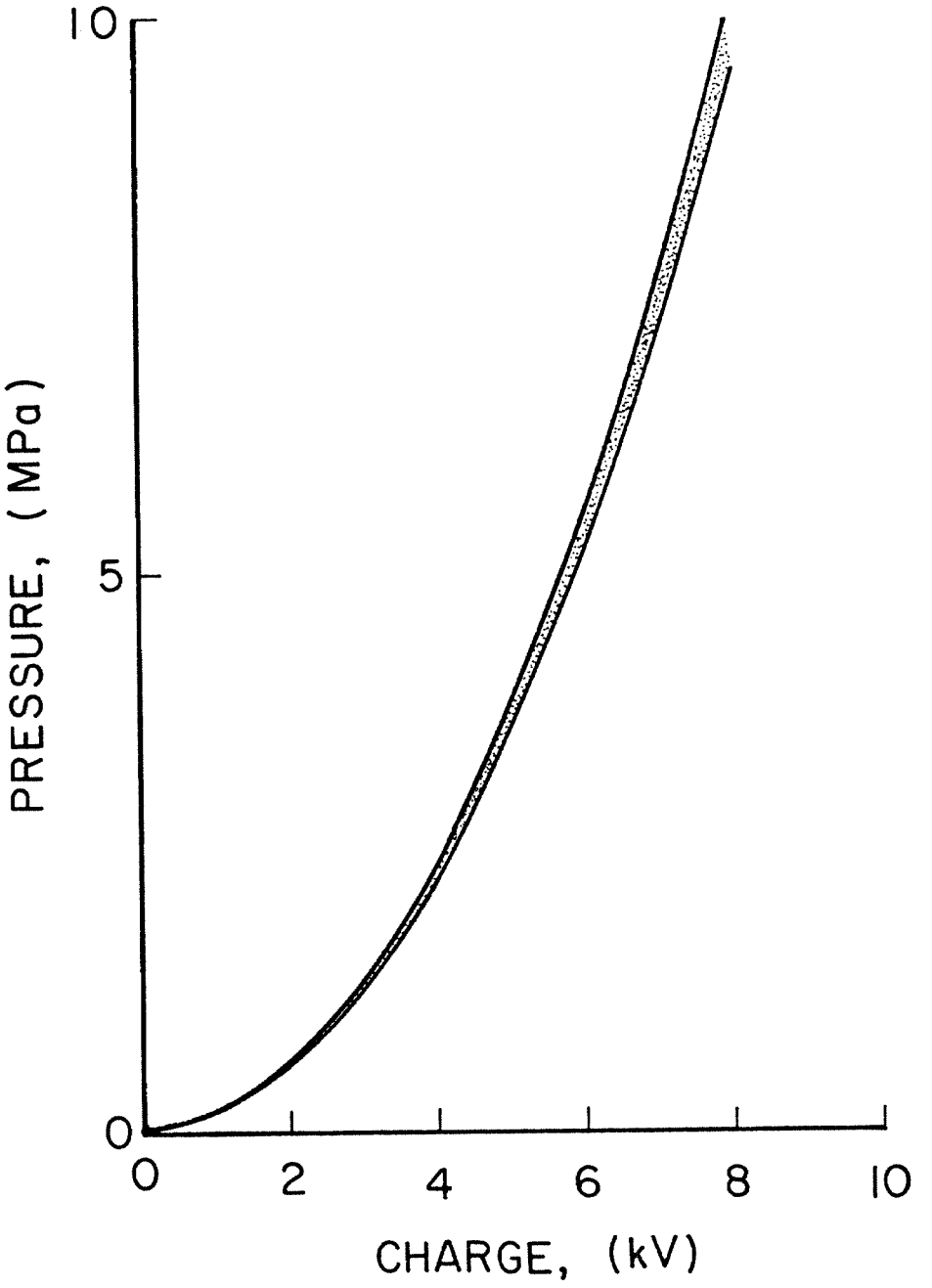

Figure 5. Calibration curve for the loading device.

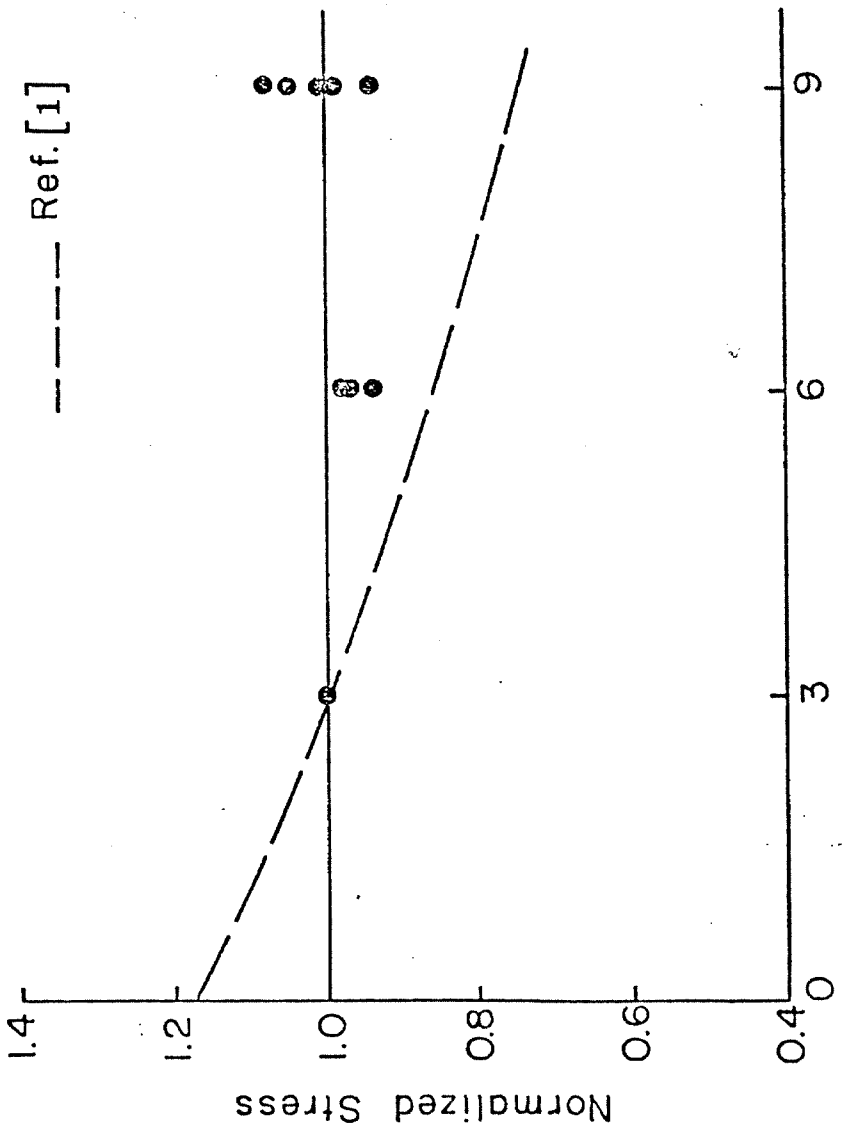

Figure 6. Amplitude of the stress pulse as it traverses along the plate.

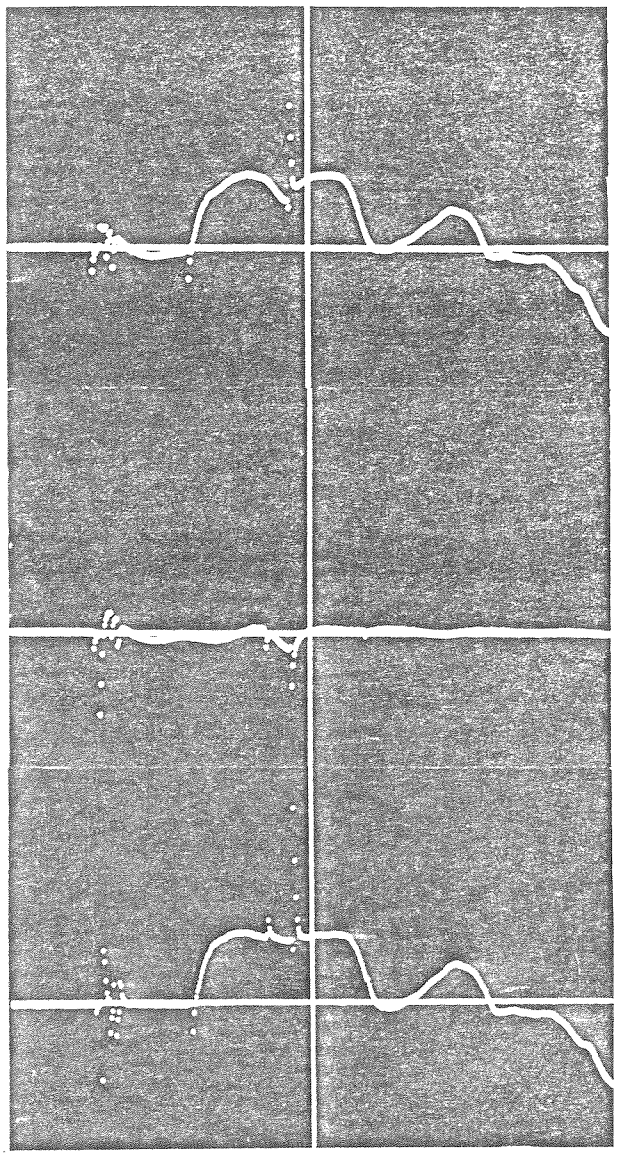

Figure 7. Noise elimination procedure for the strain gauge data.

exactly the same voltage in all the three discharges. The three traces fall on top of each other and are indistinguishable in the oscilloscope record.

2.2 Specimen

In order to effect a comparison of the experimental results with available analyses for the infinite domain, the test specimen configuration must be so large that wave reflections do not enter the field around the (moving) crack tip for the 150 μsec duration of the experiment. With the lateral dimensions of the plate thus dictated by this infinite domain condition, the thickness needs yet to be determined. Two limiting factors govern the thickness of the plate. The electromagnetic loading principle requires the width of the strip - here equal to the thickness of the plate - to be large enough compared to the copper strip separation. On the other hand, considerations of geometrical dispersion require that the thickness be small compared to the wavelength of the predominant Fourier components of the frequency spectrum in order to allow a two dimensional approximation. The pulse shape shown in figure 4 was analysed to yield the predominant Fourier components and the highest frequency pulse that carried about 0.5% of the total energy of the loading pulse was required to show no dispersion. With these two constraints the thickness of the specimen is essentially bounded. As mentioned earlier, the strain gauge data did not reveal the presence of any dispersion. Thus, the approximation of the plane stress theory of elasticity should adequately represent the experimental configuration. The specimen size and configuration are shown in figure 3. In order to relate our results to those of previous investigators we used Homalite 100 as a model material, the elastic and optical characteristics of which are summarized in Table 1.

TABLE 1. Elastic and optical properties of Homalite-100.

Modulus of elasticity (dynamic)	E	4550	MN/m^2
Poisson's ratio	ν	0.31	
Density	ρ	1230	kg/m^3
Plate wave speed	C_d	2057	m/s
Shear wave speed	C_s	1176	m/s
Rayleigh wave speed	C_r	1081	m/s
Index of refraction	n	1.5	
Direct stress-optic coefficient	c_1	-0.906×10^{-10}	m^2/N
Transverse stress-optic coefficient	c_2	-1.140×10^{-10}	m^2/N

2.3 Crack Tip Stresses

We are interested in the time dependent stress field at the tip of a stationary or moving crack and in identifying it in terms of the stress intensity factor. The methods available for the determination of the latter are the dynamic photoelasticity[2] and the dynamic caustic[3] methods. Constraints on the specimen discussed earlier limited the specimen thickness in the present case to such an extent that the photoelastic fringe count would be too low to yield reliable information. Although fringe multiplication offers a possible remedy we note that such techniques reduce the light intensity and, therefore, pose problems for our high speed recording system. Hence dynamic caustics were chosen to determine the stress intensity factor.

The method of caustics was introduced by Schardin[4] and later developed further by Manogg,[5] Theocaris[6] and Kalthoff *et. al.*[7] The basis of the method is that a light ray passing through a stressed plate is deviated from its straight path partly due to thickness variation and partly due to the change in refractive index caused by the stress optic effect. If the plate contains a crack, the rays are deviated from the region around the crack tip and these form a singular curve called variously "stress corona", "shadow spot" or "caustic" on a reference plane some distance away from the specimen. A schematic illustration of the method of caustics is shown in figure 8a. The size of the caustic is related to the stress intensity factor. Corresponding to the caustic curve on the reference plane, there is defined on the specimen plane a curve called the initial

2. Wells,A.A., and Post,D., *Proceedings,SESA,***16**,(1958) p.69.
3. Kalthoff, J.F., *et. al.*VDI Berichte Nr.313, (1978), p.791. and Rosakis,A.J.,*Engineering Fracture Mechanics,***13**,(1980),p.331.
4. Schardin, H., *Fracture*(ed. Averbach *et. al*), MIT Press and John Wiley,(1959),p.297.
5. Manogg, P., in *Proceedings, International Conference on the Physics of Non-Crystalline Solids*,Delft,(1964),p.481.
6. Theocaris, P.S., *Applied Optics,***10**,(1971),p.2240.
7. Kalthoff *et. al., op. cit.*,

curve. Light rays from the outside of this initial curve fall outside the caustic, rays from the initial curve fall on the caustic and rays from inside the initial curve fall on or outside the caustic curve. Hence, the caustic curve is a bright curve surrounding a dark region.

Since the interpretation of the stress field at the crack tip in terms of the stress intensity factor is appropriate only in a very small region around the crack tip the reliability of the method of caustics depends on the size of the initial curve. From static tests on compact tension specimens performed in an Instron testing machine, we determined the distance between the specimen and reference plane that would provide very small initial curves.

For optically birefringent materials, the stress optic effect in the two principal stress directions differs in magnitude and hence two caustics - corresponding to two initial curves - are expected. However, initial recordings of caustics in Homalite did not show such double caustic and therefore the correctness of that statement seemed in doubt. The subsequent analysis[8] clarified the lack of double caustics for Homalite-100

Consider the optical configuration in figure 8b. If ΔS is the retardation in the optical path length as a ray traverses the thickness of the plate, then the deviation of light rays at a plane $z = z_0$ is

$$\mathbf{W} = -z_0 \, \mathbf{grad} \, \Delta S(r, \varphi) \tag{7}$$

With reference to figure 8b. let the image of a vector $\mathbf{r}$ in the specimen plane be $\mathbf{R}$ in the reference plane. Then,

$$\mathbf{R} = \mathbf{r} - \mathbf{W} = \mathbf{r} - z_0 \, \mathbf{grad} \, \Delta S(r, \varphi) \tag{8}$$

is the transformation relation between the specimen and reference planes. If a

8. Ravi Chandar, K., and Knauss, W.G., *GALCIT SM79-17*,California Institute of Technology, (1979).

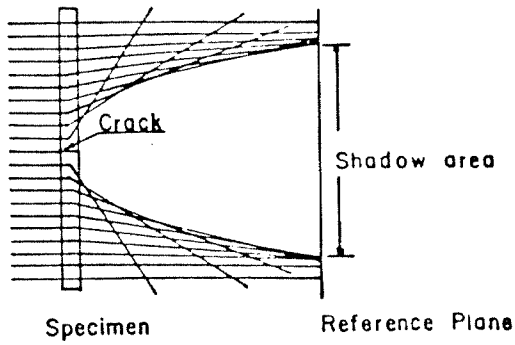

(a)

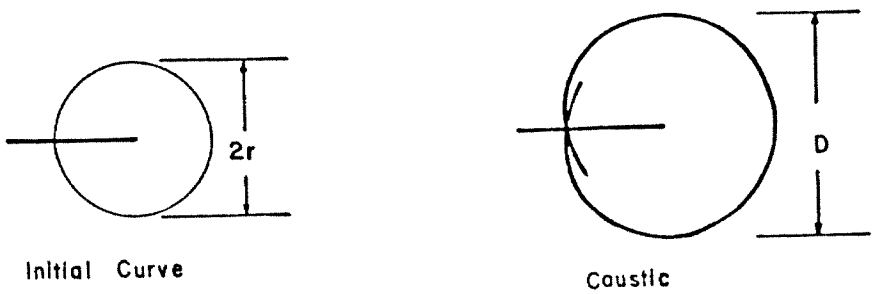

(b)

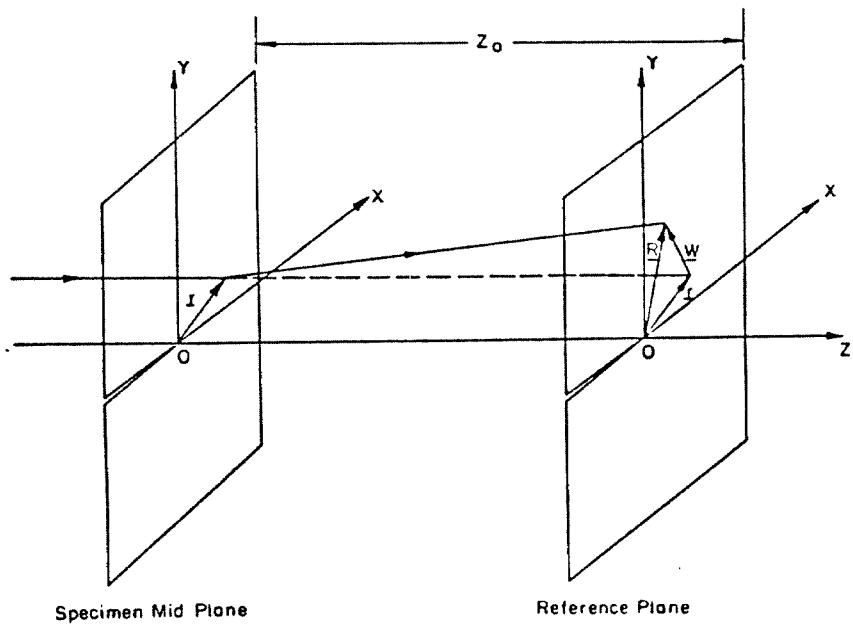

Figure 8. Optical configuration for the method of caustics.

singular curve exists in the reference plane, the Jacobian of the transformation must vanish, i.e. in the coordinate notation of figure 8b.

$$J=\frac{\partial(X,Y)}{\partial(x,y)}=0 \tag{9}$$

In order to evaluate equation (9) we choose to compute the retardation in optical path length ΔS for the plane stress case consistent with our choice for the specimen plate thickness. From the Maxwell-Neumann stress optic laws and Hooke's law one obtains the optical path retardation in the two principal directions as

$$\Delta S_{1,2} = dc[(\sigma_1+\sigma_2)\pm P(\sigma_1-\sigma_2)] \tag{10}$$

where

c_1, c_2 = stress optic constants

d = thickness of plate

σ_1, σ_2 = principal stresses

E = modulus of elasticity

ν = Poisson's ratio

n =index of refraction

$$c=\frac{c_1+c_2}{2}-(n-1)\frac{\nu}{E}$$

$$P=\frac{c_1-c_2}{(c_1+c_2)-2(n-1)\frac{\nu}{E}}$$

The asymptotic stress distribution at the tip of a mode I crack is used in evaluating equation (10). The Jacobian condition (9) results in

$$J = 1-\left[\frac{9}{4}(1+P^2)\mp\frac{9}{16}P\sin\frac{\varphi}{2}\pm\frac{63}{16}P\sin\frac{\varphi}{2}-\frac{9}{8}P^2\sin^2\varphi\right](\alpha r^{-5/2})^2 \tag{11}$$

$$\pm P\sin\varphi\ \alpha r^{-5/2} = 0$$

with

$$\alpha = \frac{K_I z_0 cd}{\sqrt{2\pi}}$$

Equations (11) describe the initial curves in the specimen plane. The equations have to be solved numerically to yield $\alpha r^{-5/2}$ as a function of φ. Applying the transformation (8) to these initial curves one obtains the caustic curves in the reference plane. Two caustics are defined corresponding to the two principal retardations ΔS_1 and ΔS_2 and the magnitude of separation of the two depends on the factor P in equation (10). The shapes and sizes of the initial curves and caustics for non-birefringent and birefringent materials are shown in figure 9. In the case of non-birefringent materials, $c_1=c_2$ and P = 0; the two caustics coalesce. Although Homalite-100 is strongly birefringent, it turns out that the combination of elastic and optical constants is such that P is small, namely P = 0.087. The separation of the caustics is therefore also so small that it is masked by the thickness of the caustic and thus only one caustic is observed with Homalite-100 in agreement with our initial experiments. For non-birefringent materials, P = 0 and equation (11) is easily solved to yield $\alpha r_0^{-5/2} = \frac{2}{3}$. Substituting for α and rearranging, one finds

$$K_I = \frac{2}{3}\frac{\sqrt{2\pi}}{z_0 cd}\left[\frac{D}{f}\right]^{5/2} \qquad (12)$$

where D is the transverse diameter of the caustic and is related to r_0 through $D=fr_0$. The value of f is determined from the equations for the caustic and initial curve and is 3.17.

Having explained the absence of a double caustic for Homalite-100 we turn now to the consideration of inertial effects. The requisite analyses have been performed previously.[9] These results are approximate but represent the true situation with an accuracy of about 1-2%. Using the definition

9. Kalthoff, J.F., *et.al.*, *op. cit.* and Rosakis, A.J., *op.cit.*

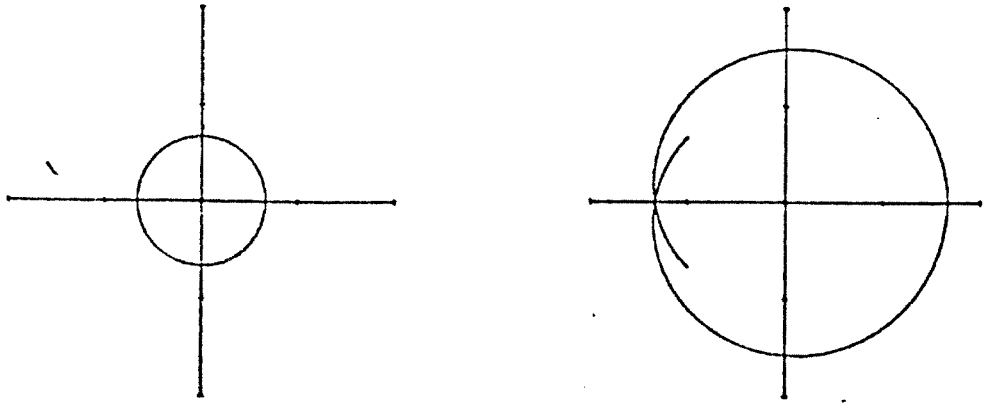

INITIAL CURVE

CAUSTIC CURVE

NON-BIREFRINGENT MATERIAL, P=0

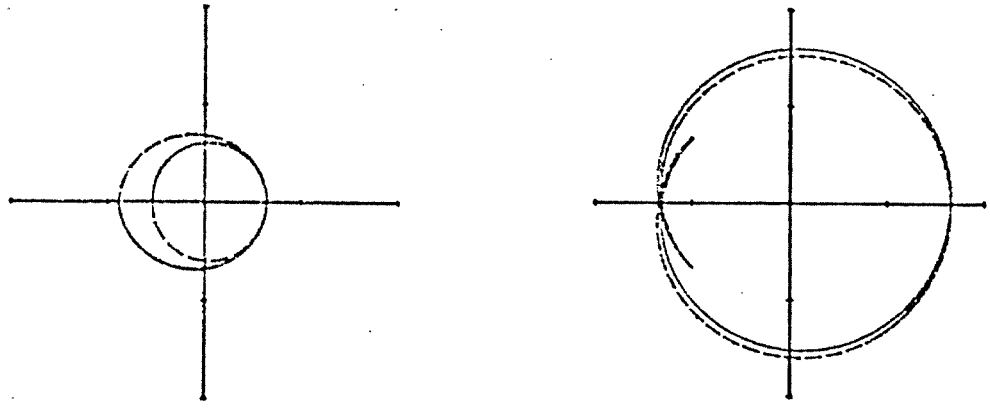

INITIAL CURVES

CAUSTIC CURVES

BIREFRINGENT MATERIAL, P=0.25

Figure 9. Caustics and initial curves for non-birefringent and birefringent materials. (For Homalite-100, P = 0.087).

$$\alpha_1=\left\{1-\frac{v^2}{C_d^2}\right\}^{1/2};\quad \alpha_2=\left\{1-\frac{v^2}{C_s^2}\right\}^{1/2}$$

and

v = crack velocity

C_d = longitudinal wave speed

C_s = shear wave speed

z_0 = distance specimen reference plane

c = optical coefficient

d = specimen thickness

D = transverse diameter of caustic

the dynamic stress intensity factor is given by

$$K_I^{dyn}=\frac{2}{3}\frac{\sqrt{2\pi}}{z_0 cd}\left[\frac{D}{3.17}\right]^{5/2}\frac{4\alpha_1\alpha_2-(1+\alpha_2^2)^2}{(\alpha_1^2-\alpha_2^2)(1+\alpha_2^2)} \tag{13}$$

Note by comparing this expression with the static analysis in equation (12) that the dynamic stress intensity factor derives from the static one through the factor:

$$F=\frac{4\alpha_1\alpha_2-(1+\alpha_2^2)^2}{(\alpha_1^2-\alpha_2^2)(1+\alpha_2^2)} \tag{14}$$

Rosakis[10] has given a similar approximate correction factor, which differs in detail from the above but is numerically within 1-2%.[11]

2.4 High Speed Photography

The photo-recording system contains two major elements, namely a camera derived from an Ellis design[12] and a 5 watt Argon ion pulsed laser as the light source. The light beam passes through the specimen and is collected into the camera by a series of lenses. Figure 10 shows a schematic and a photograph of the experimental apparatus.

10. Rosakis, A.,*op. cit.*

11. There is no reason for our preference of one result over the other except that Kalthoff's analysis was available to us at an earlier date.

12. Ellis,A.T., Ph.D. Thesis, California Institute of Technology, (1953).

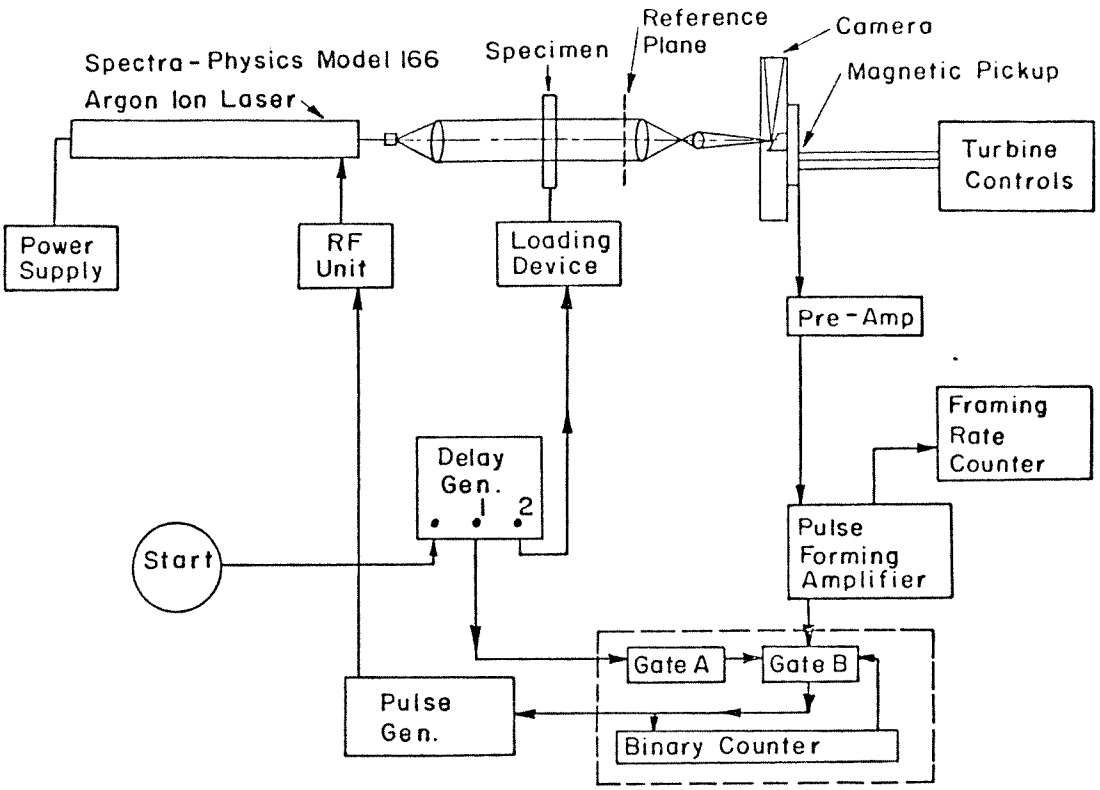

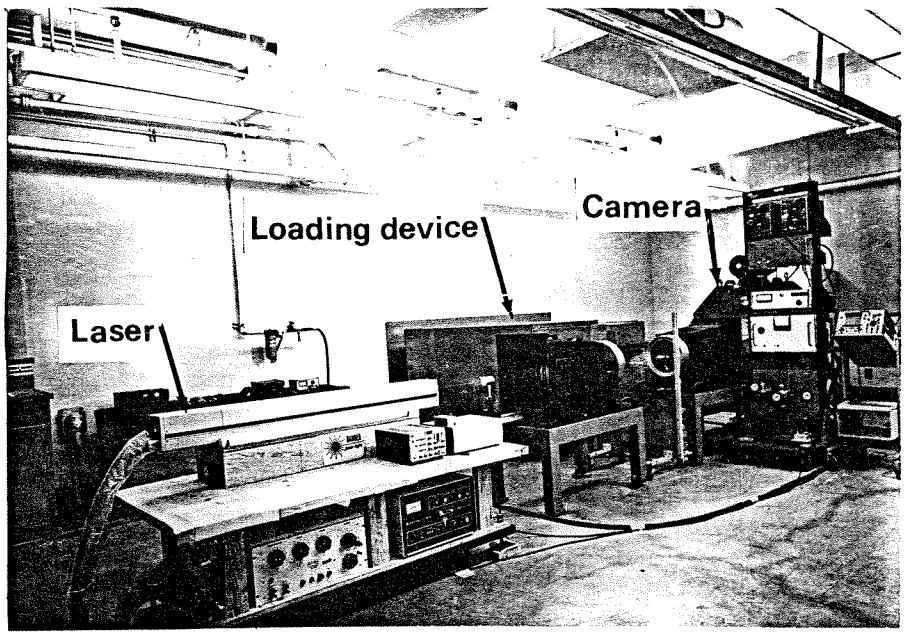

Figure 10. Experimental apparatus and schematic.

An essential component of the camera is a mirror oriented at 45°with the optical axis and mounted on the shaft of an air turbine. This mirror projects the image onto a stationary circular 35 mm film track as the turbine rotates. A 128 toothed wheel which rotates with the turbine generates a timing signal as each tooth passes a magnetic pick up and this signal is used to synchronize the pulsing of the laser with the rotation of the turbine. Each laser pulse lasts 20 nsec and forms a discrete image on the film plane. Overlapping of frames, i.e., double exposure, is prevented by a binary counter that permits only 128 laser pulses corresponding to one complete revolution of the turbine. The framing rate can be varied continuously from about 10,000 to 200,000 frames per second and is controlled through the rotational speed of the turbine. Our tests were conducted at 200,000 frames per second using a field of view of 7 inches in diameter. Even at the highest crack speed, the crack remains in the field of the camera for about 250 μsec. As remarked earlier the camera can be triggered prior to the loading and this facilitates the observation of the crack-tip from the initial stages of loading, through the initiation of crack propagation and arrival of reflected waves from the boundary at the moving crack-tip.

2.5 Calibration of the Experimental Apparatus

2.5.1 Theoretical Considerations: As stated earlier, the main advantage of using large sheet specimens is the ease with which the experimental results can be compared to available theoretical analysis. For a stationary semi-infinite crack in an infinite medium, a fundamental Green's function solution was obtained by Freund[13] for plane strain. As illustrated in figure 11, he considered concentrated unit step loads applied at a distance "L" from the crack tip and determined the resulting stress intensity factor for all time. We employ this solution via superposition to generate the stress intensity factor for any load varying arbitrarily

13. Freund, L.B.,*International Journal of Engineering Science*,**12**,(1974) ,p.179.

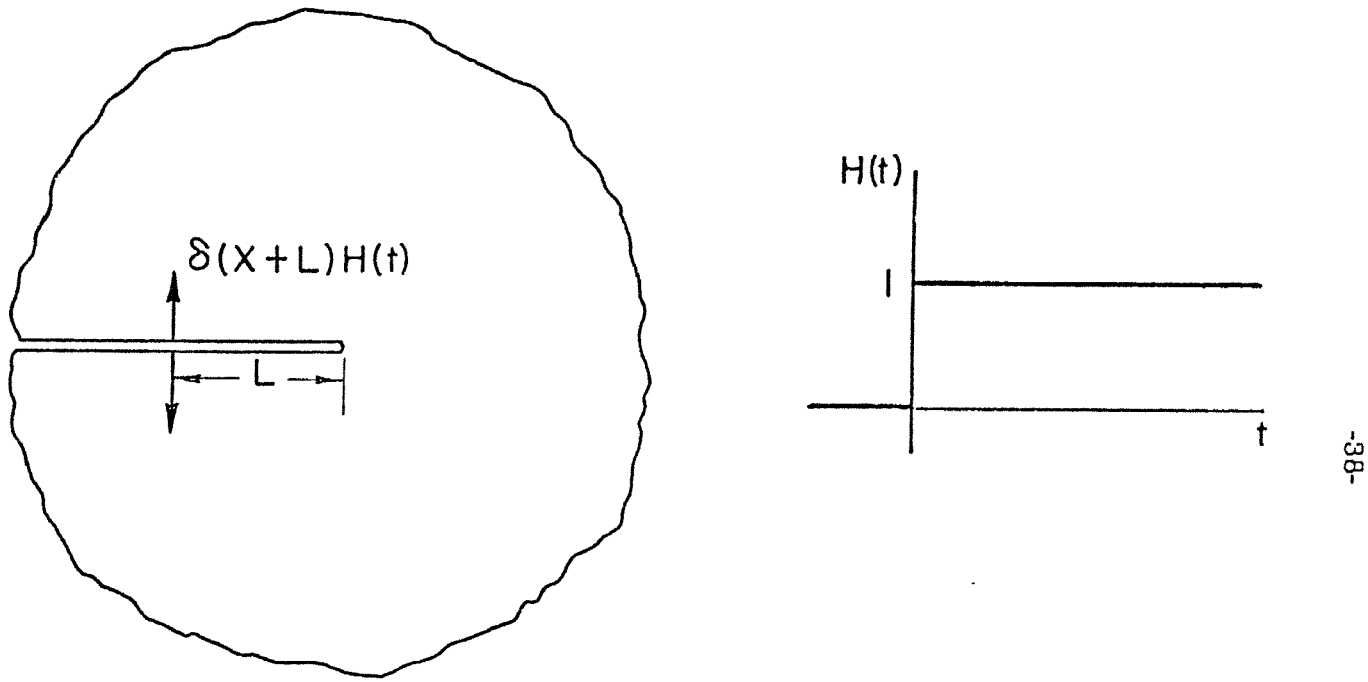

Figure 11. The Green's function problem.

both temporally and spatially on the semi-infinite crack. Let K_0 be the stress intensity factor for the Green's function problem; then for arbitrary loading the stress intensity factor K is

$$K(t)=\int_0^t ds \int_{-\infty}^0 K_0(t-s,\xi)p(\xi)\dot{f}(s)d\xi \tag{15}$$

where

$p(\xi)$ = spatial distribution of load

$\dot{f}(s)$ = time derivative of the time history of the load.

For our purposes we convert the plane strain solution to plane stress by appropriate changes in the elastic constants which replaces the dilatational wave speed by the plate velocity. In our experiments the load is distributed over the crack and the time dependence is (always) as shown in figure 4. The integral is evaluated numerically.

The stress intensity factor $K(t)$ for a crack running with the velocity v is given by[14]

$$K(t,v;l) = k(v)\, K(t,0;l) \tag{16}$$

where $k(v)$ is a velocity dependent function and $K(t,o;l)$ is the instantaneous stress intensity factor appropriate to the instantaneous crack length l. The latter is obtained from the superposition integral (15) by suitably changing $p(\xi)$. In evaluating the function $k(v)$ we make use of the experimentally determined velocity values. We defer the discussion of the results until needed in the context of comparison with experimental measurement.

2.5.2 Experimental Considerations: Before proceeding to the dynamic tests and results we describe the influence of the size of the initial curve of the caustic on the accuracy with which the stress intensity factor may be determined. The size of the initial curve has to be small in order that the interpretation of the caus-

14. Rose,L.R.F., *International Journal of Fracture*, **12**,(1976),p.799.

tic size in terms of the stress intensity factor be adequate . Since the size of the initial curve depends on the reference distance z_0 (cf. figure 8b) and also on the stress intensity factor, for a given optical configuration (fixed z_0) the radius of the initial curve increases with the stress intensity factor. In order to minimize the error due to the varying size of the initial curve, it is necessary to determine the reference distance (z_0) that would provide small initial curves over a large range of stress intensity factors. This reference distance was determined from quasistatic tests on compact tension specimens loaded in an Instron tester. The caustic diameters corresponding to various reference distances and loads were measured and the stress intensity factors computed from equation (12). Srawley[15] determined the stress intensity factors numerically for this type of specimen by using the boundary collocation technique. From a comparison of the theoretical and experimental values, as shown in figure 12, one determines that the initial curve has to be about 3 mm in diameter for reliable results. The maximum error involved is about ± 10% and arises from the fact that the reference distance is fixed and the initial curve varies in size.

We turn now to the dynamic test results. The method of caustics has been demonstrated to provide satisfactory results under static loading here and by other authors.[16] However, for the case of dynamic loading, involving stationary as well as moving cracks, several authors have utilized the dynamic caustics[17] but either due to the lack of an analytical solution for the geometry at hand or due to experimental difficulties in obtaining loading conditions for which analyses are available, no comparison of analytical results and dynamic caustics has been demonstrated to date. Because our experimental

15. Srawley,J.E., and Gross,B.,*Engineering Fracture Mechanics*,**4**,(1972), p.567.

16. Theocaris, P.S., *Journal of Applied Mechanics*,**37**,(1970),p.409.

17. Goldsmith,W. and Katsamanis,F.,*Experimental Mechanics*,**19**,(1979),p.235. and Katsamanis,F., Raftopoulos,D. and Theocaris,P.S.,*Journal of Engineering Materials and Technology*,**90**,(1977),p.105.

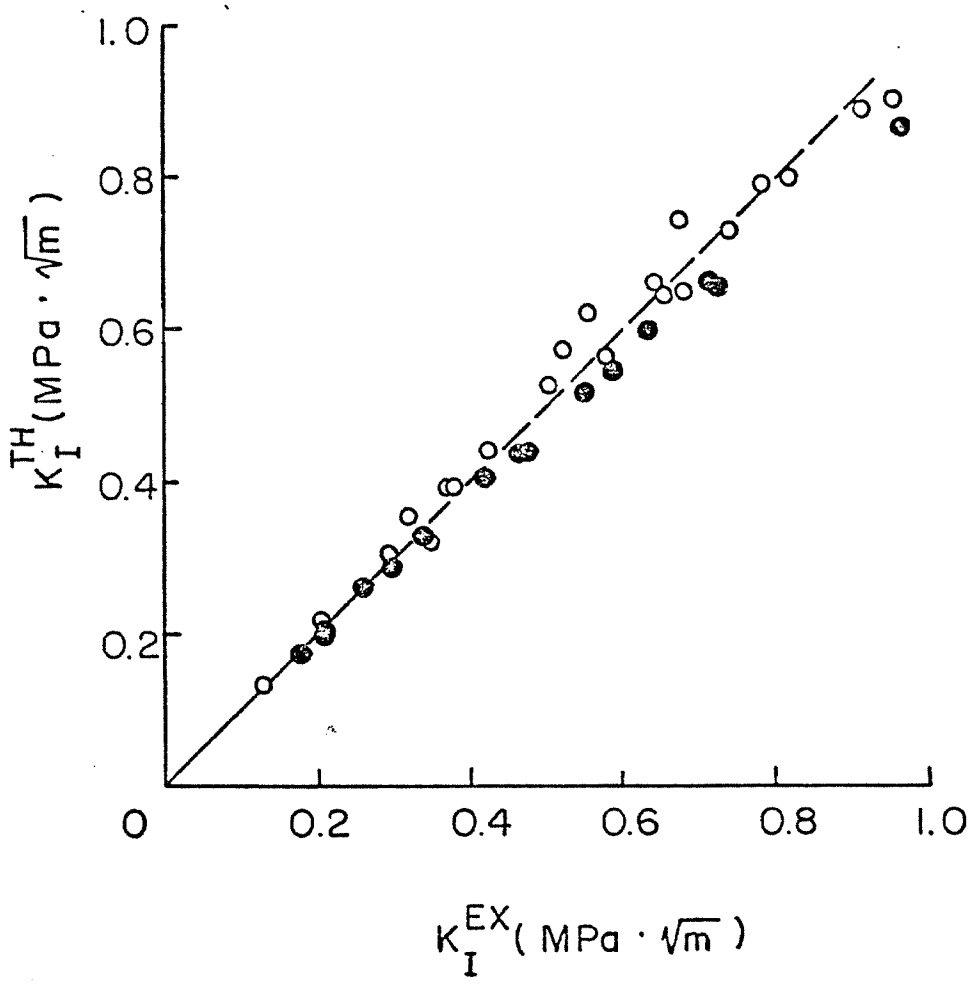

Figure 12. Results of quasi-static tests. (o - PMMA; ● - Homalite-100)

configuration is such that available theoretical results are directly applicable it is appropriate that we provide that comparison here. Moreover, the need to investigate the reliability of the method of caustics in the dynamic case in our particular problem arises for two additional reasons. First, the caustic analysis is derived from plane stress theory and depending on the steepness of the loading pulse (frequency content) three dimensional effects could be more important than would be evident from the earlier mentioned Fourier analysis of the loading pulse. Secondly, the stress-optic coefficients c_1 and c_2 are temperature dependent and could be rate dependent. To determine these effects, two experimental configurations, as shown in figure 13 are considered. In the first configuration, a semi infinite crack in an infinite medium is loaded by uniform pressure p on the semi-infinite crack faces; in the second case the loading is confined to a small length of the semi-infinite crack face at some distance a from the crack-tip. The first configuration is realized by inserting the doubled-up copper strip into the crack as in figure 3 and the second configuration is obtained by inserting the copper strip in the transverse direction. The theoretical values of the stress intensity factor for these two cases are obtained from equation (15) by suitably substituting for $p(\xi)$. The corresponding results are plotted in figures 15 and 16.

A selected number of frames from a typical dynamic test are shown in figure 14. Here the load application starts at frame 0 and 0 μsec. The caustic diameter and crack tip position are measured from the high speed cinematographs. Since no additional measurement errors are introduced in the dynamic tests, above and beyond those incurred in the static calibrations, the error factor of $\pm$ 10% determined for the latter tests is used here. Figures 15 and 16 show the stress intensity factor histories from two experiments. Figure 15 also shows the crack position as a function of time for the first configuration. In the second

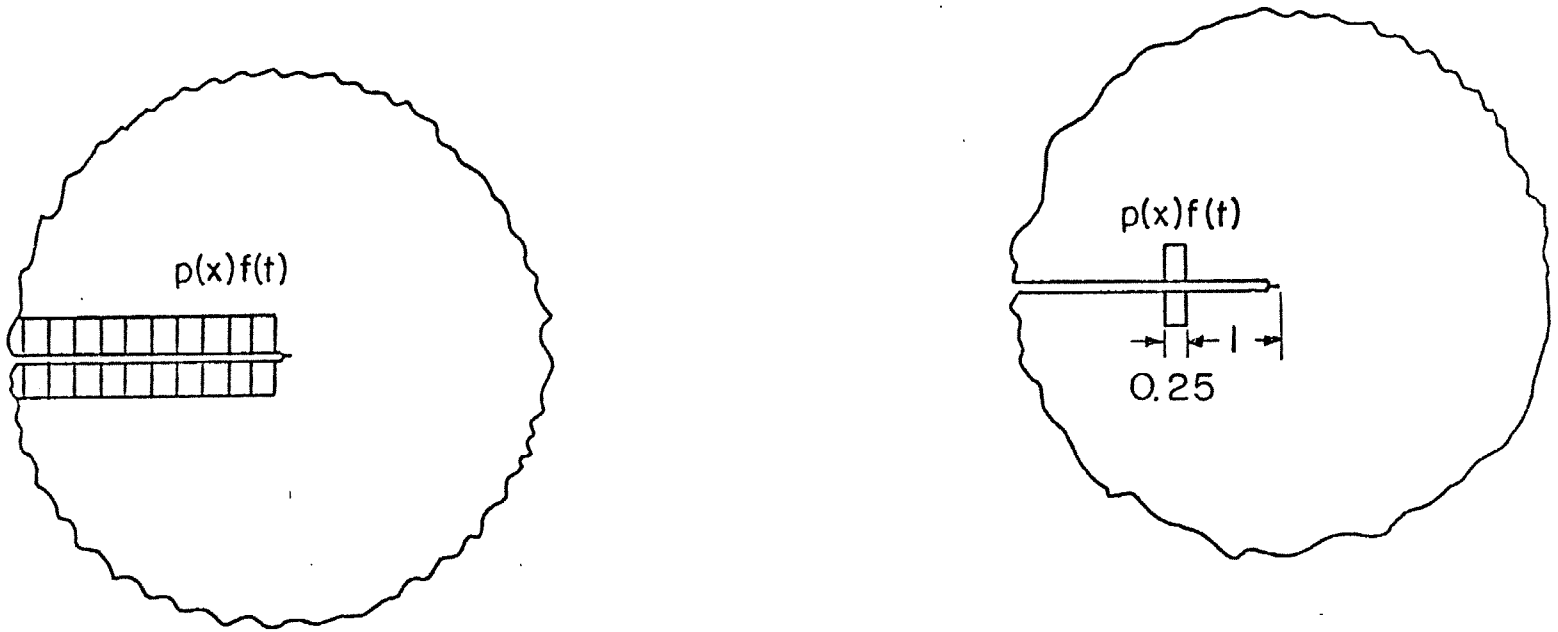

Figure 13. Dynamic test geometries and load distribution. f(t) is given by the trace in figure. 4.

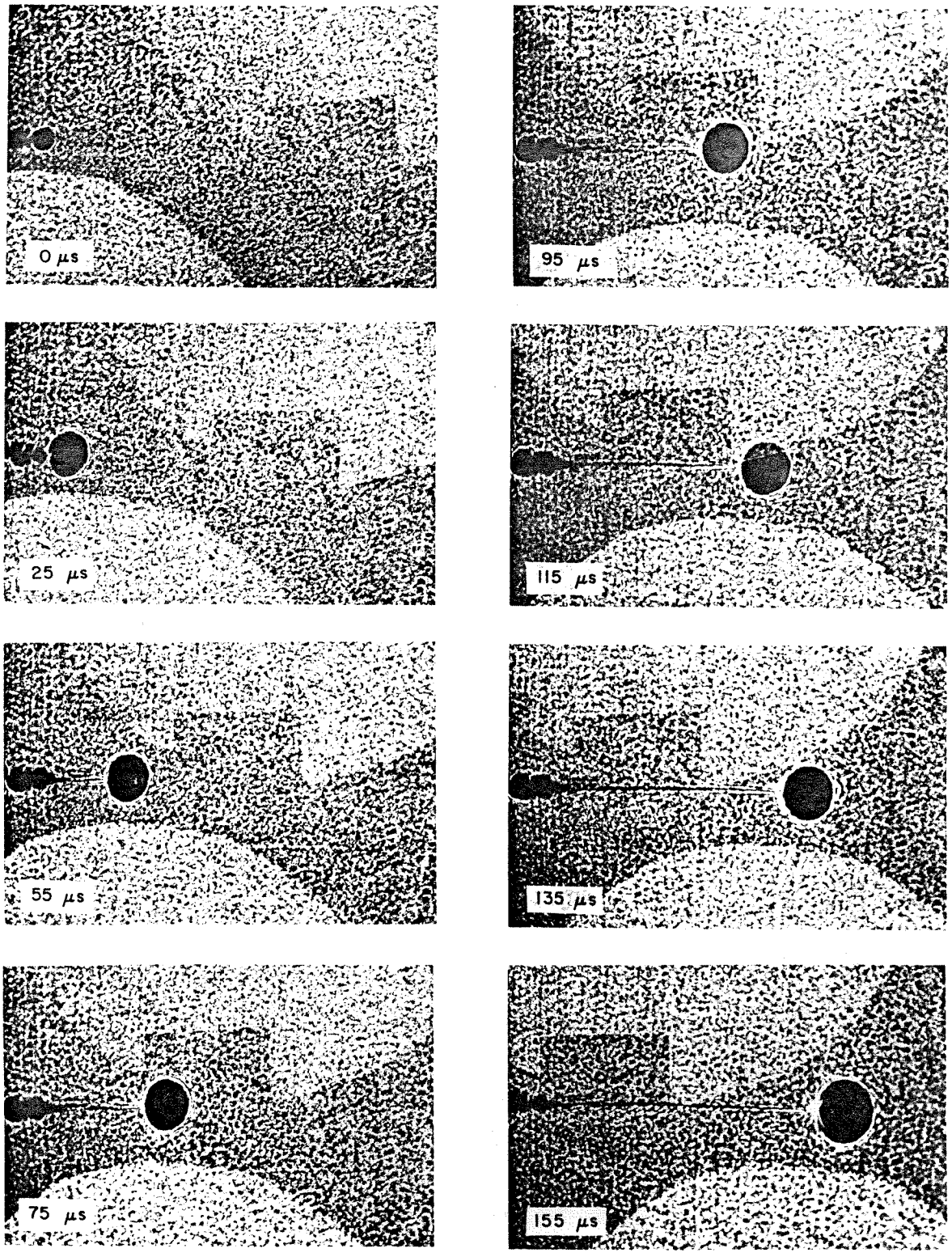

Figure 14. High speed cinematographs of a running crack.

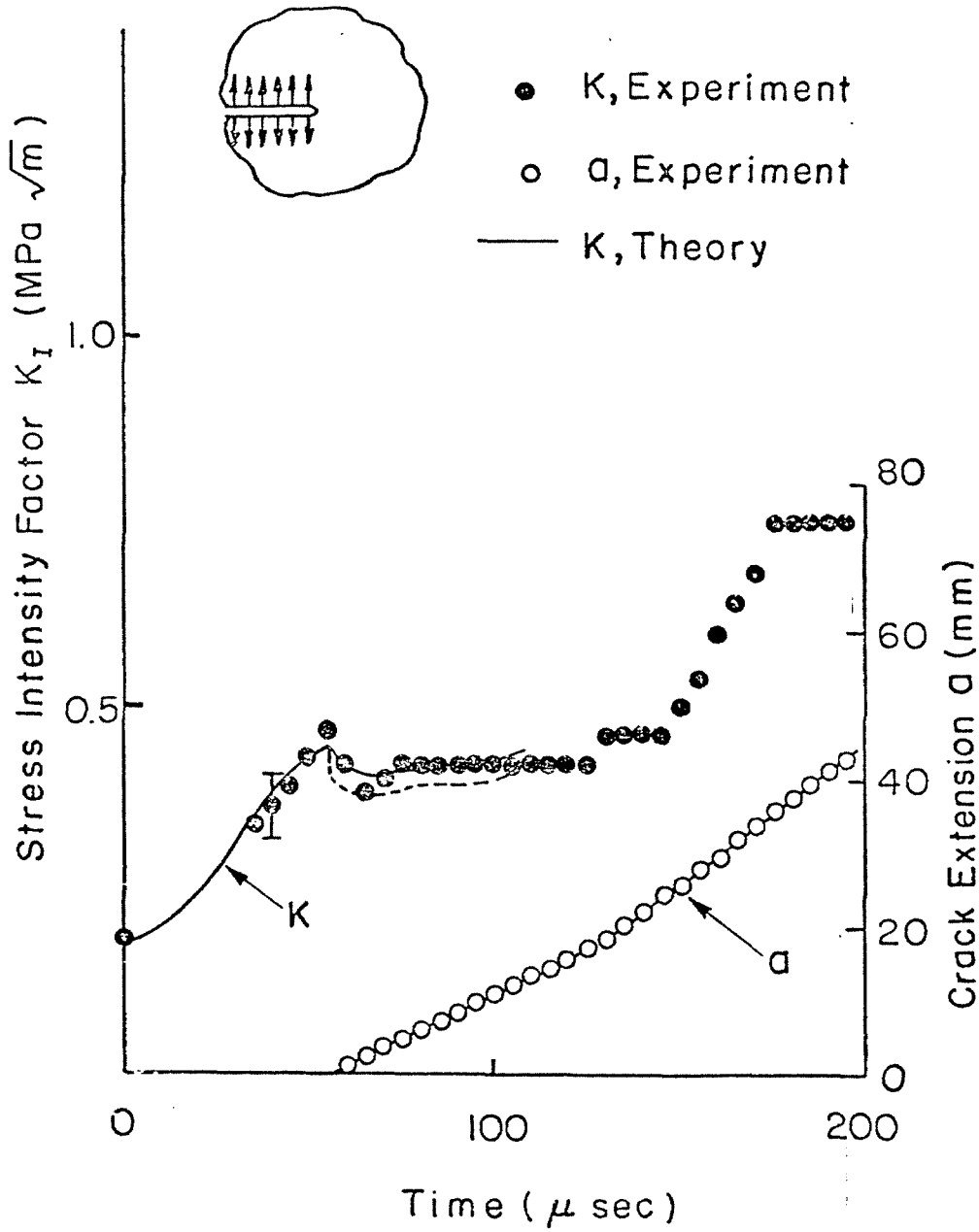

Figure 15. Stress intensity factor and crack extension history.

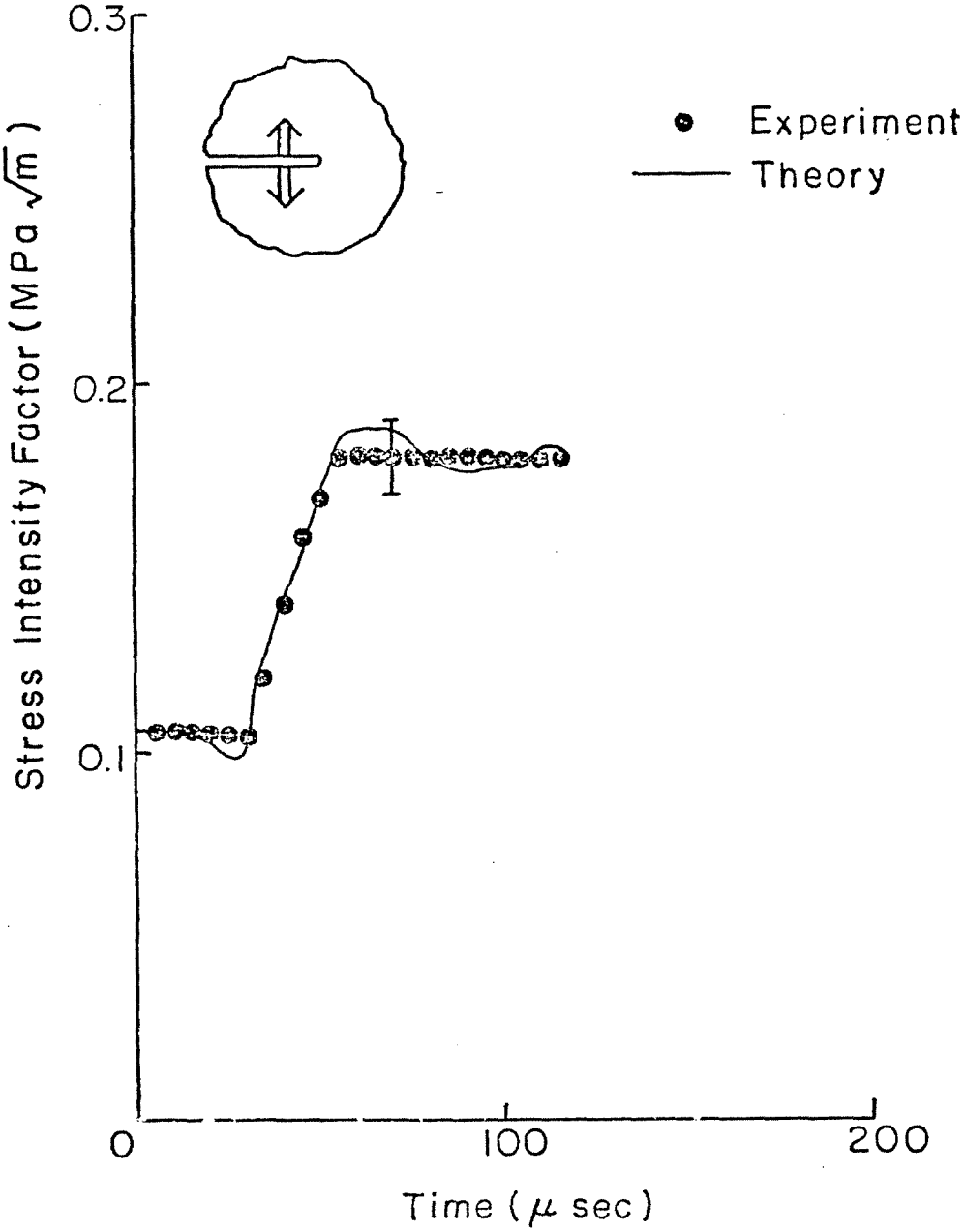

Figure 16. Stress intensity factor history.

configuration, the load was insufficient to initiate crack-growth. From figure 14 we note that the caustic evident prior to loading in frame 0 indicates a preloaded crack which results from the copper strip inserted into the machined crack faces. In making a comparison with the theoretically calculated stress intensity factors, the effect of this preload has to be considered. Since the electromagnetic loading device provides a load in addition to the preload, a constant stress intensity factor, equal to the initial value, is added to the theoretically computed stress intensity factors for the stationary crack. It is likely that the stress intensity factor due to the preload will decrease with increasing crack length, but in order to compute this effect, the detailed distribution of the preload along the crack surface is needed. Because this distribution is not known we indicate two estimated adjustments for the theoretical values for the growing crack. These corrections are computed as follows: The first estimate (solid line in figure 15) assumes that the effect of the preload is constant and is the same as for the stationary crack. The second estimate (dotted line in figure 15) corresponds to the assumption that the effect of the preload is a constant, but that value is taken to be $k(v)$ (cf. equation(16)) times the initial value. Taking into account the experimental error we see that both estimates agree well with the measured intensity history.

The crack extension history is shown in figure 15, and in order to determine the velocity of crack propagation, a least square curve fitting programme was used to fit a polynomial to the experimental data and the velocity was then obtained by differentiating the curve fit equation. The polynomial fit can be expressed as

$$a = \sum_{i=1}^{N} A_i t^{i-1} \tag{17}$$

where a is the crack position and t denotes the time. The coefficients A_i are

determined by minimizing the likelihood function:

$$\chi^2 = \sum_{i=1}^{N} \frac{\left[a_i - \sum_{j=1}^{M} A_j t_i^{j-1}\right]^2}{\delta_i^2} \tag{18}$$

where (t_i, a_i) represent experimentally measured time and crack position data, δ_i is the standard error on a_i, N is the number of data points and $M-1$ is the degree of polynomial fit. The degree of the polynomial fit is yet to be determined and this will be done using the 'goodness of fit' criterion as determined by the χ^2 test. For the crack extension history illustrated in figure 15, the polynomial curve fitting programme was tested with fourth and second order as well as linear fits. The linear fit was applied in two segments taking into account that stress wave interaction occurred at around 140 μsec. The value of χ^2 in the three cases was respectively 19.52, 82.60, and for the line fit 0.01 and 5.54 for the two line segments. Clearly, the two segment straight line fitting provides the best estimate of the actual crack extension history and hence the experimental data were fitted with straight lines of appropriate number of segments in order to obtain the best fits in each case. Anticipating later results, in all cases not involving arrested cracks or wave interactions, one straight line segment fit the data very well. Where there was either crack arrest and reinitiation or stress wave interactions, these events had to be taken into consideration separately in order to decide on the number of straight lines that were fit to the data.

From the plot of crack extension history, it is clear that the crack attains a constant velocity of 240 m/sec (within the time resolution of the high speed camera of 5 μsec). The quality of the experimental data is clearly sufficient to answer our potential reservations regarding the application of caustics to transient dynamic crack problems. In fact, the accuracy is ample to identify deviations from the theoretical and experimental results as evidenced by

the divergence of the experiment and analysis at 150 μsec. At this time the waves reflected at the nearest plate boundaries arrive as tension waves, thus increasing the stress intensity factor. Also, on arrival of these reflected waves, the crack velocity jumps to a new constant value (again within the time resolution of the camera).

In conclusion we note that,

1. a completely characterized loading device delivering a highly repeatable pressure pulse has been constructed for performing fracture tests under transient loadings.
2. For the time scale of the experiment and under the loading history considered, conditions of plane stress prevail. Also, the optical coefficient c is a constant on this time scale. Thus the dynamic caustics produce satisfactory results.
3. The crack acceleration phase occurs during a very short time such that the crack attains a constant velocity in less than 5 μsec.

3. CRACK INITIATION AND CRACK ARREST

The main problems of interest in dynamic fracture are those of crack initiation, crack arrest, crack propagation and crack branching. In this chapter we will investigate the first two problems, namely, crack initiation and crack arrest. Crack propagation and branching are discussed in Chapter 5.

3.1 Crack Initiation

The basic formulation of the quasi-static fracture problem was discussed briefly in Chapter 1. The main idea of this formulation is that the energy required to create new surface area, Γ, has to be obtained by the energy released by the elastic system in deforming to the new configuration. The energy released by the system per unit of crack advance is referred to as the strain energy release rate and is usually denoted by G. One may then write the failure criterion in quasi-static fracture mechanics as

$$G = \Gamma. \tag{19}$$

The energy release rate can be expressed as a function of the crack tip stress intensity factor as $G = K^2/E$ for plane stress and the stress intensity factor can be calculated for a number of practically significant geometrical configurations. The value of Γ is measured for different materials and is usually regarded as a material constant. Thus, when the stress intensity factor at the crack tip is such that the energy release rate is equal to Γ, the crack would be able to propagate. Then,

$$G = \frac{K_c^2}{E} = \Gamma. \tag{20}$$

The value of the stress intensity factor that satisfies the energy equation is referred to as the critical stress intensity factor and is denoted by K_c. The failure criterion is thus expressed as a critical value of the stress intensity

factor and when the applied load is such that the stress intensity factor exceeds the critical stress intensity factor, the crack will propagate. This quasi-static formulation is used quite profitably in designing fracture critical structures.

There are many applications in which the assumption of quasi-static loading is not justifiable and in such cases, one would like to know in advance the validity of applying the quasi-static fracture criterion. It is known that under high rates of loading, the mechanical behaviour of materials is different from their behaviour at relatively low rates of loading. The yield stress of a material, for example, depends on the rate at which the material is loaded. In viscoelastic solids, the rate of loading determines whether the short time or long time material behaviour is invoked. One would thus expect that the fracture properties of materials would also be dependent on the rate at which the external loads are applied. The present investigation into crack initiation was aimed at determining the nature of the variation of the fracture properties under stress wave loading conditions with the rate of loading varying between 10^4and10^5 MPa/sec. The electromagnetic loading device described in the previous chapter was ideally suited to carry out this investigation since the rate of loading generated by the loading device was determined by the charge voltage in the capacitor bank which could be changed very easily. Also, since the load that is applied is triggered using an electrical pulse, time sequencing of the loading with the high speed camera is achieved quite easily and the initiation behaviour of the crack can be photographed with the high speed camera. When mechanical loading schemes are used, in general, the initiation behaviour is not readily captured and one has to resort to special specimen configurations to be able to follow the nature of the initial motion of the crack.

In order to determine the nature of the dependence of the critical stress intensity factor, experiments were conducted at various rates of loading.

The loading geometry used was that of a pressure loaded semi-infinite crack in an infinite meduim. The capacitor bank was charged to different levels in order to apply various loading rates at the crack faces. From the high speed cinematographs of these experiments, the stress intensity factor history and the crack position history were determined. The stress intensity factor at initiation was determined by interpolating the stress intensity factor data at the instant of initiation as indicated by the crack position history. The result of this experimental scheme is shown in figure 17 where the stress intensity factor at initiation is plotted against the time at which the crack was initiated, since this time was a measure of the rate of loading. Also shown on this plot are the results of quasi-static tests that were obtained by Bradley.[1] Smith[2] investigated the initiation behaviour of Homalite-100 at high and low rates of loading and his results are also plotted in figure 17. The low rate data were obtained from Instron tests and the high rate data were obtained from experiments similar to those discussed here. If the present data are taken together with the low rate data of [2] and the quasi-static data of [1], it is seen that the effect of the rate of loading on the initiation stress intensity factor is negligible when the time to fracture is on the order of 50 μsec, which corresponds to a loading rate of 10^4 MPa/sec, but, at higher rates of loading, the stress intensity factor at initiation increases with an increasing rate of loading. Although the experiments of [2] were conducted under conditions identical to those described here, the results for the high rates of loading seem to be in disagreement. The reason for this is now clear to us: The photoelastic set up used in [2] was not sensitive enough to reliably determine the stress intensity factor; therefore the stress intensity factor at initiation was obtained from analytical computations of the stress intensity factor history for the given dynamic problem and using the experimentally determined

1. Bradley, W.B., Ph.D., Thesis, University of Washington, (1969).
2. Smith,G.C., Ph.D., Thesis, California Institute of Technology,(1975).

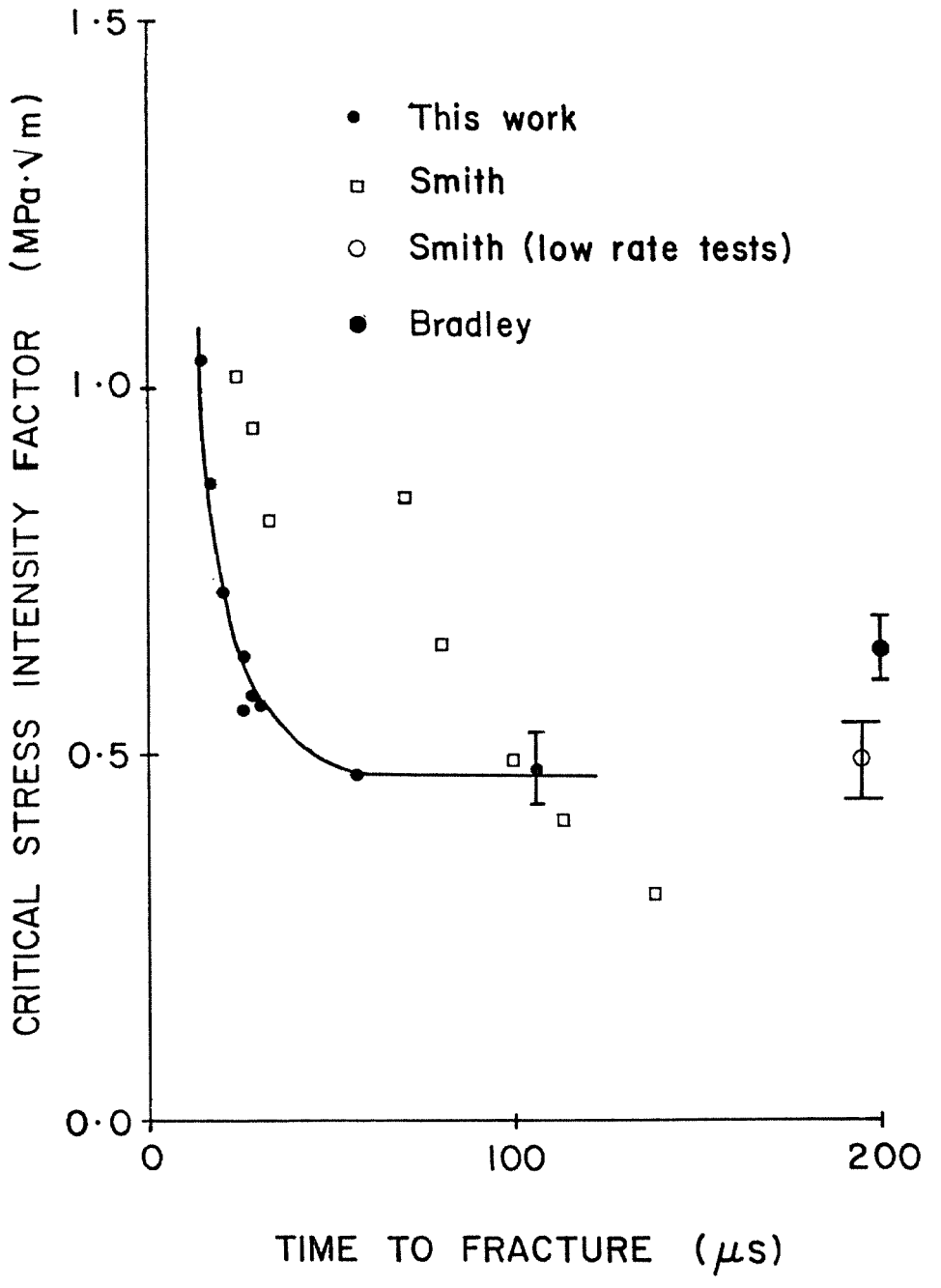

Figure 17. Rate dependence of the critical stress intensity factor.

initiation time. In the present investigation, the method of caustics was used to obtain the stress intensity factor history experimentally. It was noted that there exists an initial loading on the crack tip even when the dynamic load was not applied as can be verified from the small caustic that is seen in figure 14. This preload occurs due to the fact that the doubled up copper strip is inserted into the machined crack faces and tends to push the crack faces apart. This preload was ignored in the experimental results of [2] and accounts for the variation of the results of [2] from the present work.

In conclusion then, the dependence of the critical stress intensity factor on the rate of loading has been established for Homalite-100. The critical stress intensity factor is independent of the rate of loading and equal to the quasi-static value for rates of loading lower than 9×10^4 MPa/sec, but above this value, the initiation stress intensity factor increases rapidly with the rate of loading. From this result, we draw an interesting conclusion: Refer to figure 18, and assume that the crack is loaded such that the stress intensity factor increases upto 0.75 MPa $\sqrt{m}$, and then decreases to zero along the loading path indicated by the solid line. It is seen that the crack will not initiate, since the critical stress intensity factor is not exceeded. But if the same peak load is retained, and the loading rate is decreased to cause the loading along the path indicated by the dotted line in figure 18, the crack will initiate at the point indicated by the asterisk. This indicates that the question of whether a structure will fracture under a given loading will depend not only on the amplitude of the loading, but also on the complete history of load application. Further experimentation along these lines is required in order to investigate the effect of the pulse duration etc., on the crack initiation.

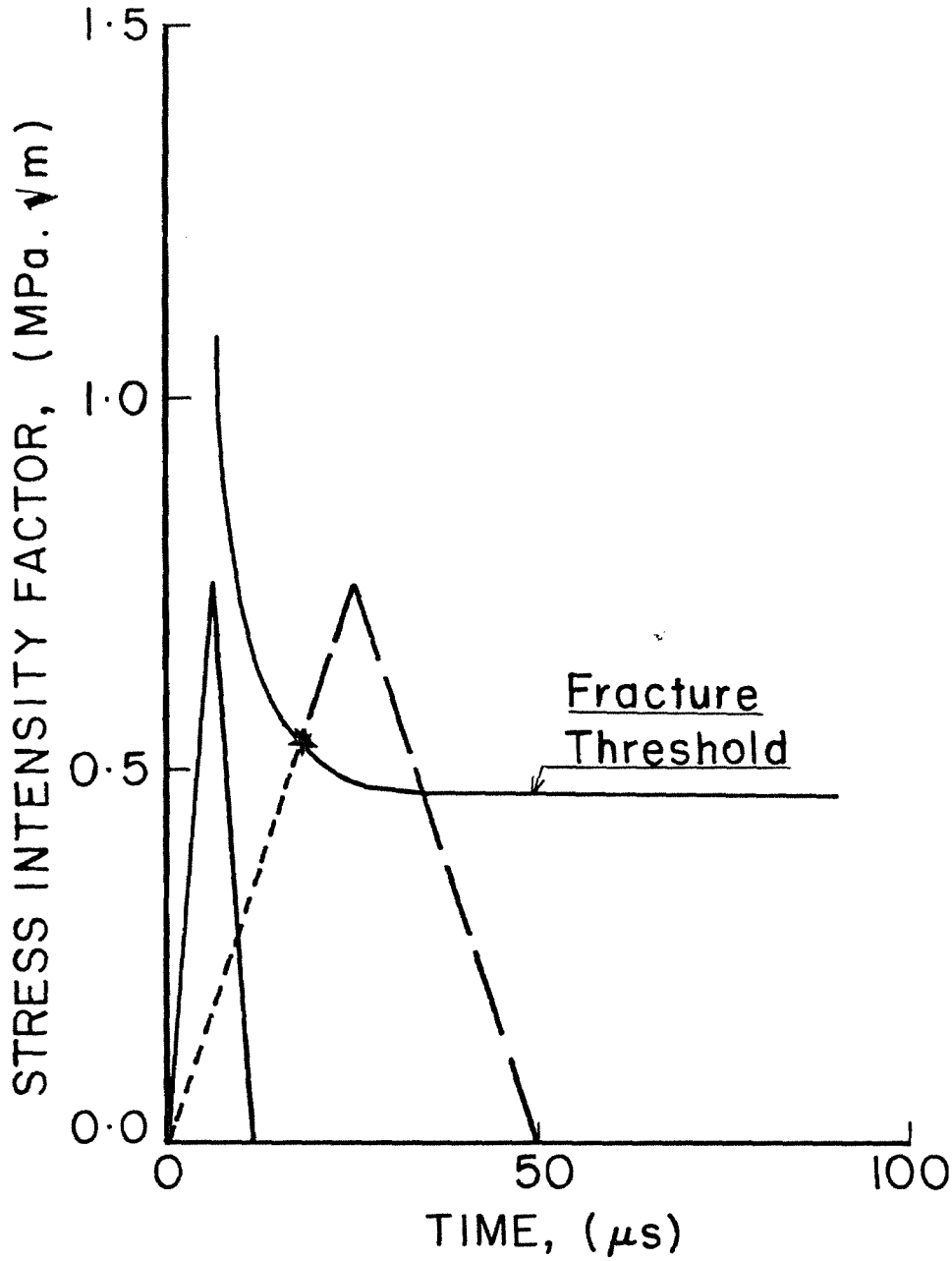

Figure 18. Effect of the loading pulse shape on crack initiation.

3.2 Crack Arrest

Crack arrest problems are of enormous practical significance in that they provide the answer to the key question: can a fast running crack be brought to rest before the complete failure of the structure? What criteria operate to control crack arrest? An important question in this connection is whether there exists a critical value of the stress intensity factor below which a crack can no longer propagate and which may be termed the "arrest stress intensity factor," analogous to the initiation stress intensity factor. Is this quantity a material parameter or is it dependent upon the geometry? Up to now, crack arrest experiments have been performed on small specimen with the attendant complicated stress wave interaction, and the crack arrest has usually been attained through the use of prescribed displacements on the specimen. The presence of stress waves leads to oscillatory behaviour of the stress intensity factor after crack arrest.[3] Also, due to the complicated nature of the stress wave interactions, the stress intensity factor a long time after arrest may be quite different from that obtained at the moment of crack arrest, and is probably one reason for the interpretation of the "crack arrest stress intensity factor" as a geometry dependent parameter.[4]

In the present investigation, crack arrest was obtained in a pressure loaded semi-infinite crack. By loading the crack faces with a very small magnitude load, just sufficient to start crack growth, and decreasing the duration for which this loading pulse lasts, the total energy put into the plate is decreased considerably and results in very little energy being available at the crack tip for further crack propagation. The pulse shape that was used for the crack arrest experiments is shown in figure 19. This is achieved by disconnecting all but four

3. Kalthoff,J.F.,*et. al.*, in *Fast Fracture and Crack Arrest*, *ASTM STP 627*,, (1977),p.161.
4. Freund, L.B., in *The Mechanics of Fracture*, (ed. Erdogan, F.), *AMD-Vol.19*, *ASME*, New York,(1976),p.105.

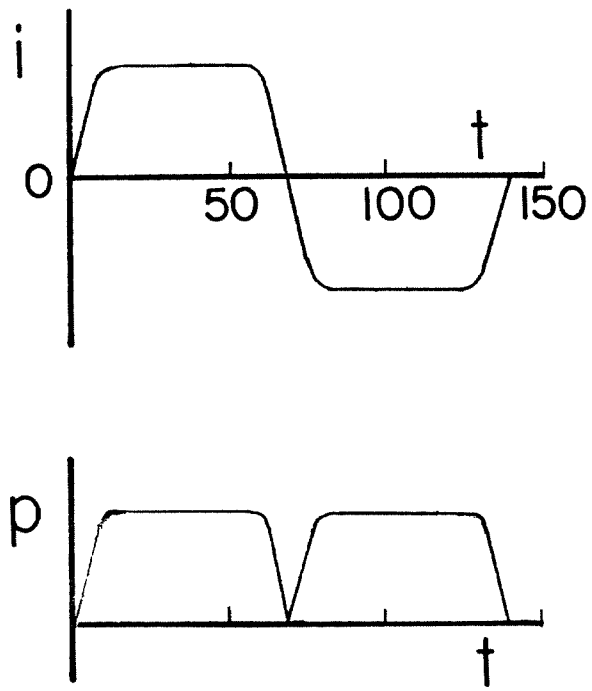

Figure 19. Time history of the current and pressure pulses that were used in the crack arrest experiments.

of the twelve capacitors in the circuit shown in figure 3. The rise time remained the same at 25 μsec, but the duration of the pulse is now only 70 μsec. The capacitor-inductor circuit now 'rings' back and forth and causes a reloading of the crack faces after 70 μsec, but, the major effect of this reloading is to cause reinitiaion of the arrested crack.

The stress intensity factor history and the corresponding crack extension histories from four different tests are shown in figures 20 and 21, respectively. The initial loading on the crack varied from test to test due to variations in the specimen preparation. Also, the starter crack was made using a razor blade leading to slightly different starter cracks for each specimen. This variability leads to differences in the stress intensity factors at initiation, although they are indeed reasonably close to one another. Finally, the loading rate in each test was not kept the same, since the charge in the capacitors was varied in each case to obtain different peak loads on the crack faces. From figure 20, it is seen that when the stress intensity factor reaches the critical value, the crack starts to propagate at a constant velocity as shown in the crack extension history in figure 21. The constancy of the velocity has already been discussed in detail in Chapter 2. As the crack propagates, the resulting unloading causes the stress intensity factor to decrease as indicated in figure 20. When the stress intensity factor decreases to a level such that the energy release rate is no longer sufficient to maintain stable crack propagation, the crack arrests. Note from figures 20 and 21, that at around 70 μsec, when the cracks are arrested, the stress intensity factor is indeed constant within the accuracy of measurement, with a value of about 0.4 MPa$\sqrt{m}$, which is 11% less than the quasi-static critical stress intensity factor for crack initiation. Since these tests were conducted in equivalent infinite specimen configurations, stress waves from the boundary do not interact with the crack (thus the question of the effect of

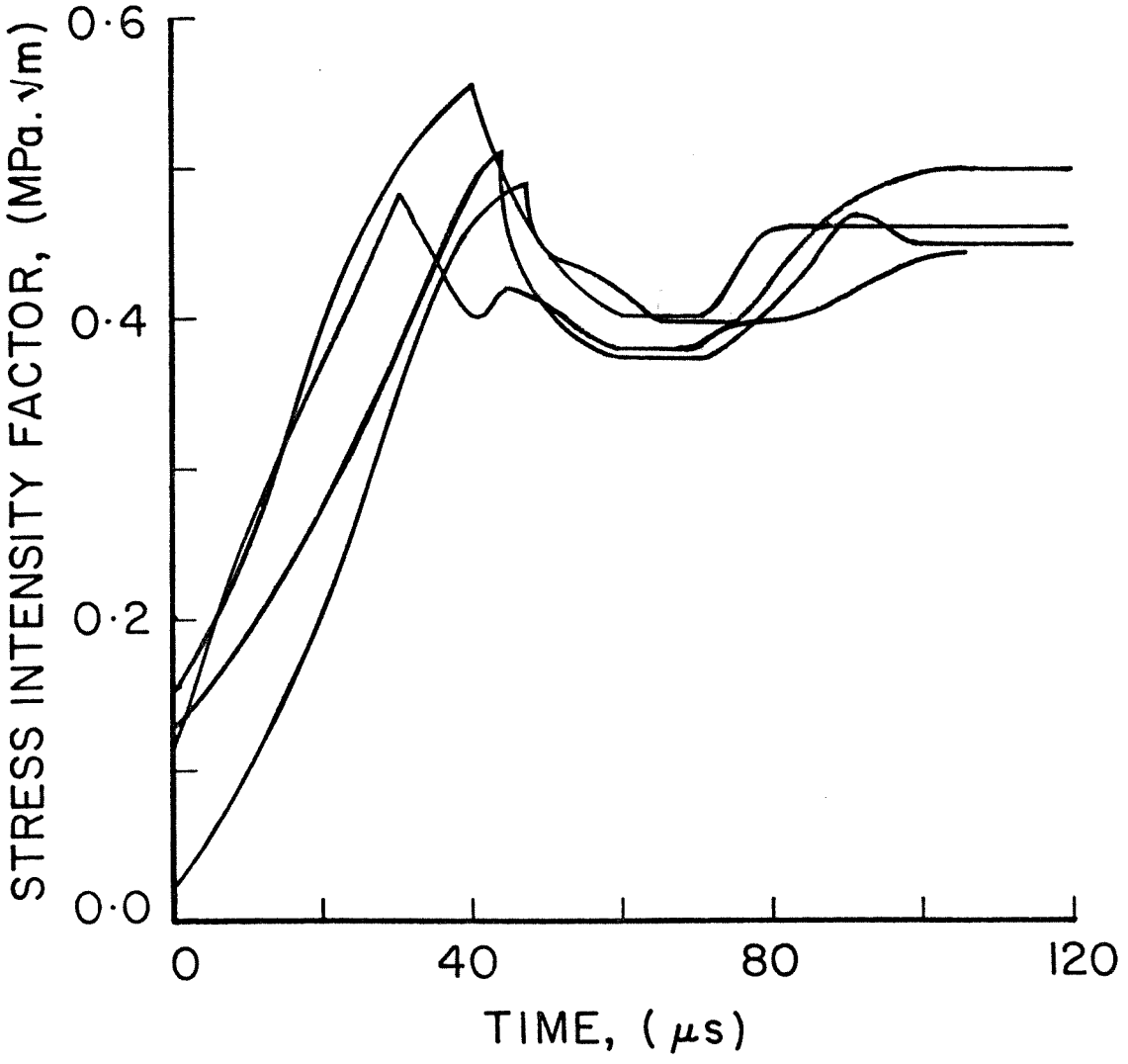

Figure 20. Stress intensity factor histories for the crack arrest experiments.

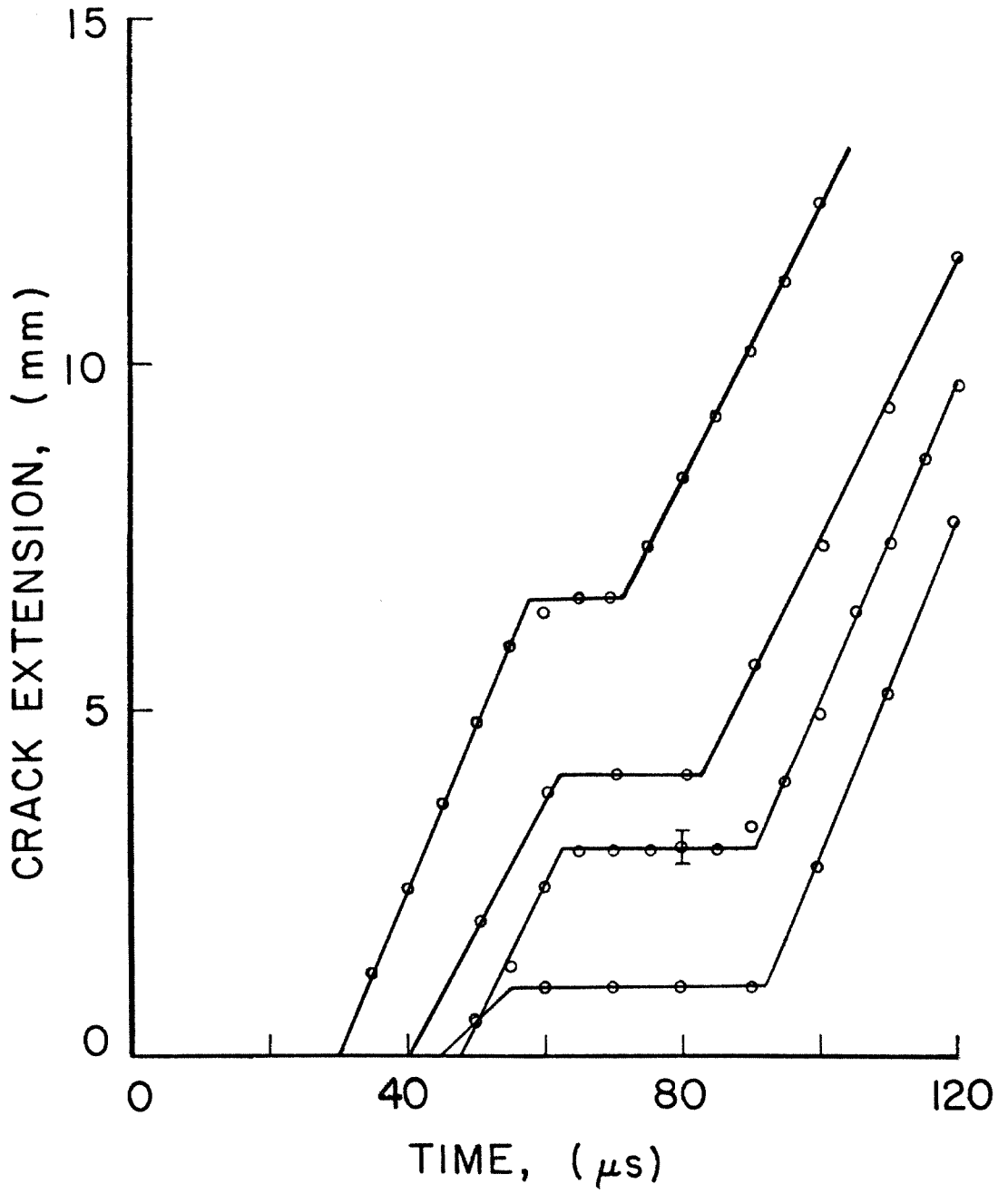

Figure 21. Crack extension histories for the crack arrest experiments.

oscillatory behaviour of the stress intensity factor on the results is circumvented).[5] Also, from these tests, there is no evidence of a crack deceleration phase prior to crack arrest within the resolution of our equipment, which is 5 μsec in time and 0.25 mm in crack position measurement.

From these experiments on crack arrest one concludes that there is a value of the stress intensity factor for crack arrest and that this crack arrest stress intensity factor appears to be a material parameter.

5. Kalthoff, J.F., ***et. al.***, ***op. cit.***

4. MICROSTRUCTURAL ASPECTS OF DYNAMIC FRACTURE

Current mathematical models of the crack propagation process appear rather inadequate in explaining some of the salient features of the propagation process. In these models it is usually assumed that a sharp planar crack traverses along a line in a plane stress or plane strain field. The advantage of such modelling is the relative ease with which the problem could be solved analytically. Until now no mathematical analysis has predicted the existence of a bifurcation in the solution to the problem of a rapidly propagating crack. Also, the assumption of a constant energy of formation of a new surface leads to the prediction of a terminal velocity for crack propagation of the Rayleigh surface wave velocity, as discussed in Chapter 1. This velocity is considerably higher than those actually observed experimentally.

We suppose that this discrepancy is due to the inadequacy of the model to represent the actual physical processes taking place, and that there are some fundamental characteristics of the process that are neglected in the current continuum formulation for crack propagation. The main idea of the experimental observations documented in this chapter is to examine the process of crack propagation from a microscopic point of view and to understand the physics of the fast fracture phenomenon. The results of these observations will then be used in the next chapter to propose a new view of the crack propagation process.

Ideally brittle fracture should occur along a single plane resulting in a perfectly smooth surface. Such a fracture is indeed possible in crystals without defects and is the main advantage of brittle fracture in gem cutting operation. However, in most materials, the surface of fracture is not a smooth plane and a detailed post-mortem examination of the markings in the fracture surface

reveals information about the microscopic nature of the fracture process, the presence of plasticity effects etc. There are three main reasons for the appearance of fracture surface markings. First, there are material inhomogenieties, microscopic deviations from a continuum solid such as the presence of voids in amorphous materials and the presence of preferred cleavage planes in crystalline materials. A second kind of marking is due to the interaction of the microstructure with the propagating crack front. Conic markings observed in many polymer fracture surfaces are due to such interaction of the microstructure with the propagating crack front.[1] A third kind of marking is due to the interaction of stress waves with a propagating crack front. The well known phenomenon of Wallner lines is due to the interaction of stress waves generated by the fracture process interacting with the crack front itself. Also, the ultrasonic modulation technique for measurement of crack velocity relies on the interaction of stress waves transmitted to the crack plane and the crack front.[2] Here we are interested in only the first two kinds of markings. In the figures in this chapter the crack travels from the left to right unless noted otherwise by an arrow.

One of the obvious consequences of the fact that the fracture surface is not smooth on a microscopic scale is that the energy required to create the new surface is generally greater than that calculated by assuming a smooth fracture surface. Thus the energy dissipated in the fracture process is greater than that assumed in the mathematical models. This might at least partially account for the lower terminal velocities observed. Also, one needs to investigate the causes for the appearance of such markings in detail and determine the influence of the microscopic processes on the macroscopic nature of crack

1. Feltner, C.E., *University of Illinois, T&AM Report No 224*, (1962).
2. Kerkhof, F., in *Proceedings of the Third International Congress on High Speed Photography*,Butterworths, London, (1957),p.194.

propagation. In the following, we examine, therefore, the origin and nature of the fracture surface markings in detail and also investigate the problem of crack branching, all from a microstructural point if view. This examination is accomplished in three stages. First, the fracture surface is examined, post-mortem, at relatively low magnifications and the details of the surface are interpreted in terms of the macroscopic parameters of the problem. Second, the fracture surfaces are examined in greater detail under high magnifications (using a scanning electron microscope) and the microstructural details of the fracture process are investigated. Thirdly, the fracture process is examined in real time, using high speed microphotography, to investigate the evolution of the crack propagation process and the crack branching process. The resulting interpretation of the dynamic crack propagation process leads to a new unified view of crack propagation and crack branching.

4.1 Macroscopic Observations of the Fracture Surface

Macroscopically the surface generated by a crack running at a high velocity generally has the appearance as illustrated in figure 22. This has been called the "mirror", "mist" and "hackle" pattern.[3] At the end of the hackle pattern, the crack splits into two or more branches. The "mirror" is a smooth fracture surface, which reflects light specularly, the "mist" pattern is a matte surface and the "hackle" pattern is a relatively coarse fracture surface. We examine the results from four experiments conducted at different load levels. These results are representative of the crack propagation behaviour in this material, and the selected experiments that will be dealt with in detail here contain all the major features of the crack propagation process that are experimentally observed. Figure 23 shows the assembled plates and also the corresponding fracture surface. In all the four cases, the loading simulated pressurization of a

3. Andrews, E. H. *Journal of Applied Physics*, **30**, (1959), p.740.

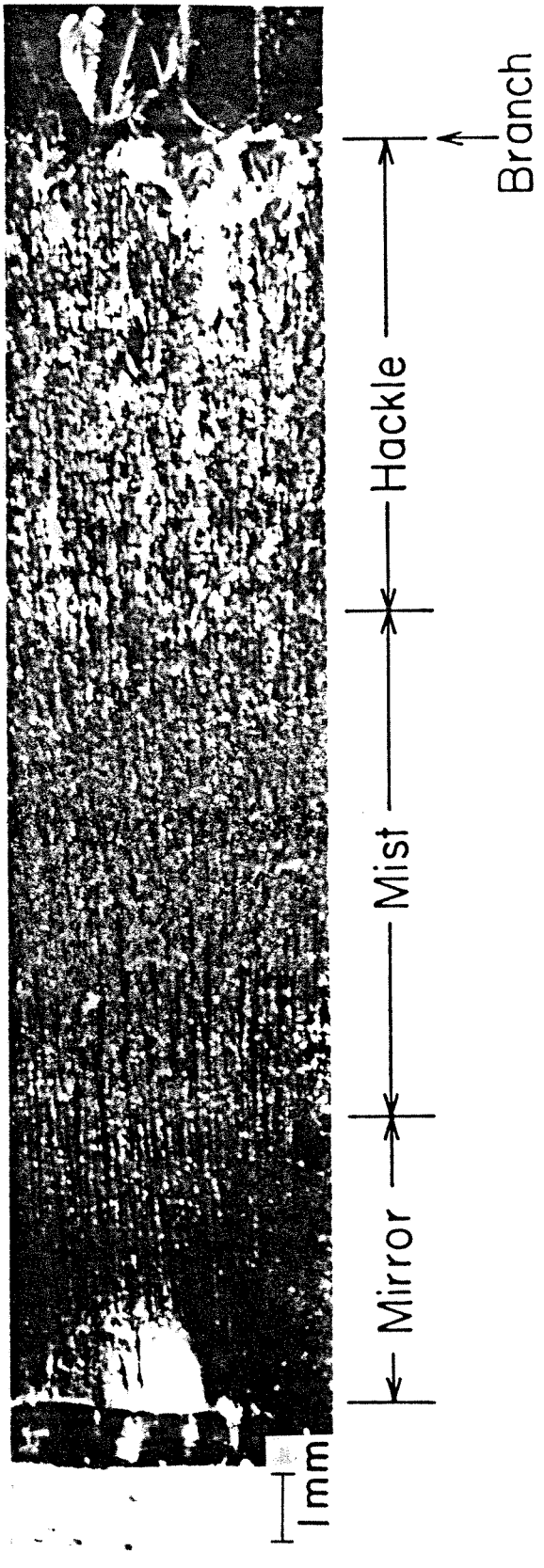

Figure 22. Appearance of the fracture surface.

semi-infinite crack in an infinite medium. The magnitude of the pressure load was varied in the four cases, but in all cases, the crack propagated with a constant velocity as indicated. The only parameter that changed as the crack propagated was the stress intensity factor (figure 24). In the first case (figure 23a) the crack propagates along the line of symmetry until waves reflected from the boundaries arrive. Since these waves did not contain the symmetry of the outgoing waves due to varying support conditions, the crack deviates from the straight line path along the path such that K_{II}=0. The fracture surface exhibits only the "mirror" pattern while the crack propagates at a constant velocity of v= 363 m/sec. Upon arrival of the waves reflected from the boundaries of the specimen, at around 150 μsec, the stress intensity factor increases as in figure 24 (curve a), and *the velocity remains constant*. Now the fracture surface turns more rough and has the "mist" appearance. In the second case (figure 23b), the pressure load on the crack was higher. The crack propagated at 410 m/sec and since the pressure load was higher, the stress intensity factor continued to increase after crack initiation (curve b). The fracture surface once again starts out mirror-like but quickly changes to mist and later to hackle. The boundary reflections arrive again at about 150 μsec and now induce crack branching. The third and fourth cases (figure 23c,d) are at progressively at higher load levels and branching of cracks occurs *prior* to the arrival of the reflected waves. The fracture surfaces in these two cases seem to exhibit the typical mirror, mist and hackle pattern although the "lengths" of these zones vary, becoming smaller as the load level increases. Since in all cases the crack tips travel at constant velocity, the apparent transitions of the surface markings are noted on the stress intensity factor history plot in figure 25. Note that these transitions are not discrete and hence they are shown as bands. Also, within the mist and hackle zone, the surface roughness is not constant, but increases with increasing stress

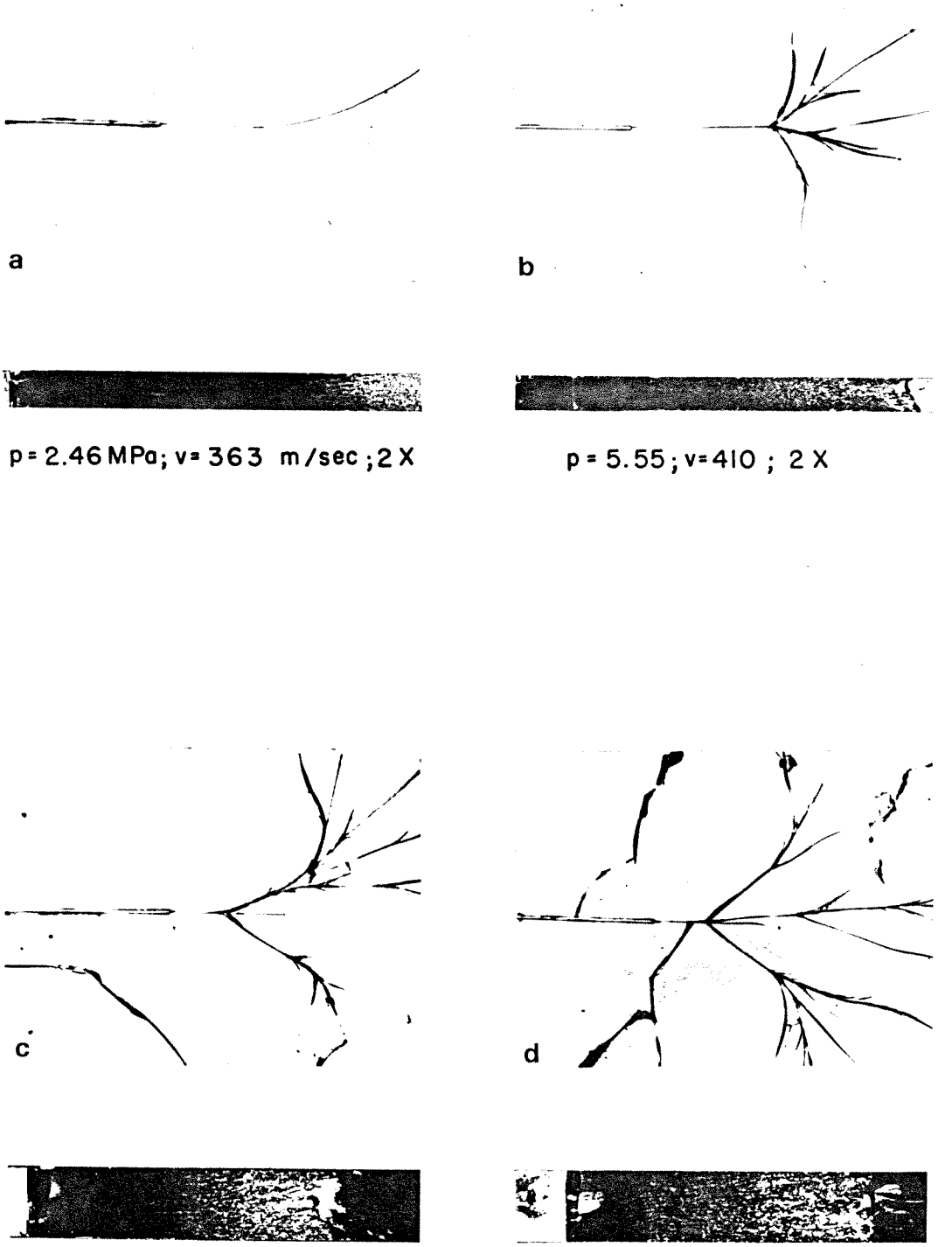

Figure 23. Assembled plates and the corresponding fracture surfaces from four experiments.

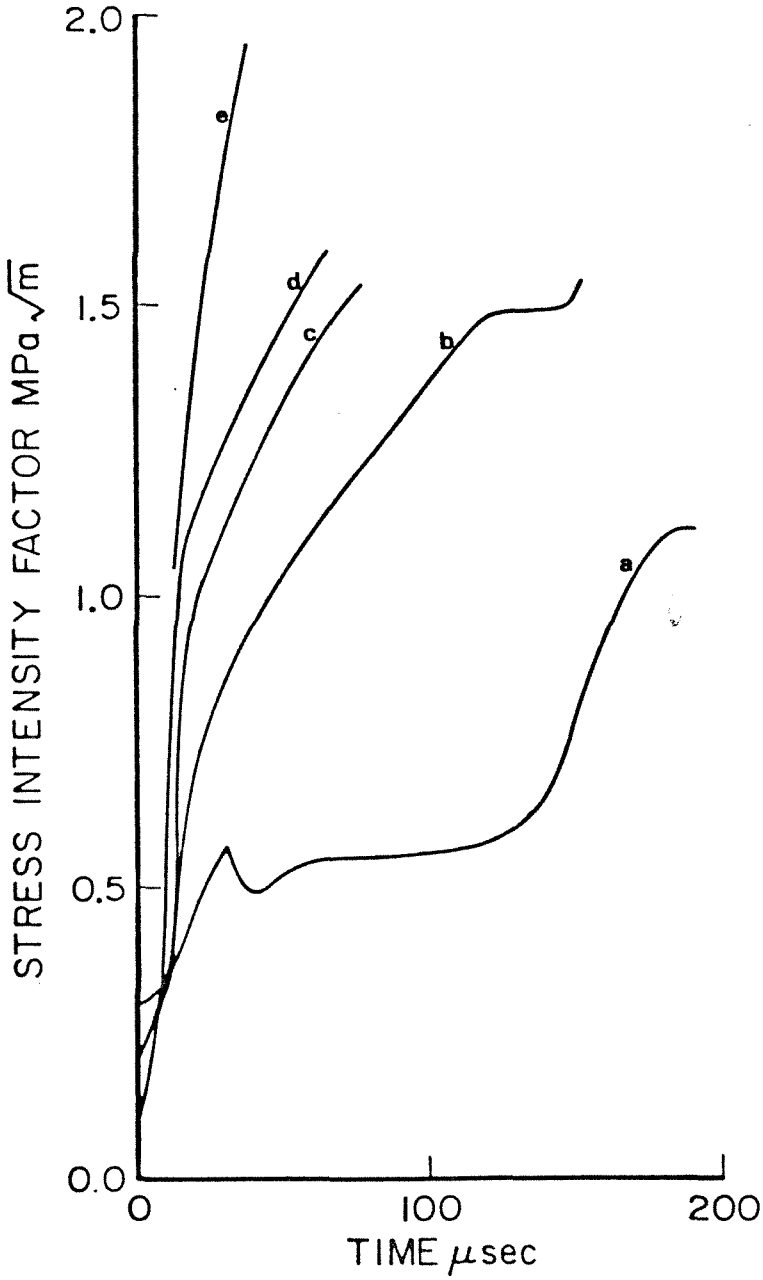

Figure 24. Stress intensity factor histories for the four cases in figure 23.

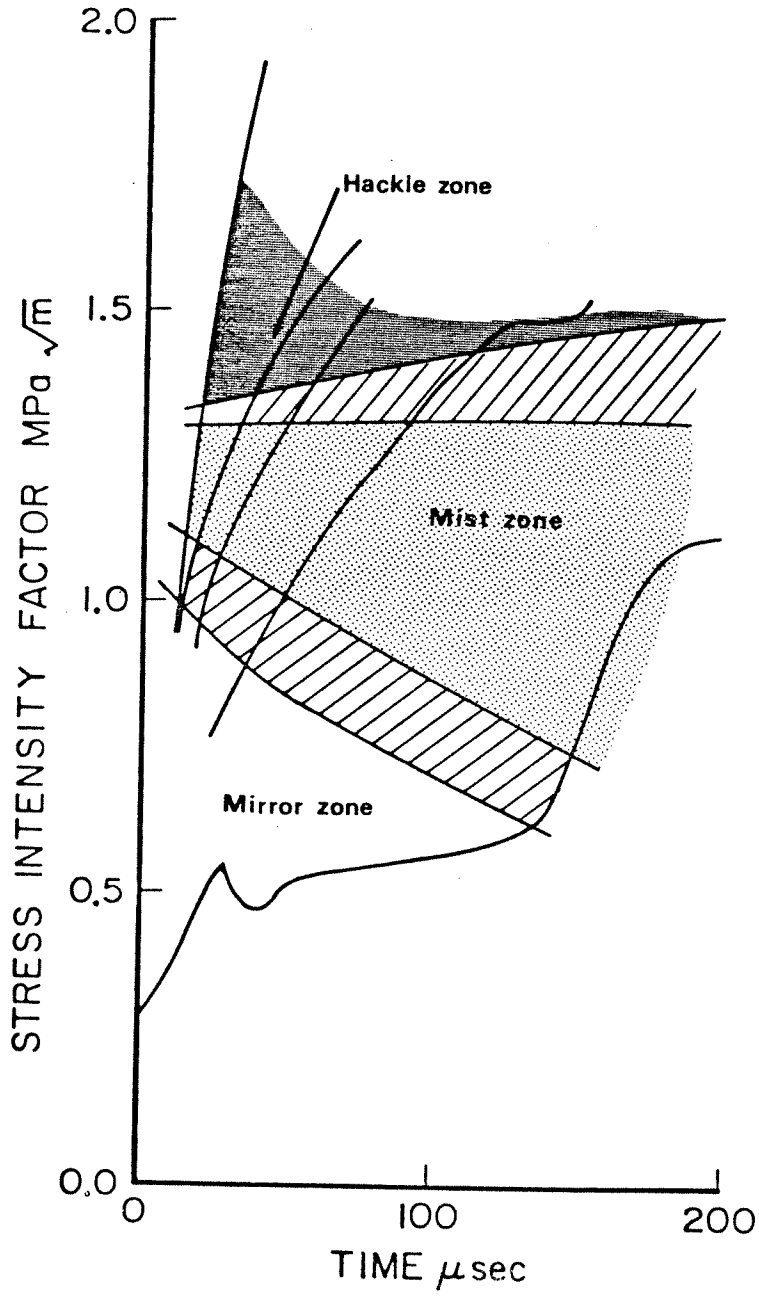

Figure 25. Surface roughness transitions marked on the stress intensity factor history plot.

intensity factor. We will return to this important point later.

From the above macroscopic examination of the fracture surface, the following conclusions can be drawn. At constant velocity, a propagating crack dissipates excess energy supplied to the crack tip by creating a rough surface. The exact mechanism by which this is done is not yet clearly revealed but becomes distinct under the microscopic examination to be discussed later. The actual surface area created by the fracture process is greater than that obtained by multiplying the crack length by the plate thickness. This fact should have implications in applying Griffith type energy blance equations to crack propagtion.

4.2 Microscopic Observations of the Fracture Surface

Although the fracture surfaces appear, to the naked eye, to be of the mirror, mist and hackle type, an examination of surface at high magnifications reveals surface discontinuities of small dimensions which provide further insight into the fracture process. Figure 26 shows an enlarged view of the fracture surface (of figure 23c). It is seen that the fracture surface roughness increases **continuously** along the crack path, with no apparent transitions in the surface marking. From the stress intensity factor history for this case, (shown in figure 24), and noting that the crack velocity is constant along the crack path the crack surface roughness may be interpreted as varying with the stress intensity factor. The mirror zone, which appears featureless under small magnifications (figure 22), exhibits lines running in the direction of crack propagation. These lines indicate that the crack propagated along different planes and the lines that are observed are really steps in the fracture plane. (The initial starter crack is introduced by a razor blade. This does not provide a smooth crack in one plane. Thus, the crack starts to run along different planes, but

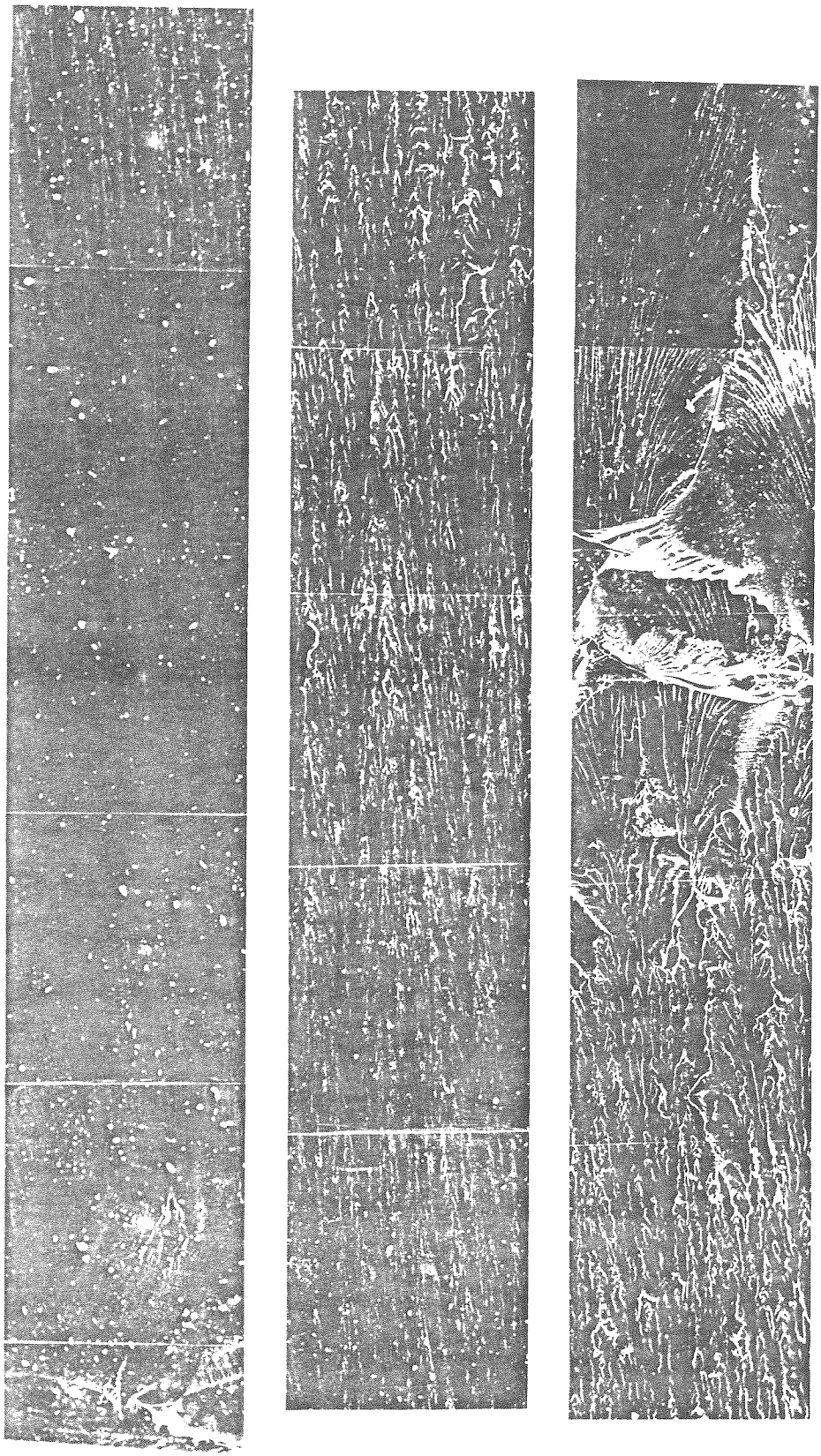

Figure 26. Fracture surface showing continuous change in roughness.

exhibits a definite tendency to merge into one crack plane in the mirror zone). Also, under high magnification, circular or nearly circular markings are seen in the mirror zone (figure 27) which represent interaction of the crack with voids. The interaction of the propagating crack with the voids can lead to crack propagation along different planes. This is illustrated in figure 28, where we see the line demarking the surface steps as running parallel to the crack propagation direction, but emanating from a void. This presents us with the first evidence that the microscopic details of the material may affect the crack propagation behaviour at least in the microscopic sense. Microscopic examination of the virgin material also reveals the presence of many flaws that are on the order of 10 to 25 μm in size as shown in figure 29. There is a surface and volume related distribution of these flaws in the material. Thus the main observations on the mirror zone are that there is a tendency to propagate along one plane and that the crack passes through many pre-existing voids, although some of the voids tend to alter the plane of propagation of the crack.

The mist zone exhibits some more interesting features. The stress intensity factors associated with this zone are higher than in the mirror zone. Therefore, the stresses ahead of the crack are high enough to "activate" isolated small flaws present in the specimen. When such growing flaws interact with the main crack front, conic markings are formed.[4] If the flaw and the crack grow with the same velocity, the resulting conic is a parabola. Many such parabolas are present in the mist zone (figure 30). These parabolas vary in size and depth, indicating that flaws of various sizes and at various depths below the average fracture surface were initiated into growing. Also, the crack begins to propagate along several planes and the interaction of these results in lines along the direction of crack propagation suggesting that flaws of various sizes were initiated

4. Feltner, C.E., *University of Illinois, T&AM Report No 224*, (1962).

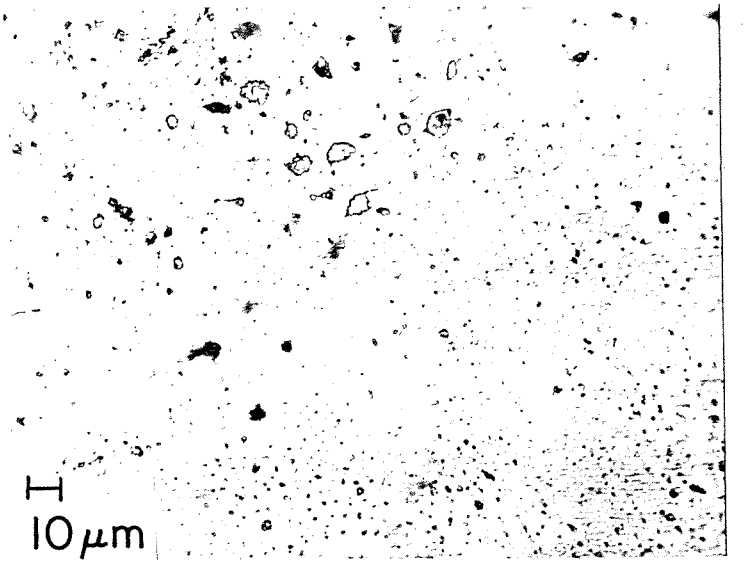

Figure 27. Magnified view of the 'mirror' zone showing the voids.

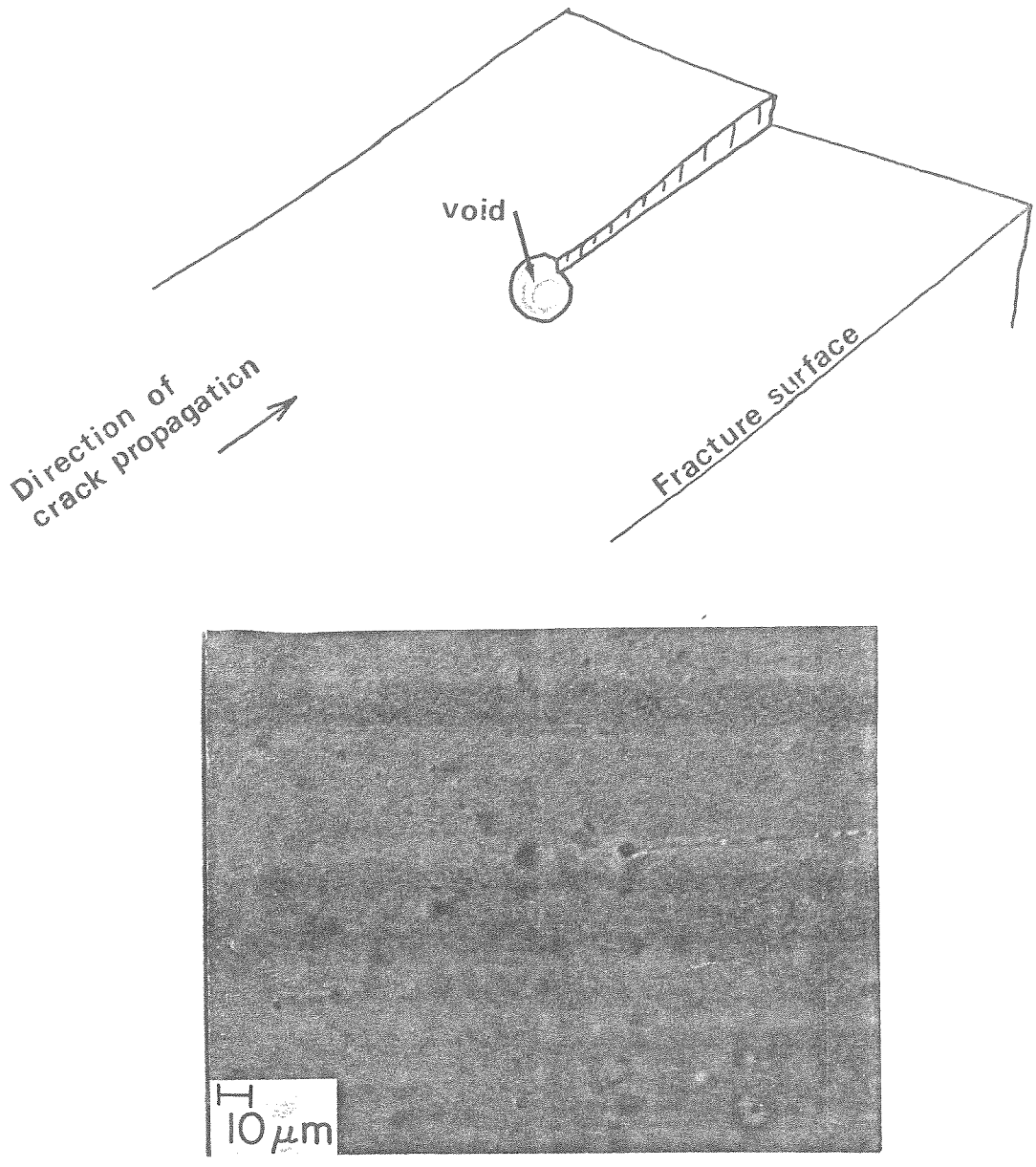

Figure 28. Effect of crack interaction with the voids.

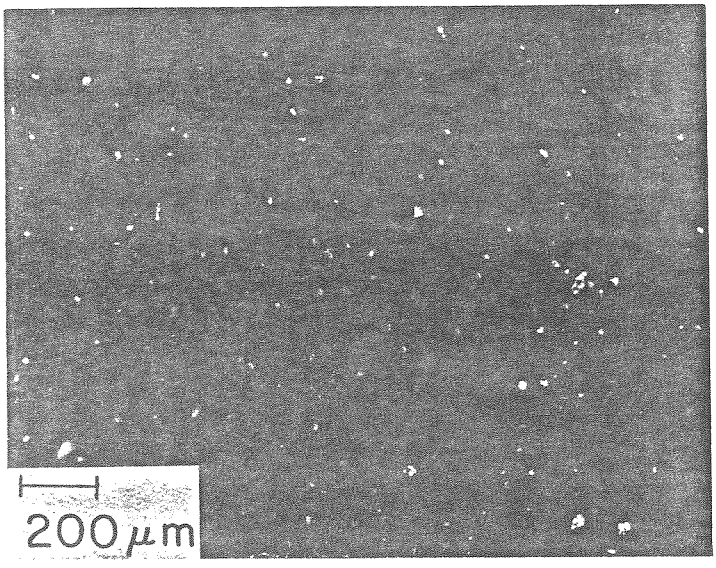

Figure 29. Microscopic view of the virgin material showing voids.

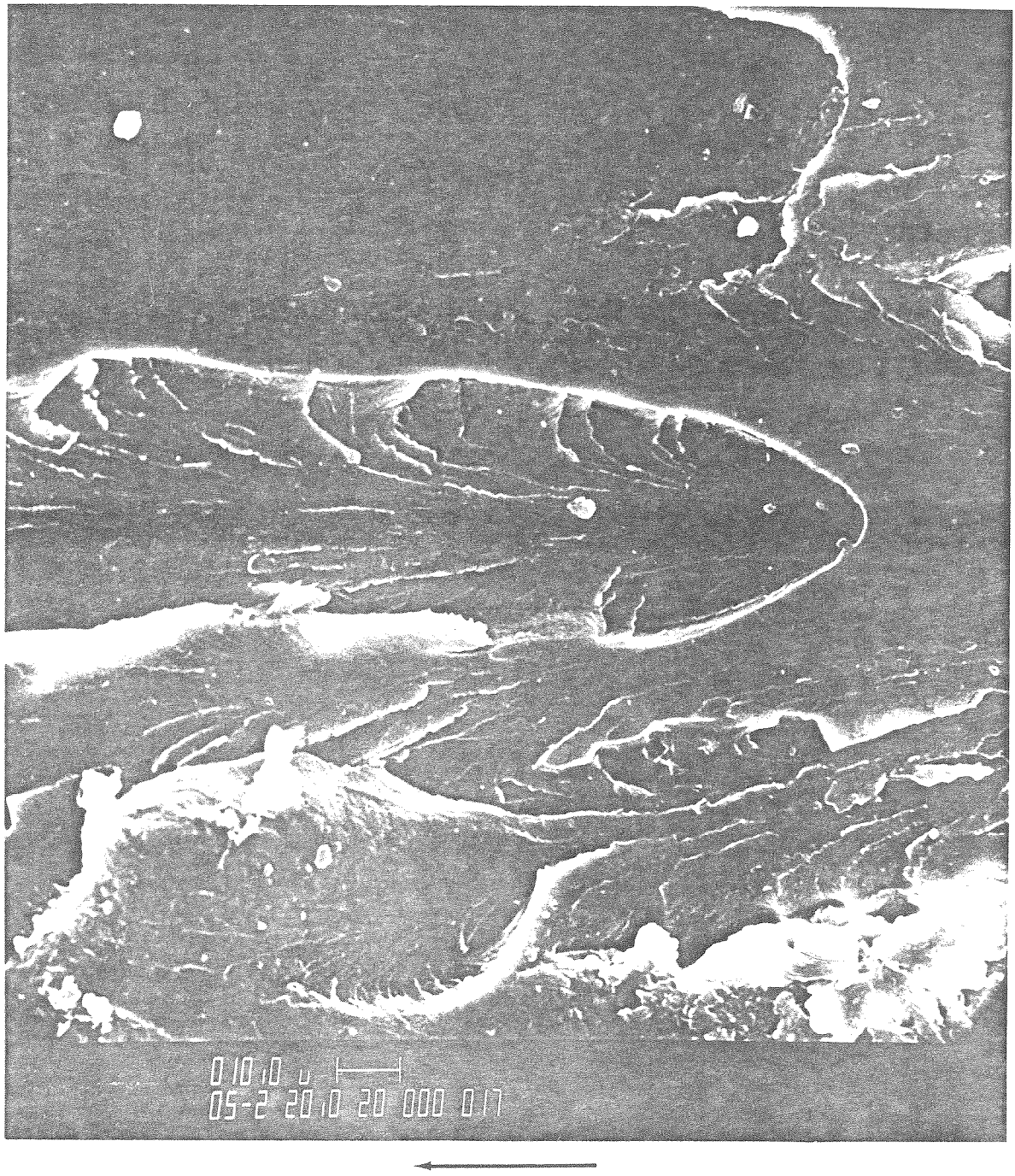

Figure 30. Magnified view of the 'mist' zone showing a parabolic marking.

into growing more or less simultaneously and also that voids away from the main crack plane started to grow *before* the arrival of the main crack front.

In the hackle zone it was found that parabolic markings similar to those in the mist zone exist, but these are deeper than those in the mist zone indicating that flaws farther away from the main crack plane are activated in this zone. The crack also propagates along different planes leading to lines along the direction of crack propagation. There exist also "river" markings (figure 31) nearly perpendicular to the direction of main crack propagation. These are markings that are caused by crack propagation perpendicular to the propagation direction of the main crack front. They are due to the interaction of secondary cracks or microcracks that are formed ahead of the main crack front and that interact with one another and link up in a direction perpendicular to the main crack propagation direction.

Let us summarize the observations on the microscopic nature of the fracture surface: The crack starts to grow along many planes due to initial imperfections in the starter crack, but has a definite tendency to merge into one plane in the "mirror zone." The voids that are naturally present in the material are not activated into growing individually, but some of the voids do influence the propagation of the crack in that they may alter the plane of propagation of the crack. At higher stress intensities, in the "mist zone," the flaws are activated into growing and the crack propagates along different planes and voids grow before the arrival of the main crack front. The size of the fracture process zone, i.e. the zone in which the small flaws are activated, increases. In the "hackle zone" all of the mist zone features exist, only more pronounced. There is also evidence of crack growth perpendicular to the main crack growth direction. The fracture process zone is much larger.

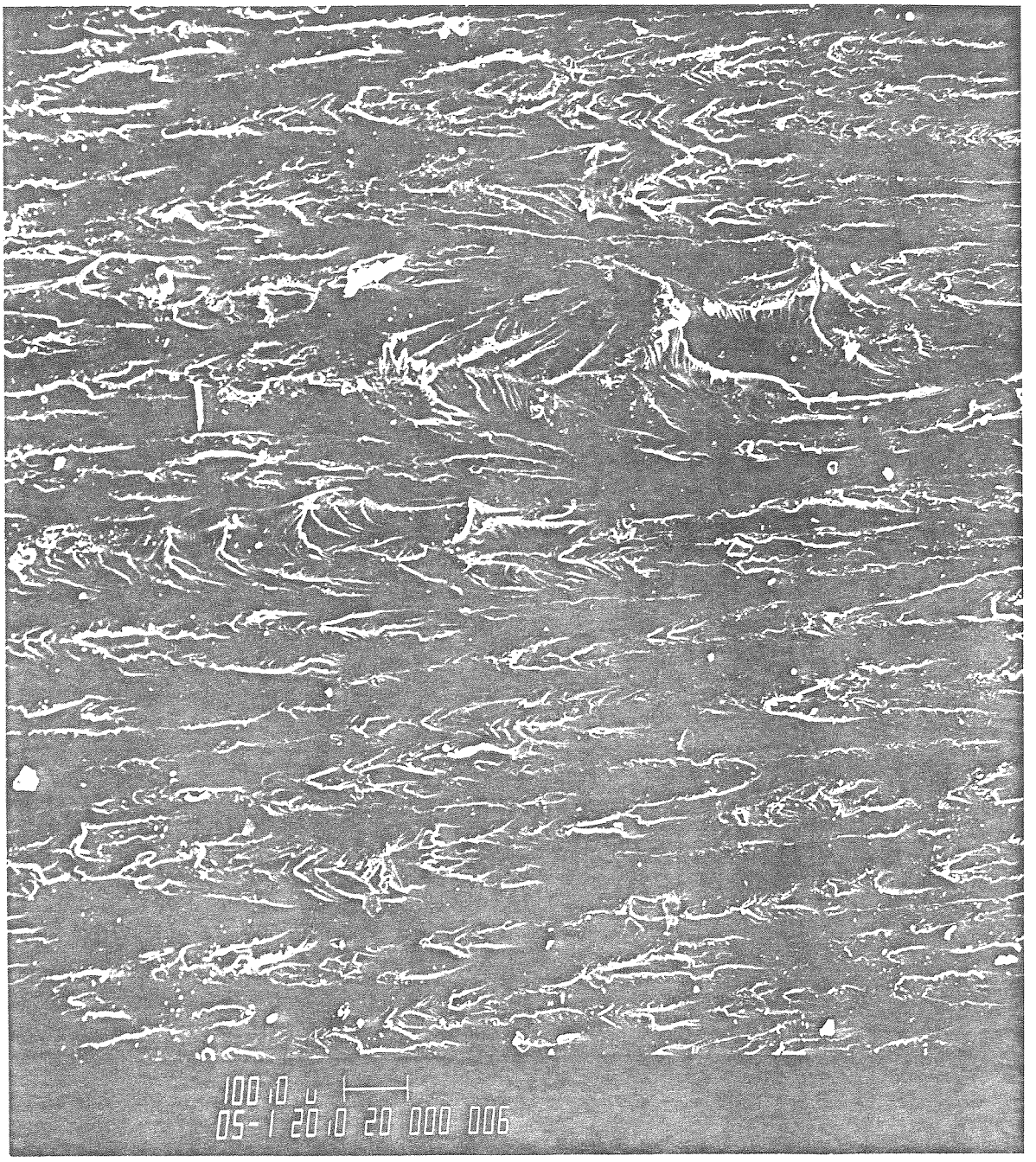

Figure 31. Magnified view of the 'hackle' zone showing 'river' markings.

So far the examination of the fracture surface has been of a qualitative nature. A quantitative estimate of the fracture process zone can be obtained by using a light section microscope and determining the maximum depth of the fracture surface markings at each location along the crack path. The variation of the depth of the fracture surface along the crack path as obtained from the light section microscope is shown in figure 32. The thickness of the fracture process zone increases with distance along the crack path and since the stress intensity factor increases monotonically along the crack path, this may be interpreted as the variation of the fracture process zone with the stress intensity factor. This fact leads to a reinforcement of a statement made earlier, namely, that the actual energy dissipation during the crack propagation process is larger than that calculated for simple models.

4.3 Real Time Observations of the Dynamic Fracture Process

So far the observations on the microstructural aspects of dynamic fracture have been based on post mortem examination of the fracture surface markings which provide some information about the nature of the fracture process. However, the time history of the evolution of the fracture surface is not revealed directly. In order to accomplish this time resolution, we have to resort to high speed motion pictures of the fracture process in real time, but the experimental difficulties involved in such a task are enormous. First, it is impossible to obtain a "head-on" look at the newly created fracture surface in real time. Even looking at the back side of the fracture surfaces, that is through the material, poses problems since the light rays have to travel through a long optical waveguide and the distortions involved make it very difficult to obtain photographs. It is possible, however, to view the crack at an angle, under backlight conditions, although some details of the fracture surface are lost and only the crack front can be seen. Secondly, since the fracture process is viewed under

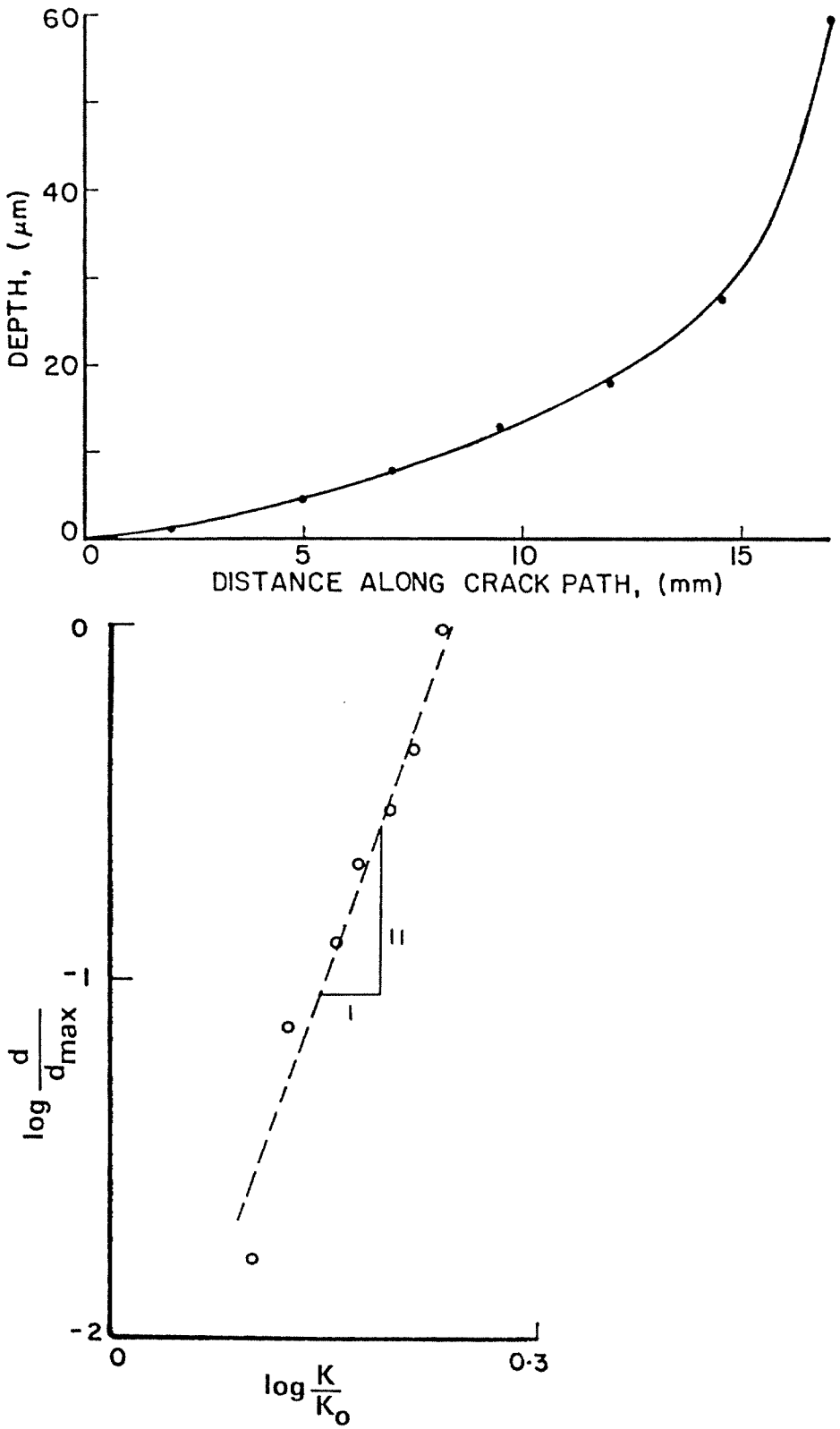

Figure 32. Variation of the depth of the fracture process zone.

high magnifications, the crack passes through the field of view (8 mm) in a time on the order of a couple of tens of microseconds, and with our high speed camera at most two frames may be obtained. Thus many repetitions of the fracture tests are necessary in order to be able to follow the evolution of the crack front.

The optical arrangement for the high speed photomicrography of the crack front is illustrated in figure 33. Since the specimen is at an angle to the optical path, only a projection of the crack front is recorded on film, but this does not pose any problem regarding interpretation of the photographs. Figure 34 shows typical frames from three different specimens under identical loading conditions, but the center of the viewing was located in the mirror, mist and hackle zones, respectively. In the mirror zone, from figure 34a, one notes that the crack front in the middle of the specimen leads the crack front at the plate ends by about 0.5 mm and that there is a smooth variation in the crack front between the middle and faces of the plate. At the faces of the plate the crack front forms caustics and this leads to the crack front appearing to be larger than the plate width. Figure 34b shows the crack front in the mist zone and it appears distinctly different from that in the mirror zone. Again caustics are formed at the faces of the plate, and these are larger because of the hogher stress intensity factors associated with the mist zone. The most striking difference is that the "crack front" is nearly straight but exhibits a number of small caustics. This indicates that there is no longer a single crack front, but an *ensemble of cracks* propagating along the apparent crack front and generating multiple caustics. The next frame (figure 34c) shows the appearance of the "crack front" in the hackle zone which seems to be similar to that in the mist zone but represents the coarser structure of the fracture surface in the process of forming. This might have been expected in view of the fact that the post mortem examinations of the mist and hackle surfaces exhibited similarities.

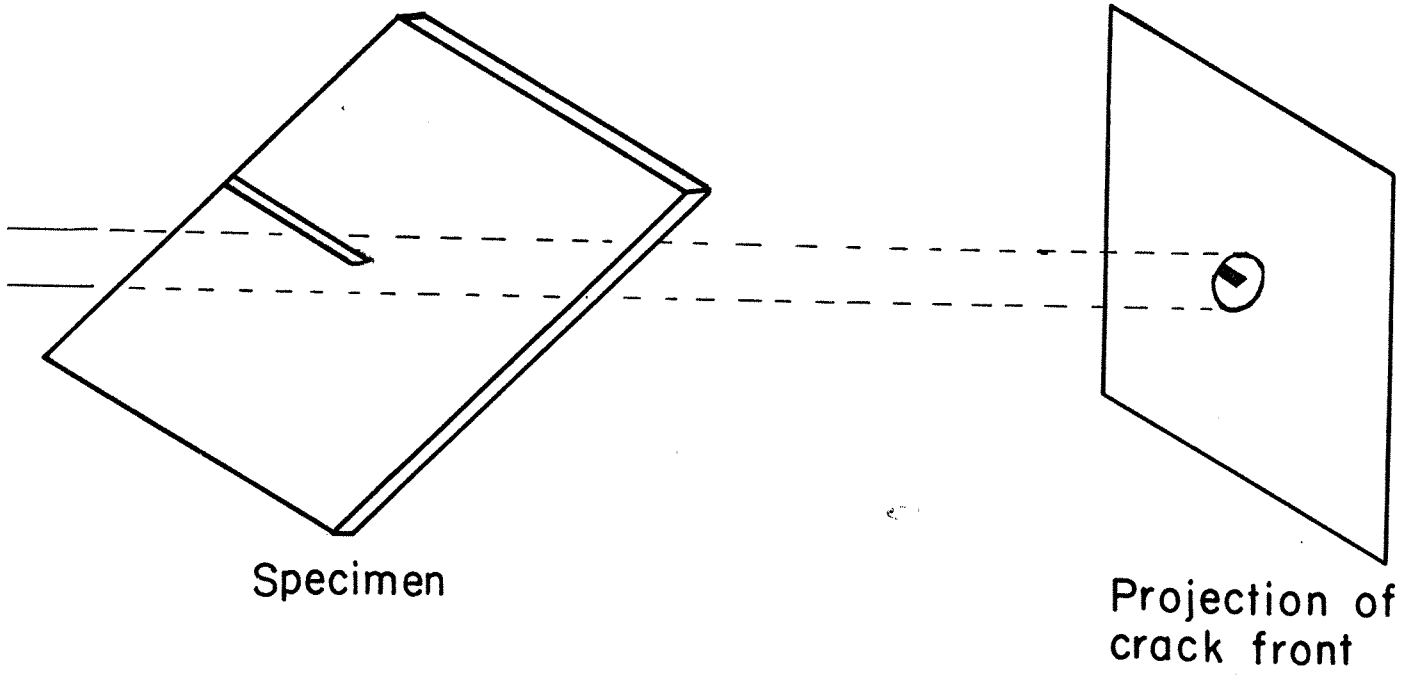

Figure 33. Optical arrangement for high speed photomicrography of the crack front.

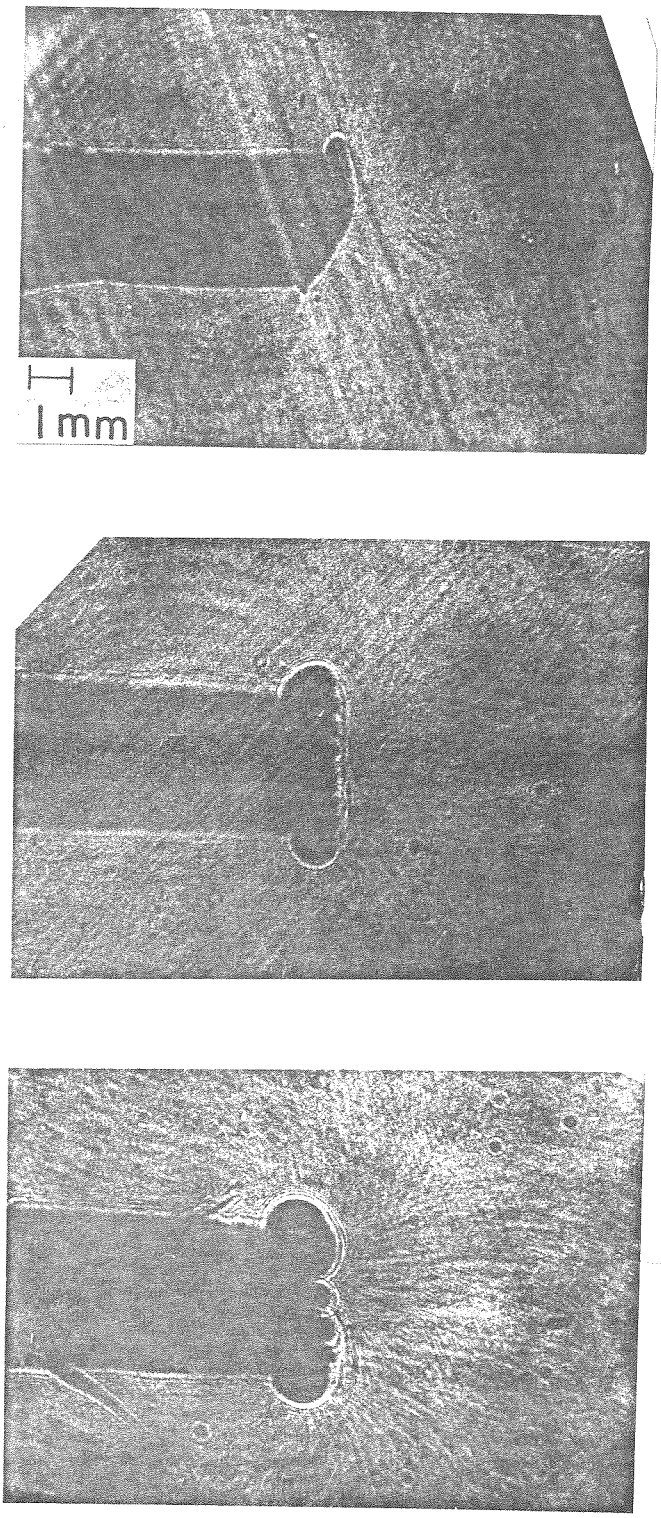

Figure 34. High speed photomicrograph of the crack front in the mirror, mist and hackle zones.

However, the caustics are larger than in the mist zone, again indicating higher loading and along the crack front fewer but larger caustics are observed. Photomicrographs of the crack front after branching, also exhibits *ensemble crack propagation* (cf. figure 35).

From the above examination of the fracture process we conclude that initially in the mirror zone a single crack propagates with a curved front, similar to what is observed in quasi-static crack propagation. In the mist zone several small cracks propagate simultaneously and the ensemble crack front is nearly straight. Further crack propagation is really governed by the details of the interaction between the microcracks. In the hackle zone many of the small cracks coalesce and form larger cracks, but crack propagation is still in terms of many cracks propagating along a straight front. Based on this microscopic investigation of the crack propagation process,

It appears that the propagation of cracks under a high stress intensity factor in a material containing voids and other defects is essentially governed by the growth of these voids into microcracks their coalescence and further by the interaction of these microcracks.

One of the main goals in this study is the investigation of the problem of crack branching from a microscopic view point; while we have looked, so far, into the fracture process in detail, we have not yet at this stage examined the branching process microscopically. An obvious question about the branching phenomenon, from the microscopic point of view, is whether the branching process is continuous or discontinuous: in examining the broken plates, as shown in figure 36, one is struck by the number of attempted branches that are left arrested, while a few of the branches develop into full fledged successful ones. The attempted branches are almost always *part-through* cracks appearing either at the faces of the plate or *totally interior* to the plate. Furthermore,

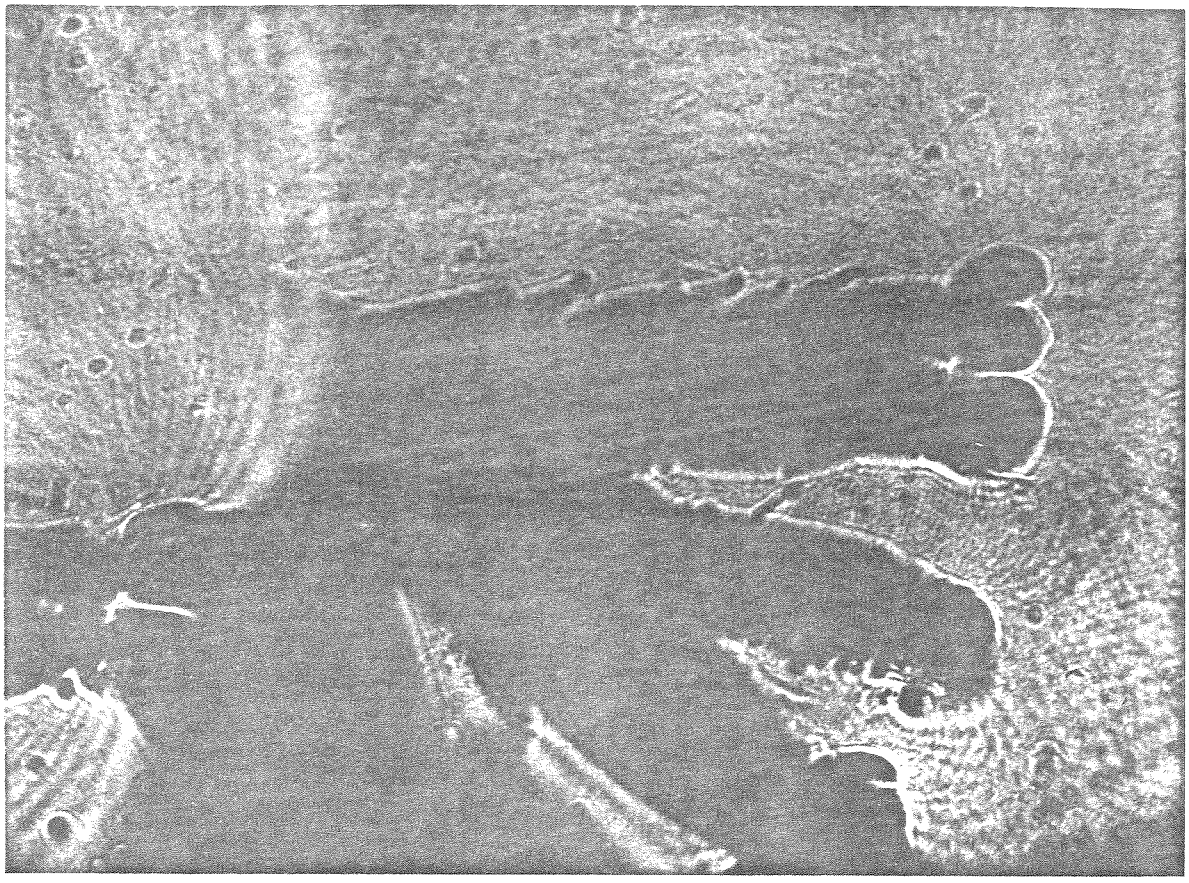

Figure 35. High speed photomicrograph of the crack front after branching.

Figure 36. Magnified view of a crack branch showing a number of attempted branches.

they seem to issue out from the main crack plane in a continuous way and not at an abrupt or definite angle. With the high speed photomicrography system described earlier, it is be possible to examine the evolution of the crack branches thus providing us an idea of the mechanism involved in the crack branching process. Since the loading device is extremely repeatable, it is possible to obtain repeat tests at the same load level and know with a reasonable certainty the location of the branch point. Accordingly, the camera was focussed onto this anticipated branching location and photomicrographs were taken. Figure 37 shows the high speed micrographs of the evolution of the crack branching process. Here, four frames at 5 μsec intervals are shown capturing the evolution of crack branching. Clearly, the branching process is not a simple splitting of a mathematically sharp plane crack into two sharp plane cracks! Rather, one observes a number of cracks that attempt to propagate simultaneously. Figure 38 shows a frame from another high speed photomicrogaph of the branching process, at a higher magnification. The attempted branches clearly issue out of the main crack propagation plane and continue to turn away from the main direction of crack growth smoothly without any abrupt change in the direction of propagation. The high speed photomicrographs of crack branching phenomenon then indicates that the *branching process evolves continuously from crack propagation along a straight line, governed by the microcracks.* This interpretation is consistent with the earlier observation that the pre-branch propagation of cracks is governed by the growth and interaction of small microcracks. A complete discussion of the branching mechanism is presented in section 5.2.

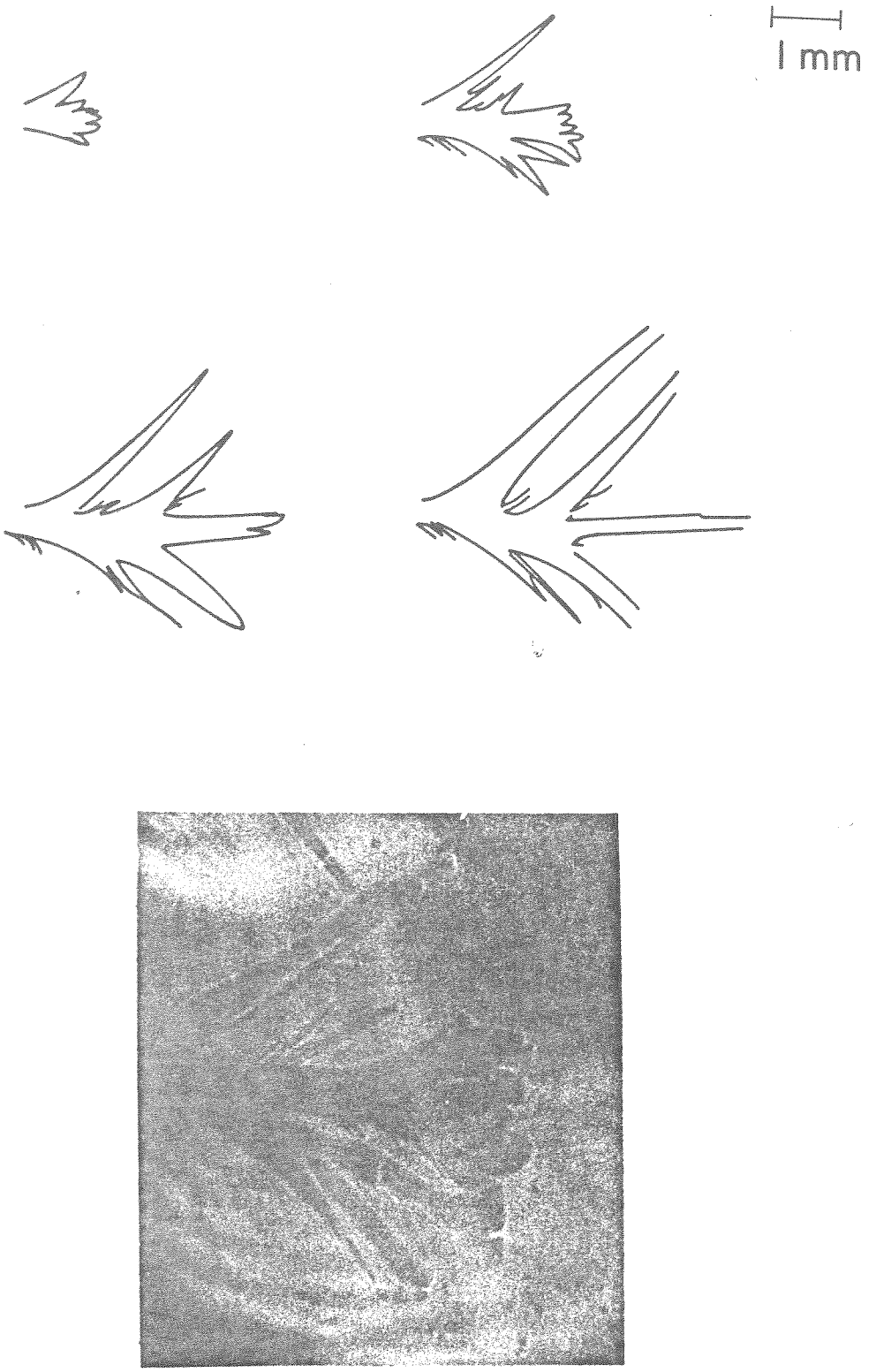

Figure 37. Photomicrograph of the evolution of a crack branch.

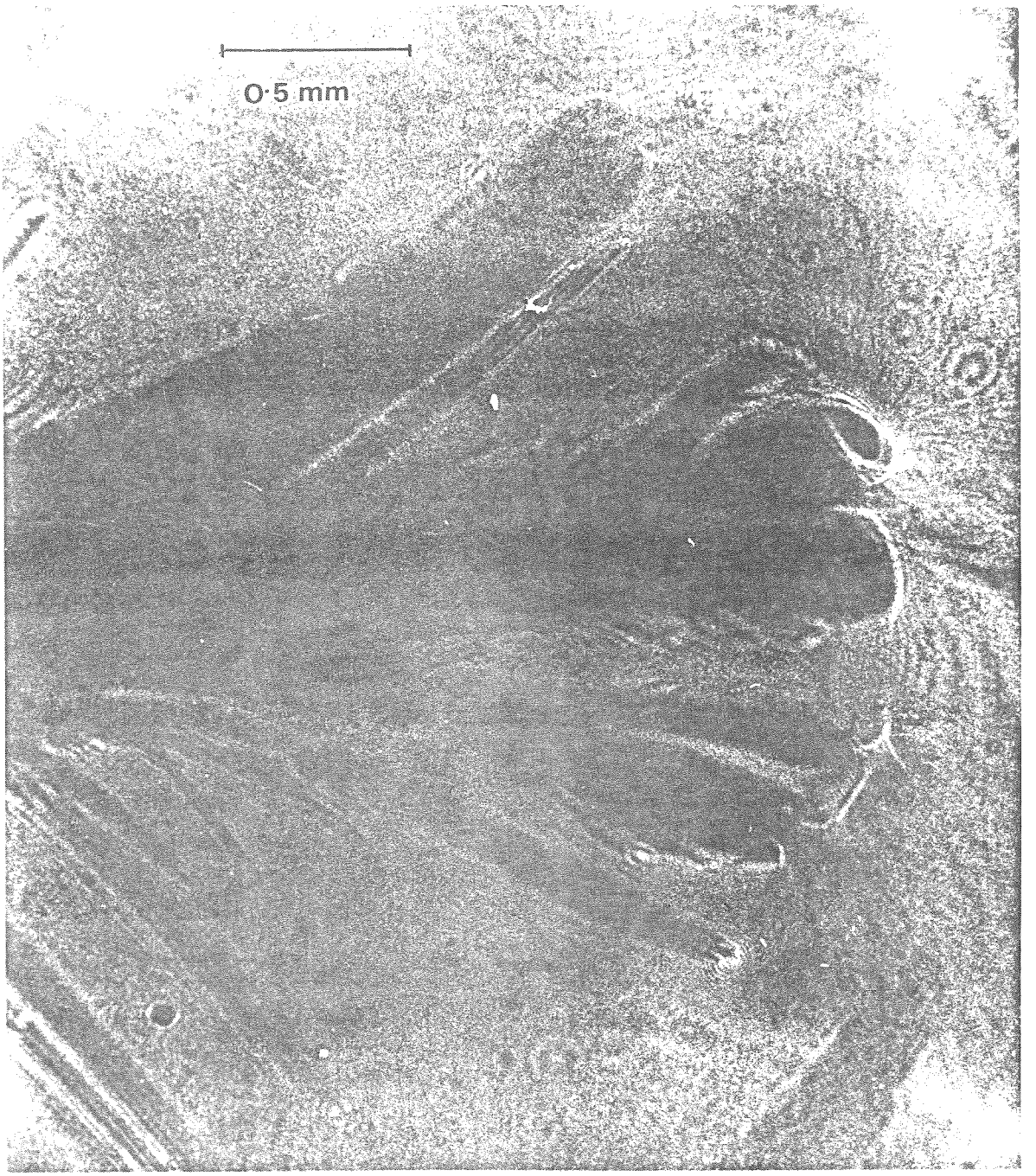

Figure 38. Magnified view of crack branching showing continuous evolution of the branch.

5. CRACK PROPAGATION AND BRANCHING

The main problems regarding crack propagation and branching have already been described in Chapter 1. The ideas and observations of the previous chapter on the microstructural aspects of dynamic crack propagation will form the basis for our tentative explanation of the observed crack propagation behaviour. We note that theoretically predicted limiting velocity of the Rayleigh surface wave velocity is not attained, the experimentally observed maximum velocities being considerably smaller. Moreover, the phenomenon of crack branching has not been explained satisfactorily. Based on our observations on the microscopic nature of the dynamic fracture process a new unified view of the dynamic crack propagation process is proposed here that would at least qualitatively (at this stage) explain the observed crack propagation behaviour, including the lower limiting velocities as well as the phenomenon of crack branching. A quantitative evaluation of this model is beyond the scope of this work and is therefore not attempted. In the following, the crack propagation aspect is examined first and branching is explained next.

5.1 Crack Propagation

In obtaining data for the rate dependence of the critical stress intensity factor for crack initiation, a number of experiments were performed on large Homalite-100 sheets and additional results from these same experiments will now be examined to analyse the propagation behaviour. The rate of loading in each case was progressively higher, resulting in the crack being loaded to various stress intensity histories. As a result, the crack propagated at various velocities in each case and provided a wealth of data on the crack propagation aspects. The stress intensity factor and the crack extension histories were determined from high speed cinematographs such as the one shown in figure 39;

they are plotted in figures 40, 41 and 42. There are two important aspects of dynamic crack propagation that are revealed by the these results and will be discussed in separate sections.

5.1.1 Constant Velocity Crack Propagation A surprising result of these investigations is that (*cf.* figures 40, 41 and 42) *the crack velocity remains constant, independently of whether the stress intensity factor decreases, remains constant or increases. Moreover, the velocity with which the crack propagates seems to be determined by the stress intensity factor at initiation.* If these data are then plotted, as is customary in dynamic fracture mechanics, on a plot of "stress intensity factor versus instantaneous crack velocity," the record shown in figure 43 is obtained. Also shown on this plot is the stress intensity factor-velocity plot as suggested by Dally.[1] who performed dynamic fracture experiments on Homalite-100 specimen using various geometrical configurations; Dally's results suggest a unique relationship between the instantaneous stress intensity factor and the crack velocity. In contrast, the present experimental data reveal a definite lack of a one-to-one relation between the instantaneous stress intensity factor and the crack velocity. It is clearly seen that the crack travels at a constant velocity while the stress intensity factor varies. Thus it appears that a different interpretation of the dynamic fracture process is necessary to explain the crack propagation behaviour.

The microscopic view of the crack propagation process outlined in Chapter 4 provides a new way of interpreting the crack propagation problem and explains at least qualitatively some of the salient features of crack propagation. As discussed in the previous chapter, the microscopic nature of the crack propagation process obeys the following scenario: when the stress intensity factor at the crack tip reaches a sufficiently high value, the propagation process is

1. Dally, J.W., *Experimental Mechanics*, **19**,(1979),p.349.

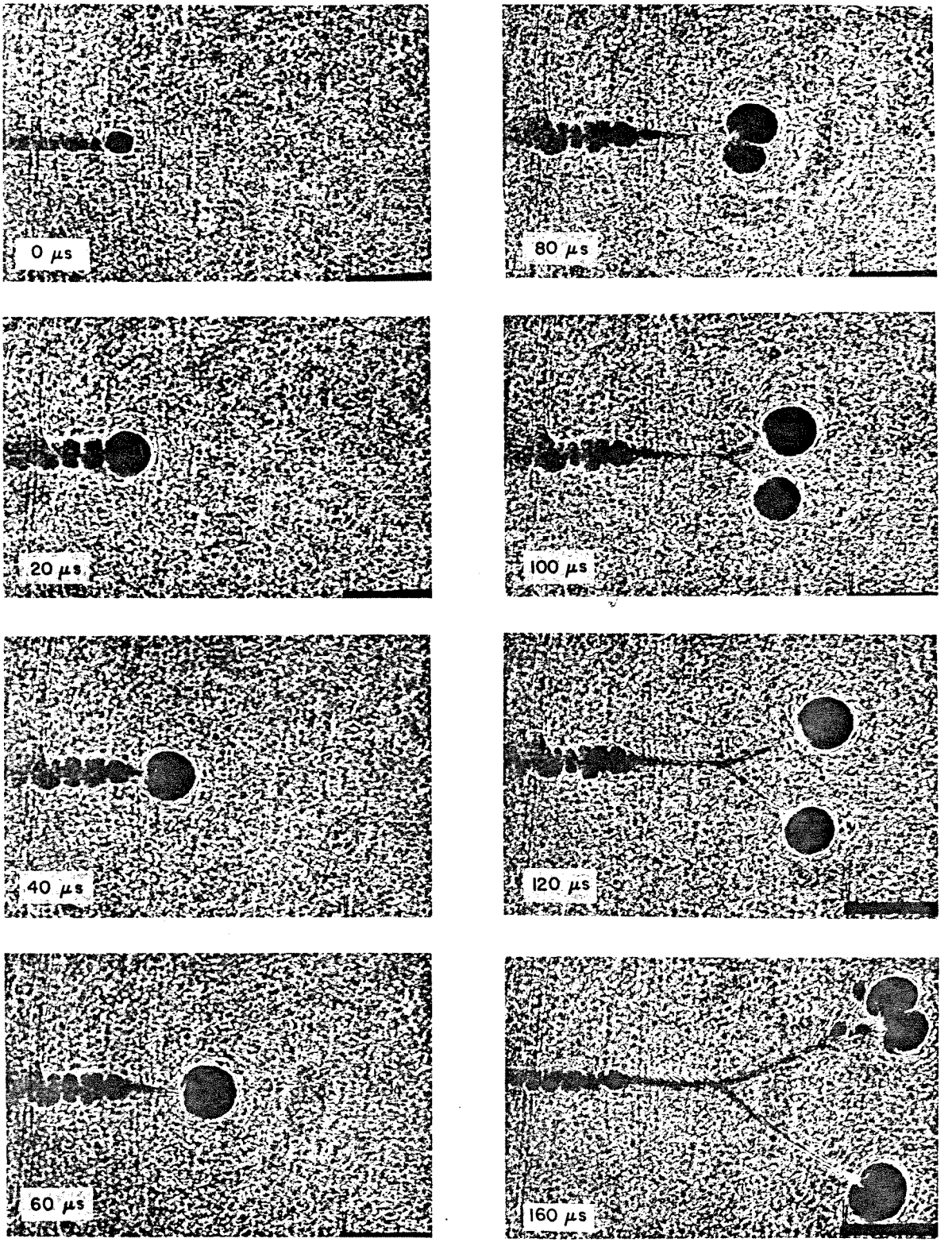

Figure 39. High speed cinematographs from a typical experiment.

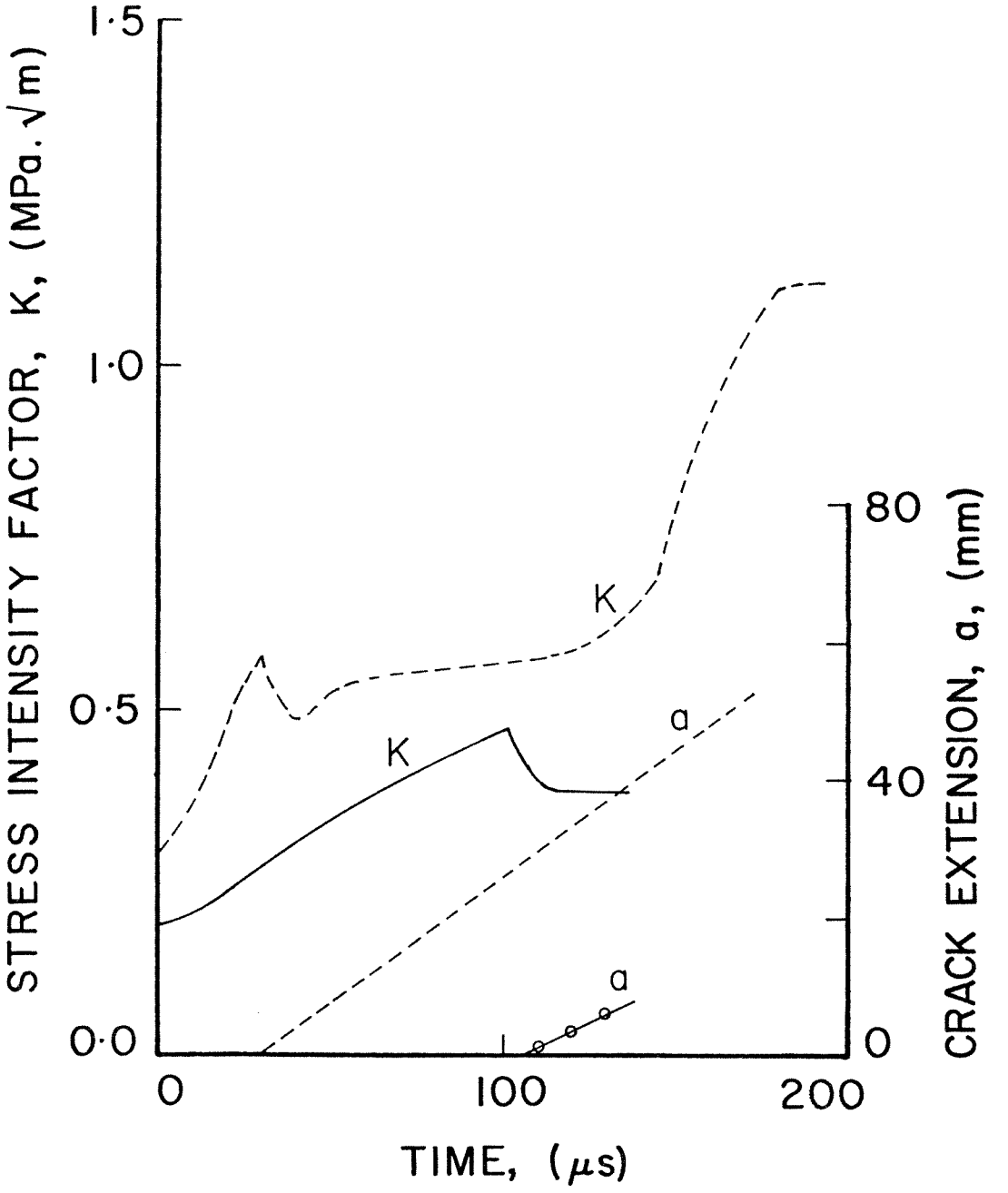

Figure 40. Stress intensity factor and crack extension histories.

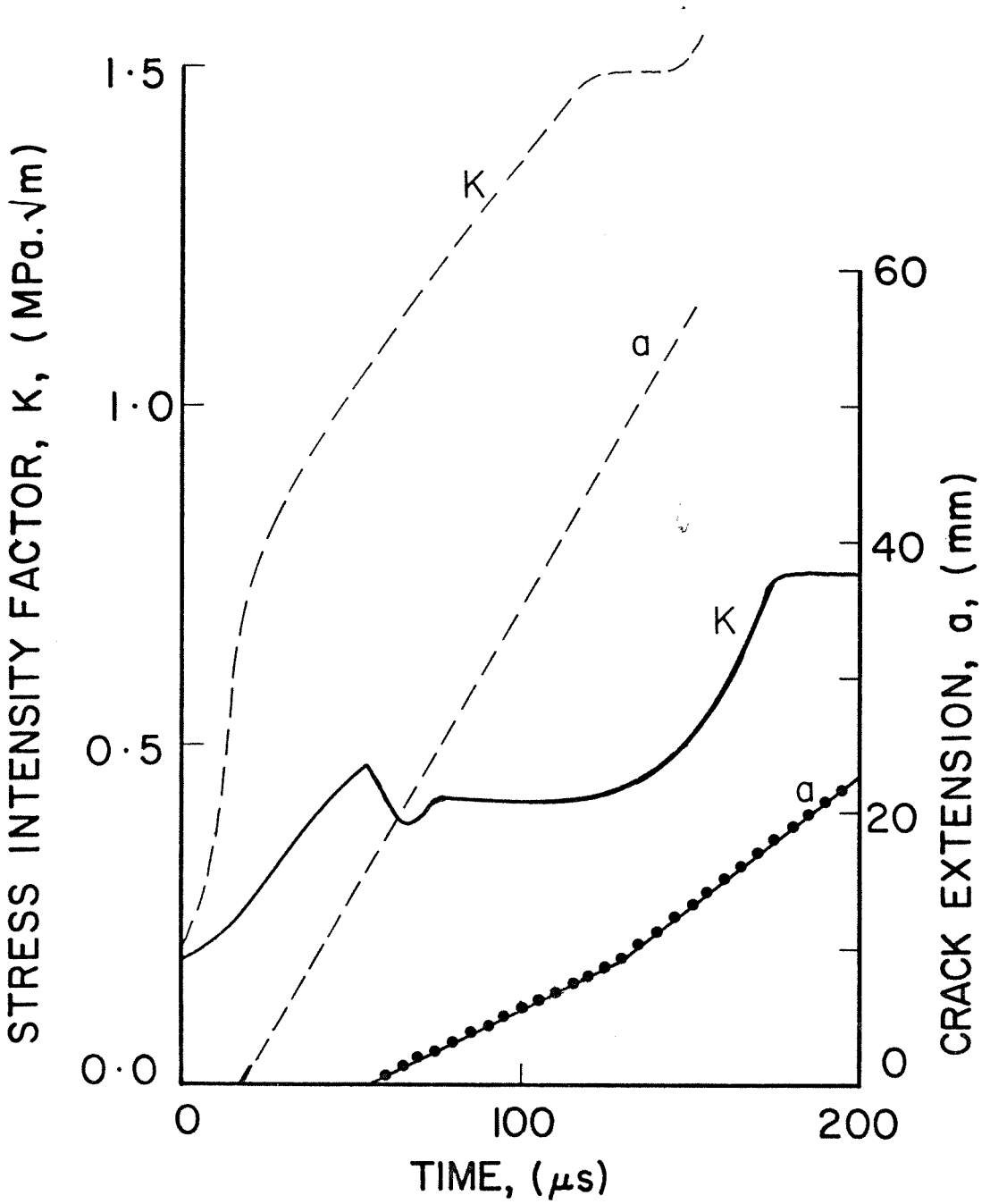

Figure 41. Stress intensity factor and crack extension histories.

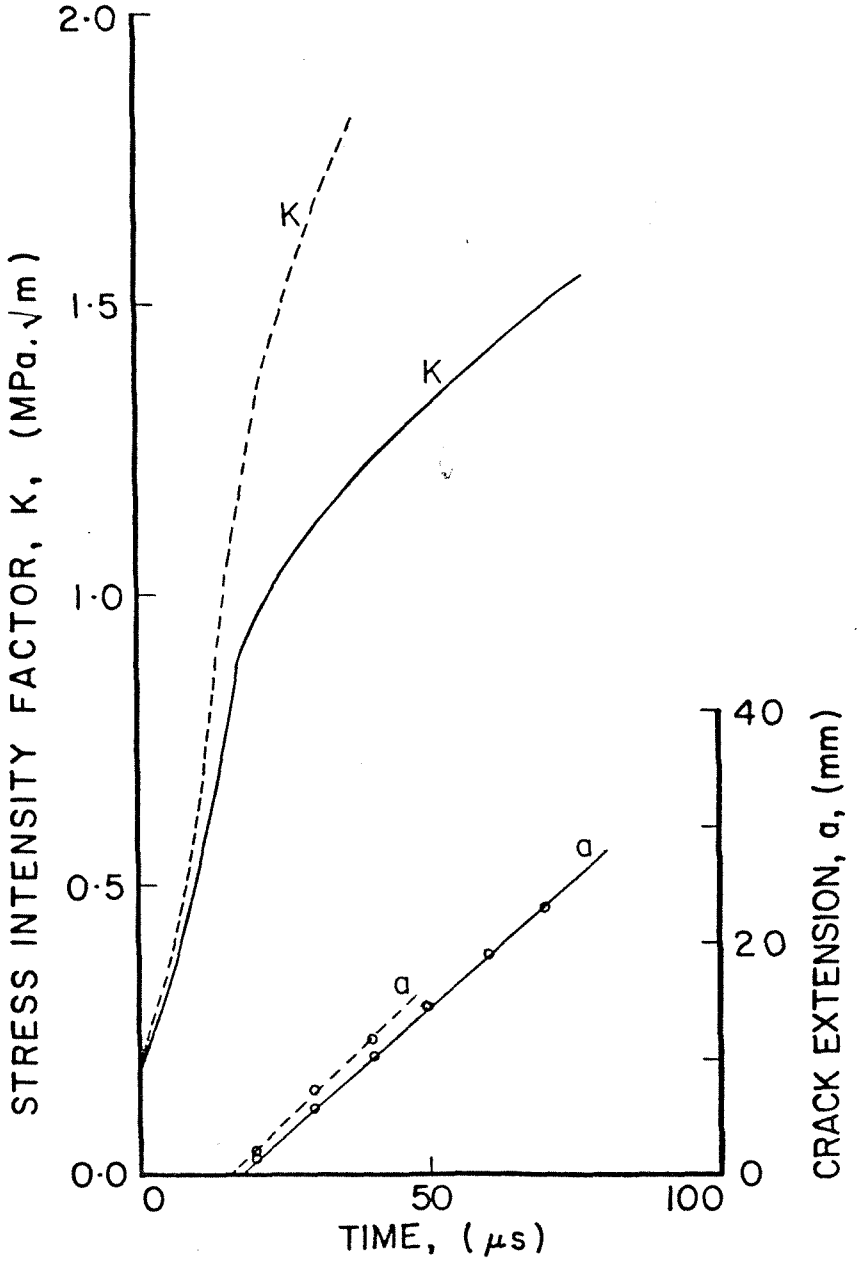

Figure 42. Stress intensity factor and crack extension histories.

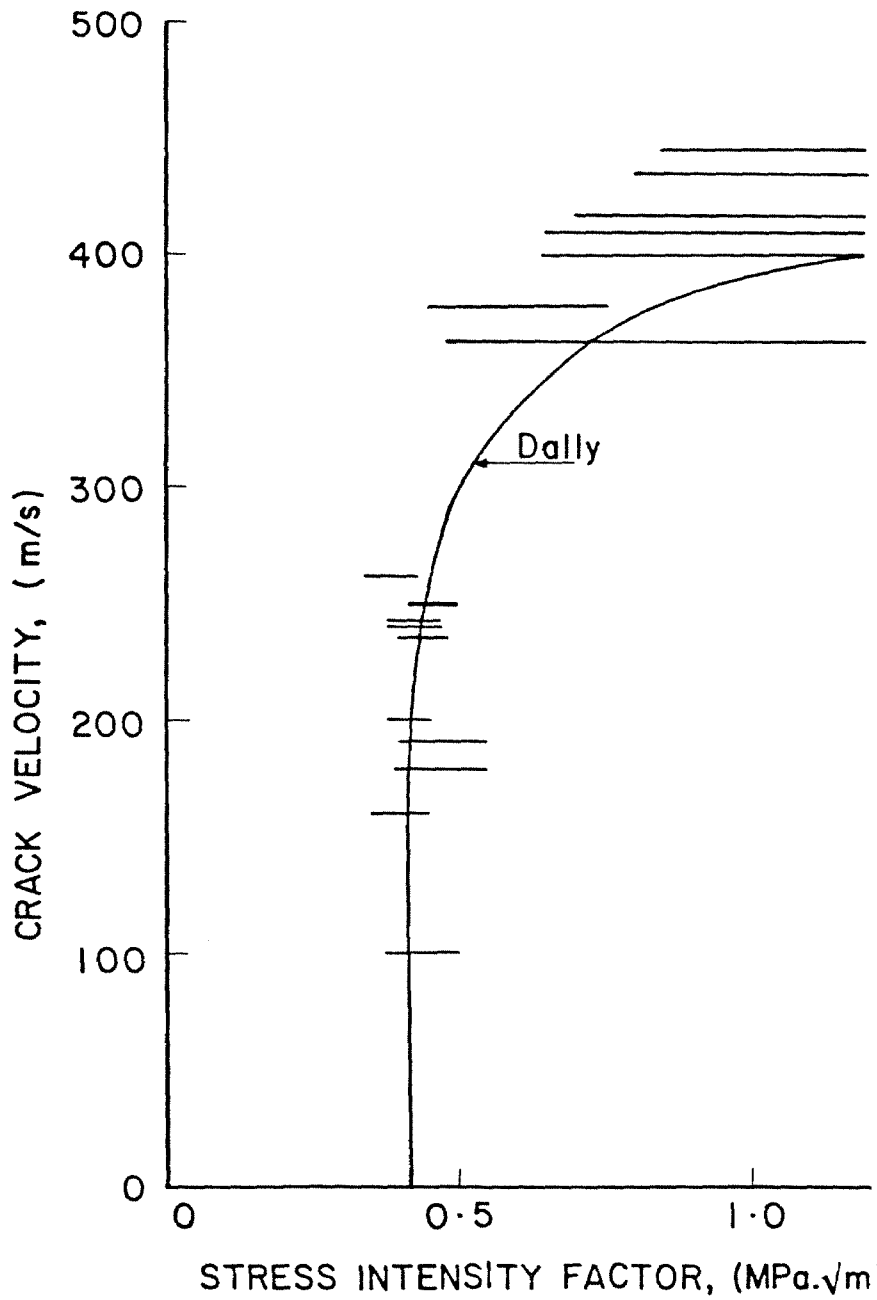

Figure 43. Relationship between the instantaneous stress intensity factor and crack velocity.

initiated. During the initial stages of this process, the stress level at the crack tip is rather low and the resulting damage zone or the fracture process zone is correspondingly small as is the attendant energy expenditure. If the fracture process continues into a decreasing stress field, the fracture process zone remains small and the energy required to create new surfaces also remains small. Finally, if the stress intensity factor drops to a sufficiently low value, the crack arrests. If the fracture process occurs under a condition where the stress intensity factor does not drop below the arrest value, then the crack continues to grow, the energy expended in creating the new surface being replenished by the energy release at the crack tip. In both cases, the size of the fracture process zone is small and the post-mortem examination of the fracture surface reveals a mirror-like appearance.

A more interesting situation arises when the fracture process occurs into an increasing stress field. In this event, the fracture process zone is initially small as in the previous cases, but as the stress intensity factor increases, the size of the fracture process zone increases rapidly in accordance with figure 32, although the velocity remains constant. This indicates that the energy required to create the new surfaces through the fracture zone also increases. Under this increasing stress level and increasing size of the fracture process zone, the crack eventually branches and we will deal with this aspect a little later. The important conclusions of this view of the fracture process are:

1. The crack propagation occurs by linking up many microcracks.

2. The number of microcracks that are activated into growing is a function of the stress intensity factor, the size of the fracture process zone, the distribution of voids in the material itself and probably the velocity of crack growth.

3. The size of the fracture process zone increases as the stress intensity factor increases (*cf.* figure 32).

4. As the fracture process zone grows in size, statistically, the number of potential microcracks contributing to the fracture process zone increases and thus the probability of initiating flaws into growth increases, thereby increasing the energy that is dissipated in the fracture process zone.

5. As the number of initiated microcracks increases, the interaction of these microcracks becomes important. An exact calculation of the nature of the interaction is very complicated and beyond the scope of this work.

We now make an attempt at explaining the experimentally observed constancy of velocity of propagation. As the stress intensity factor increases prior to crack initiation, the stresses ahead of the crack tip are high; these stresses induce microfractures and the value of the stress intensity factor at initiation then establishes the size and general geometry of the fracture process zone at initiation. Thereafter, the crack propagates due to the interaction of and communication between these microcracks in the fracture zone; the nature of the subsequent interaction is apparently determined by the size of the zone that existed when the zone started to propagate. From this viewpoint, it seems reasonable to expect the stress intensity factor at crack initiation to set the limit on the velocity with which the crack will travel subsequently.

While gradual increases in the stress intensity factor do not seem to affect the velocity with which the crack propagates, the geometry and nature of the fracture process zone are altered drastically by a large stress pulse and thus a change in the propagation velocity is enabled. From figure 41 (solid line), it is seen that the crack travels at a constant velocity of 240 m/sec prior to the arrival of the reflected waves at around 150 μsec. The arrival of the waves

reflected from the boundaries causes the stress intensity factor to increase as in figure 41 (solid line), and the crack velocity immediately changes to a new constant velocity of 350 m/sec. On the other hand, from figure 40 (dotted line), it can be seen that the crack velocity remains constant at 363m/sec even after the arrival of the waves reflected from the specimen boundaries, although the stress intensity factor increases. This behaviour was observed consistently and leads to the following conclusion. While cracks travelling at low velocities, typically below 300 m/sec, encounter stress waves, a change in the velocity of propagation is enabled. If the interaction with the stress wave occurs when the crack velocity is higher than 300 m/sec, the crack velocity does not change.

5.1.2 Terminal Velocity of Crack Propagation: As mentioned in Chapter 1, exact calculations of the energy flux at the crack tip by Freund[2] have shown that when the energy required to create a new surface is taken to be a constant, the limiting crack velocity is the Rayleigh wave velocity. One would expect on analytical grounds that the Rayleigh wave velocity would set the limit for crack propagation velocity since the energy input into the crack tip is through surface waves that travel with the Rayleigh wave velocity. It was also pointed out in Chapter 1 that the experimentally observed crack velocities were always significantly lower than the Rayleigh surface wave velocity. This is further reinforced by the present data, where the maximum observed crack velocity was 487 m/sec, ($0.45C_r$). In fact there are sufficient data available in the literature to substantiate the claim that a terminal velocity that is smaller than the Rayleigh wave velocity exists in most materials. A survey of the velocity of propagation of cracks in various materials is given in Table 2. There have been a number of hypotheses put forward in order to explain the lower observed terminal velocities and we shall examine these next.

2. Freund, L.B., *Journal of Elasticity*,**4**,(1972),p.341.

TABLE 1. Survey of brittle fracture velocities.

Material	Author	ν	v/C_d	v/C_s	v/C_0	v/C_r
Glass	Bowden	0.22	**0.27**	0.42	0.29	**0.51**
	Edgerton	0.22	0.26	0.43	**0.28**	
	Schardin	0.22	0.28	0.47	**0.30**	
	Anthony	0.22	0.36	**0.60**	0.39	
Plexiglas	Cotterell	0.35	**0.26**	0.54	0.33	
	Paxson	0.35	0.28	0.58	**0.36**	
	Dulaney	0.35	0.28	0.59	**0.36**	
Homalite-100	Beebe	0.31	0.16	0.31	**0.19**	
	Kobayashi	0.345	**0.17**	0.35	0.22	
	Dally	0.31	**0.22**	0.35	0.24	
	Smith	0.31	**0.22**	**0.38**	**0.25**	**0.41**

Note: Bold face numbers indicate values obtained from the references. Other values were calculated from the value of Poisson's ratio shown in column 3.

1. Bowden, F.P., *et. al.*, *Nature*,**216**,(1967),p.38.
2. Edgerton, H.E. and Barstow, F.E., *Journal of American Ceramic Society*, **24**,(1941),p.131.
3. Schardin, H., and Struth, W., *Glastechnische Bertichte*,**16**,(1938),p.219.
4. Anthony, S.R., *et. al.*, *Philosophical Magazine*,**22**,(1970),p.1201.
5. Cotterell, B., *Applied Materials Research*,**4**,(1964),p.227.
6. Paxson, T.L., and Lucas, R.A., in *Dynamic Crack Propagation*, (ed. Sih, G.C.), Noordhoff, Leyden,(1973),p.415.
7. Dulaney, E.N., and Brace, W.F., *Journal of Applied Physics*,**31**,(1960),p.2233.
8. Beebe, W.M., Ph.D., Thesis, California Institute of Technology, (1966).
9. Kobayashi,A.S., and Mall, S., *Experimental Mechanics*,**18**,(1978),p.11.
10. Kobayashi, T., and Dally, J.W.,*Fast Fracture and Crack Arrest, ASTM STP 627*, (1977),p.257.
11. Smith, G.C., Ph.D., Thesis, California Institute of Technology, (1975).

It has been suggested that crack branching occurs at the experimentally observed terminal velocity and that this phenemenon is responsible for the lower observed terminal velocities. The implication is that if branching were suppressed, cracks might then travel at or close to the Rayleigh wave velocity. Once again, experimental data seem to contradict this in the sense that, when the applied stress is increased considerably, as indicated in figures 40, 41 and 42, the velocity does not increase above $0.45C_r$, even during the constant velocity propagation phase, when there is no evidence of crack branching. On this basis, one would have to assert the existence of a terminal velocity other than the Rayleigh wave velocity and seek a different explanation for the causes of this lower terminal velocity.

Another suggestion for explaining the observed crack propagation behaviour is to consider the energy required to create a new surface Γ to be a rate dependent quantity and therefore $\Gamma = \Gamma(V)$. If Γ varied with the velocity, it is conceivable that a limiting velocity other than the Rayleigh wave velocity may be obtained as suggested by Rose.[3] While this assumption might explain the existence of a lower terminal velocity, it meets with difficulties when one considers the fact that, as observed in this investigation, cracks travel with a constant velocity although the stress intensity factor is varying. If Γ is a function of velocity alone, the energy flux equation (5) can be rearranged such that the right hand side is purely a function of velocity and the left hand side is a function of the stress intensity factor.

$$\frac{E}{K^2} = \frac{g(V)}{\Gamma(V)} \tag{21}$$

Thus the energy equation predicts that the velocity of crack propagation should change under varying stress intensity factor situations. However,the stress

3. Rose, L.R.F., *International Journal of Fracture*,**12**,(1976),p.341.

intensity factor and crack extension histories presented in figures 40, 41 and 42 indicate that while the stress intensity factor changes considerably, the velocity remains constant. Thus allowing Γ to be a function of crack velocity creates a problem in explaining the constancy of crack velocity. The causes for the existence of a terminal velocity lower than the Rayleigh wave velocity then has to be explained by some other mechanism and a microcrack interpretation of the crack propagation process that was described in Chapter 4, yields a satisfactory explanation for the lower observed terminal velocities.

If the crack propagation process is viewed as the ensemble propagation of a number of microcracks in a fracture process zone, then the speed of crack propagation is governed by the nature of interaction between these microcracks. There is a finite time involved in the interaction process and this is one source of the limitation on the maximum crack velocity. Secondly, the microcrack interaction problem is a three dimensional one and the growth of these cracks need not always be in the direction of main crack growth, but microcracks may also grow perpendicular to the direction of growth of the main crack front. These two factors together may contribute to the lower observed maximum crack propagation velocity.

5.2 Crack Branching

Before proceeding to the discussion of a new physics-based mechanism of crack branching, it is appropriate to review some of the major hypotheses that have been put forward to explain crack branching.

Branching of cracks in glass was observed by Schardin[4] and other investigators have observed crack branching in crystalline as well as amorphous materials.[5] This bifurcation is not predicted by analytical solutions to

4. Schardin, H., in *Fracture*(ed. Averbach *et. al*), MIT Press and John Wiley,(1959),p.297.
5. Field, J., *Contemporary Physics*,**12**,(1971),p.1. Beebe, W.M., Ph.D Thesis, California Institute of

propagating cracks. This failure is due in part to the fact that in analysing crack growth problems, the equations of elasticity are solved independently of the fracture criterion, and by restricting the crack to travel along a straight line. If the equations of elasticity could be solved together with the failure criterion without any *a priori* assumption regarding the nature of crack motion, the solutions might reveal some additional or different features. Solutions of such general form are not in sight for the complicated two dimensional problems and the crack motion is usually prescribed to be along a straight line.

Yoffe[6] attempted to explain the branching of cracks from an analysis of the problem of a constant length crack that travels at a constant velocity in an unbounded medium. From this solution, she found that the maximum $\sigma_{\theta\theta}$ stress acted at an angle of 60° to the direction of crack propagation when the crack velocity exceeded $0.6C_2$, and suggested that this might cause the crack to propagate along these directions whenever the crack velocity was above this value. There are three major shortcomings with this argument. First, as pointed out by Baker,[7] the $\sigma_{\theta\theta}$ stress is not a principal stress and in a brittle material, it is reasonable to expect the crack to propagate perpendicular to the direction of the maximum principal stress. Secondly, the angle of $\pm 60°$ for crack branching that is predicted by the Yoffe argument is large compared to the experimentally observed crack branching angles which range from $\pm 10° - \pm 45°$. Finally, the velocity that is required for the realignment of the $\sigma_{\theta\theta}$ stress is considerably larger than the velocities at which crack branching is observed experimentally. In fact, for the velocities at which crack branching have been observed, there is very little realignment in the stress field that is so essential to the Yoffe argument. We conclude that the Yoffe argument, while

Technology, (1966). Finkel,*et. al.*, *Fiz. Metal. Metalloved*, **15**,(1963),p.754.

6. Yoffe, E., *Philosophical Magazine*,**12**,(1951),p.739.
7. Baker, B.R., *Journal of Applied Mechanics*,**29**,(1962),p.449.

very attractive due to its simplicity, is not likely to explain crack branching satisfactorily.

Eshelby[8] approached the branching problem from the viewpoint of energy balance. It is known that the dynamic energy release rate can be expressed as the product of a velocity dependent factor g(v) and the equivalent static energy release rate G^*, that is dependent on the geometry.[9] Eshelby suggested that while the velocity factor g(v) may change in a discontinuous manner, the factor G^* should be continuous at branching, at least for small angles of crack branching. Since after branching, twice as much surface area is being created, the crack would not advance unless the velocity factor g(v) could be doubled, by a reduction in crack speed. This leads to the conclusion that at branching the velocity has to be larger than $0.5C_r$ and also that the crack will slow down after branching. This conclusion depends on assuming constancy of Γ and the effect of varying Γ would be to reduce the velocity at which branching could occur. Although the main idea that the availability of sufficient energy at the crack tip is clearly a necessary condition, the conclusions about the velocity behaviour of the branched crack is not borne out by experiment. The crack travels at a constant velocity *prior to* and *after* crack branching, with no apparent change in the velocity. The above energy argument is devoid of any mechanism by which the crack branching is achieved, but merely poses a necessary condition on the energy release rate that must be satisfied if crack branching were to occur in the idealized manner.

Another "explanation" of crack branching rests on the stress wave hypothesis.[10] It is known that when stress waves interact with propagating

8. Eshelby, in *Inelastic Behaviour of Solids*,(eds. M.F., Kanninen *et. al.*), McGraw Hill, New York, (1970),p..

9. see, for example, Rose,L.R.F., *International Journal of Fracture*, **12**, (1976),p.341.

10. Lawn, B.R., and Wilshaw, T.R., *Fracture in Brittle Solids*, Cambridge University Press, (1975),p.104.

cracks, the crack path may change abruptly. When the interaction is weak, the well known phenomenon of Wallner lines is observed. In this connection it has been suggested that when the interaction is strong - the amplitude of the stress waves is high - the resulting change in the crack path might lead to crack branching. This argument is also devoid of any specific mechanism by which crack branching is achieved. By contrast, the present experimental data show clearly that crack branching can occur without *any* interaction with stress waves, a situation which the stress wave hypothesis does not address at all. A detailed investigation of the effect of stress waves on propagating cracks is discussed in section 5.3.

To date published attempts at analysing branched cracks have all been to seek a necessary condition for branching through a comparison of the stress states prior to and after branching.[11] The post-branching stress state is obtained by assuming that a fast running crack comes to rest abruptly, radiates out the appropriate stress field and in this stress field two branches issue out at some arbitrary symmetric angles. Also, the cited analysis is for a Mode III crack problem which is analytically easier, and the conclusions are not necessarily directly applicable to the more complicated Mode I problem. Once again, this kind of analytical treatment cannot provide us with a mechanism by which crack branching is achieved.

All the above explanations were of an idealized nature and a common feature among all of the attempts at explaining the phenomenon of crack branching is that they assume a mathematically sharp plane crack to propagate in a two dimensional solid and to branch into two distinct, sharp, plane cracks. Another explanation for the crack branching problem is due to Congleton,[12] who

11. Achenbach, J.D., *International Journal of Solids and Structures*,**11** ,(1975),p.1301.
12. Congleton, et. al., *Philosophical Magazine*, **16**,(1967),p.749.

suggested that microcracks are responsible for the crack branching phenomenon. To the writer's knowledge, this is the only attempt at explaining branching by taking into consideration the real physical process of fracture. Although Congleton suggests that cracks that are nucleated ahead of the main crack front are responsible for inducing crack branching, he does explain the possible mechanism further. His remarks arose in connection with calculating the stress level at which a small Griffith crack placed ahead of the main crack will start to grow. From this he estimated the critical stress intensity necessary to achieve crack branching. By contrast our main interest here is not in computing the stress level necessary for crack branching, since we already have sufficient information on the stress intensity factor at crack branching, but in establishing a mechanism through which the crack branching process is achieved, Starting from the microscopic view of the crack propagation process as outlined in Chapter 4, a unified view of the crack propagation and branching is proposed here.

As we have shown in the previous chapter, the mathematical model of a sharp crack propagation plane is an unacceptable view for the real crack propagation process, which is essentially three dimensional in nature and governed by the microscopic phenomenon of microcrack interaction. From the microscopic model of the crack propagation process, it is possible to obtain a mechanism for crack branching, which treats crack branching not as a discontinuous process that occurs when some critical state is reached, but as a continuous process occasioned by the interaction of the microcracks.

The crack propagation and branching mechanism is illustrated in figure 44. Initially, the crack is propagating at low stress intensity factors in a material that contains a number of voids. The crack cuts through these voids and some of the voids have the effect of diverting the crack to propagate along

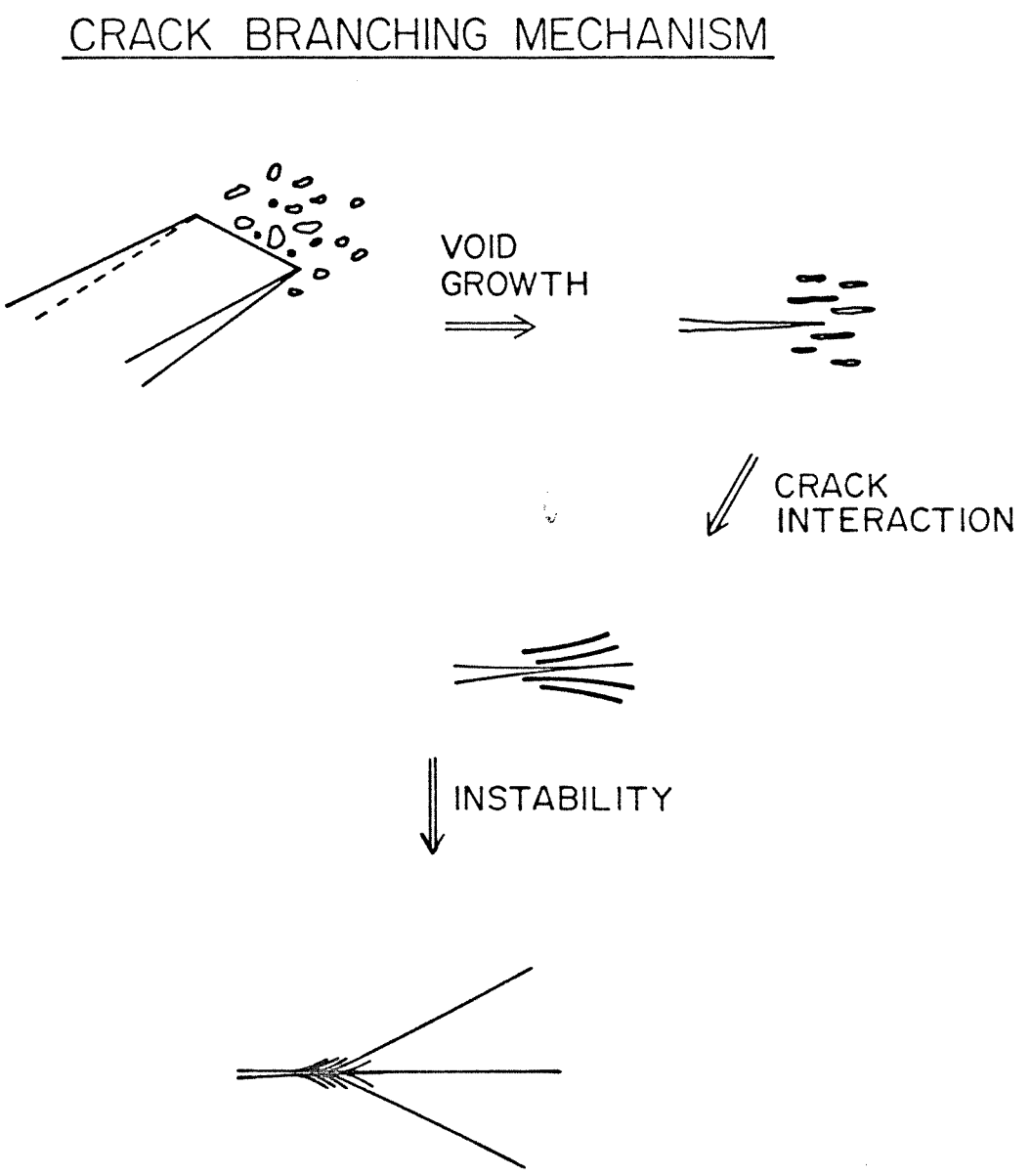

Figure 44. Crack branching mechanism.

different planes. When the stress intensity factor becomes sufficiently high, the voids start to grow ahead of the major crack front, which now becomes really an ensemble crack front. The course of further crack propagation and its branching behaviour is governed by the details of the interaction of these microcracks. The solution to the problem of dynamic interaction of even the simplest crack geometries seems to be very difficult to develop, but there exist solutions to the static interaction problems and we shall draw upon the results of quasi-static analyses to assess further crack propagation. For the present purpose, it is assumed that the quasi-static solution provides a good insight into the dynamic interaction problem, because the experimentally observed crack velocities are small enough to make the effect of inertia relatively small.

The solution to the problem of two interacting Griffith cracks was provided by Pucik,[13] who considered the crack centres to be located at arbitrary points and the cracks themselves to be oriented at arbitrary angles with respect to one another, with a uniform load p at infinity. As part of the analysis, Pucik computed the maximum $\sigma_{\theta\theta}$ stress in the immediate crack tip vicinity and also the orientation along which this stress acted. For the case of two parallel cracks of equal length $2l$, the variation of the angle at which the maximum $\sigma_{\theta\theta}$ acts is plotted in figure 45 as a function of the vertical separation Y_{12} and the horizontal separation X_{12} between the two cracks. From this plot one verifies that, depending on the proximity of the cracks, the two cracks may either attract or repel one another. A similar solution to interacting cracks has been provided by Yokobori[14] which exhibits once again this behaviour of attracting or repelling cracks depending on the separation and the sizes of the cracks.

13. Pucik, T.A., Ph.D., Thesis, California Institute of Technology,(1972).
14. Yokobori, *et. al.*, *Reports of The Research Institute for Strength and Fracture of Materials*, Tohoku University, Vol.7, No.1,(1971),p.25.

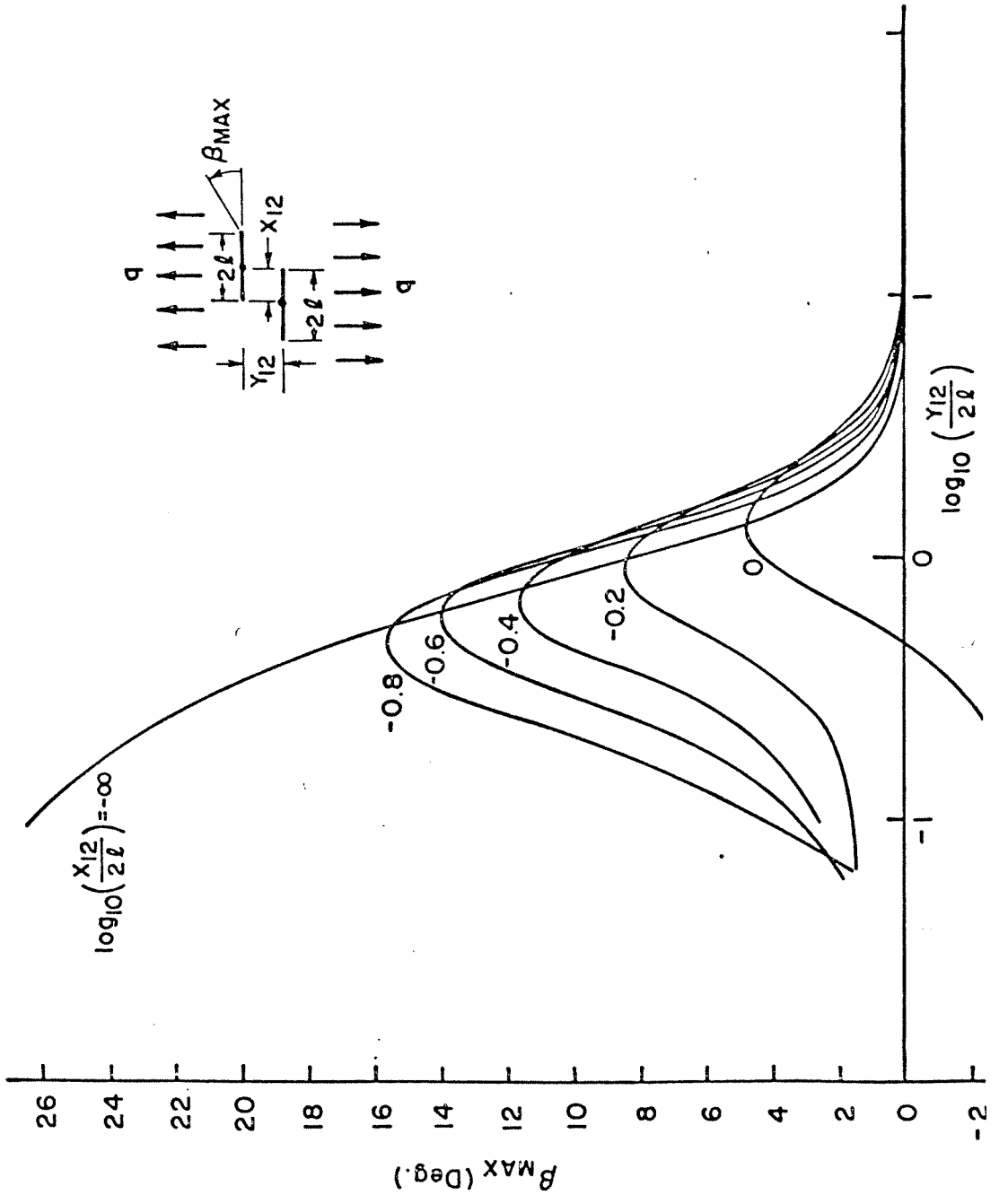

Figure 45. Variation of the angle at which the maximum $\sigma_{\theta\theta}$ stress acts. [From ref. 13]

Let us return now to the crack branching problem; in this case there are several microcracks that interact with one another, and under certain conditions, the small cracks may deviate from the main crack plane. Here we note that while the quasi-static interaction solutions indicate a sharp deviation from the original propagation direction, what is observed in the crack branching problem is a smooth deviation from the main propagation plane. We can account for this difference by considering the fact that the microcracks interact with one another continuously through stress waves, unlike in the quasi-static case where the cracks "know" of each other instantaneously. Also, in the branching problem, we deal with a number of microcracks that interact with one anothersimultaneously, making the interaction more complex than in the quasi-static case. Hence, we have to consider the quasi-static solution as giving qualitative support to the argument of deviation of cracks due to interaction. This kind of continuous deviation of the microcracks from the major propagation plane is evident from the high speed photomicrograph of the branching process shown in figure 39. The path instability of the interacting cracks results in some of the attempted branches developing into full fledged crack branches and propagating further while the rest of the attempted branches become unloaded and arrest; this situation is illustrated in figure 44.

In conclusion, we summarize here the main arguments and the supporting evidence.

1. In the 'mirror' zone, the crack propagates at relatively low stress intensity factors. It cuts through the voids present in the material and sometimes the latter cause a change in the plane of crack propagation. This is illustrated in figures 27 and 28. Also, the crack propagates with a curved front as shown in figure 34a.

2. In the 'mist' zone, the crack propagates at higher stress intensity factors compared to the 'mirror' zone. Here, the stresses ahead of the crack front are high enough to initiate voids into growing prior to the arrival of the main crack front. This is substantiated by parabolic markings such as the one shown in figure 30. In this zone, the crack front is no longer curved as in the 'mirror' zone, but we see evidence of a number of small cracks propagating along the apparent or ensemble crack front, as illustrated in figure 34b.

3. In the 'hackle' zone, the stress intensity factors are very high; several voids are initiated into growing and also voids are initiated the farther away propagation plane the higher the stress intensity factor. This is supported by the fact that the fracture surface appears the roughest in this zone. We also have evidence of crack growth in a direction perpendicular to the main propagation direction as suggested by the 'river' markings shown in figure 31. Otherwise, the crack front, shown in figure 34c, appears similar to that in the 'mist' zone.

4. The course of crack propagation in the presence of a large number of microcracks is governed by the interaction of these with one another. High speed photomicrographs of the branching process (figures 38 and 39) indicate that crack branching is a continuous process with a number of micro-branches emanating smoothly from planes parallel to the main plane of the crack.

5. Quasi-static analysis indicates that two interacting Griffith cracks may deviate from one another depending on the size and separation of the cracks. This provides the basis for the micro-branches that deviate from the main propagation plane.

6. High speed photomicrographs of the crack front after branching also indicate the presence of microcracks along the crack front (*cf.* figure 35).

The above view of the crack propagation process, predicated on the nature of microcrack growth and interaction, provides a mechanism for crack branching that follows in a natural way from propagation along a straight line.

5.3 Interaction of Stress Waves with a Propagating Crack

It was noted repeatedly that just after the waves reflected from the boundaries arrived at the crack tip the nature of crack propagation changed. Since the interaction of stress waves with a propagating crack is an important problem, we shall examine it in greater detail in the following. The interaction of stress waves with propagating cracks provides an easy way of altering the crack tip stress field. In fact, one might argue that the crack-parallel stress at the crack tip causes path instability in accordance with the analysis of Cotterell and Rice,[15] and thus provide the basis for the crack branching phenomenon. In the initial stages of this investigation this was actively pursued as a possible crack branching mechanism.

There are two ways in which stress waves can be made to arrive at the crack tip. First, the pressure pulse applied to the semi-infinite crack faces propagates through the material and is reflected at the specimen boundaries to interact with the (moving) crack tip. In this case one has virtually no control over the amplitude of the stress wave that arrives at the crack tip. A second way of obtaining wave interaction with a propagating crack is to apply a second load pulse with the aid of another loading circuit. By virtue of the present configuration of the loading devices, we can only generate compressive stress waves arriving at the crack tip. Both of the above methods were used in studying stress wave interaction with propagating cracks. We turn now to the results of these interactions.

---

15. Cotterell, B., and Rice, J.R., *International Journal of Fracture*, **16**,(1980)p.155.

5.3.1 Reflected Waves Interacting with Cracks: In order to determine the nature of the waves arriving at the crack tip, the outgoing waves have to be examined. The wavefront diagram for the diffraction at the crack tip is shown in figure 46. By judiciously selecting the proximity of the specimen boundaries one can select parts of the outgoing waves to arrive at the crack tip at predetermined times. To make this clear, consider the geometry shown in figure 47. Here only the dilatational wavefront is shown for the sake of clarity. By placing boundaries along lines labeled 'front', 'top' and 'bottom', and adjusting the distances b_1, b_2 and b_3, it is possible to obtain the waves reflected at the three boundaries at different times. The amplitude of the outgoing wave has an angular distribution and also attenuates as the distance from the crack tip increases. The amplitude has a maximum when the angle is 90°, that is, the angle corresponding to the top and bottom boundary reflections and a minimum when the angle is 0°, corresponding to the front boundary reflection. It was determined through numerical computations that the front reflection was very weak when compared to the top and bottom reflections. We will now investigate the effect of these stress waves on crack propagation under both low and high stress intensity factor situations.

The first case results when the crack face pressure is low and the stress intensity factors also sufficiently low so as to not induce branching. The specimen geometry and dimensions are indicated in figure 48. All three boundaries - top, bottom and front - are stress free and hence the reflected waves undergo a sign change and reflect back to the crack tip as tensile waves. In this case, the bottom wave arrives first, followed by the top wave with a 25 μsec delay. The resulting crack path is also indicated in figure 48. It is seen that the bottom reflection arrives first, alters the direction of the maximum principal stress and causes the crack to change its path continuously until the wave

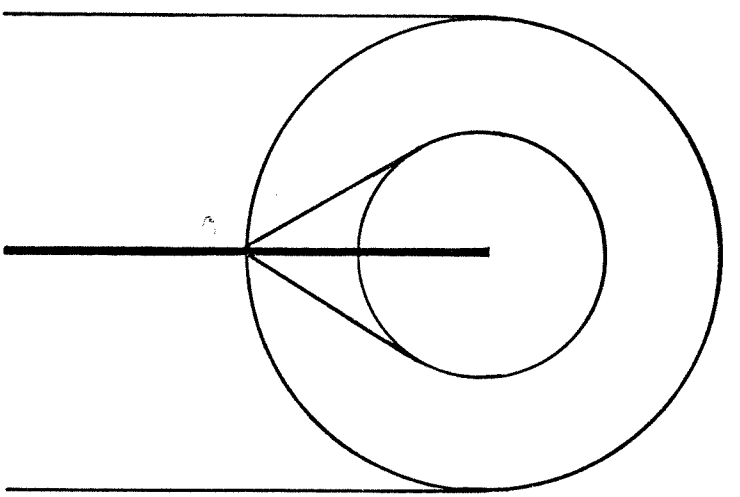

Figure 46. Wavefront diagram for the diffraction at the crack tip.

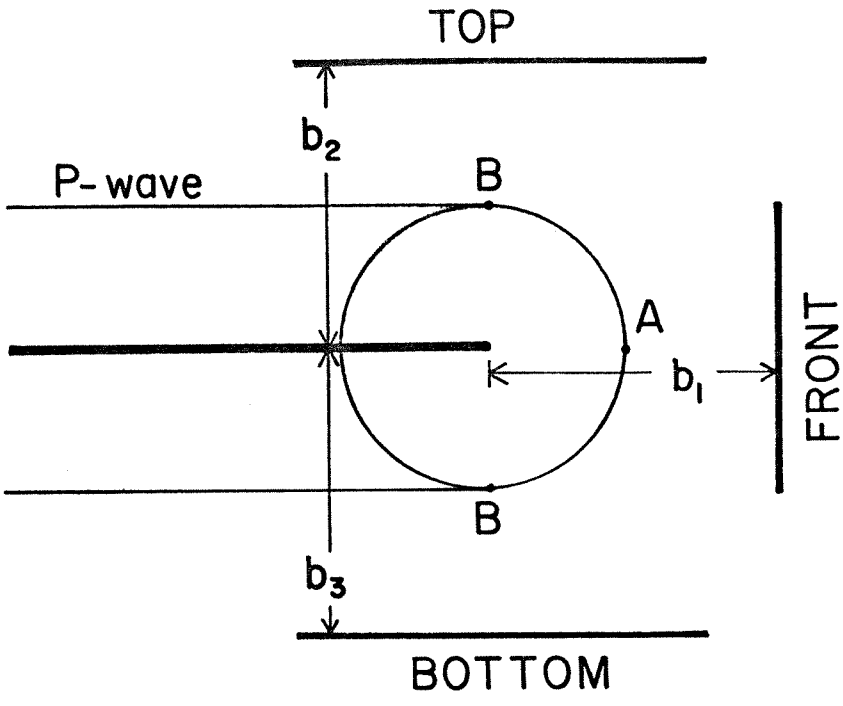

Figure 47. Geometry for the reflected wave interaction study.

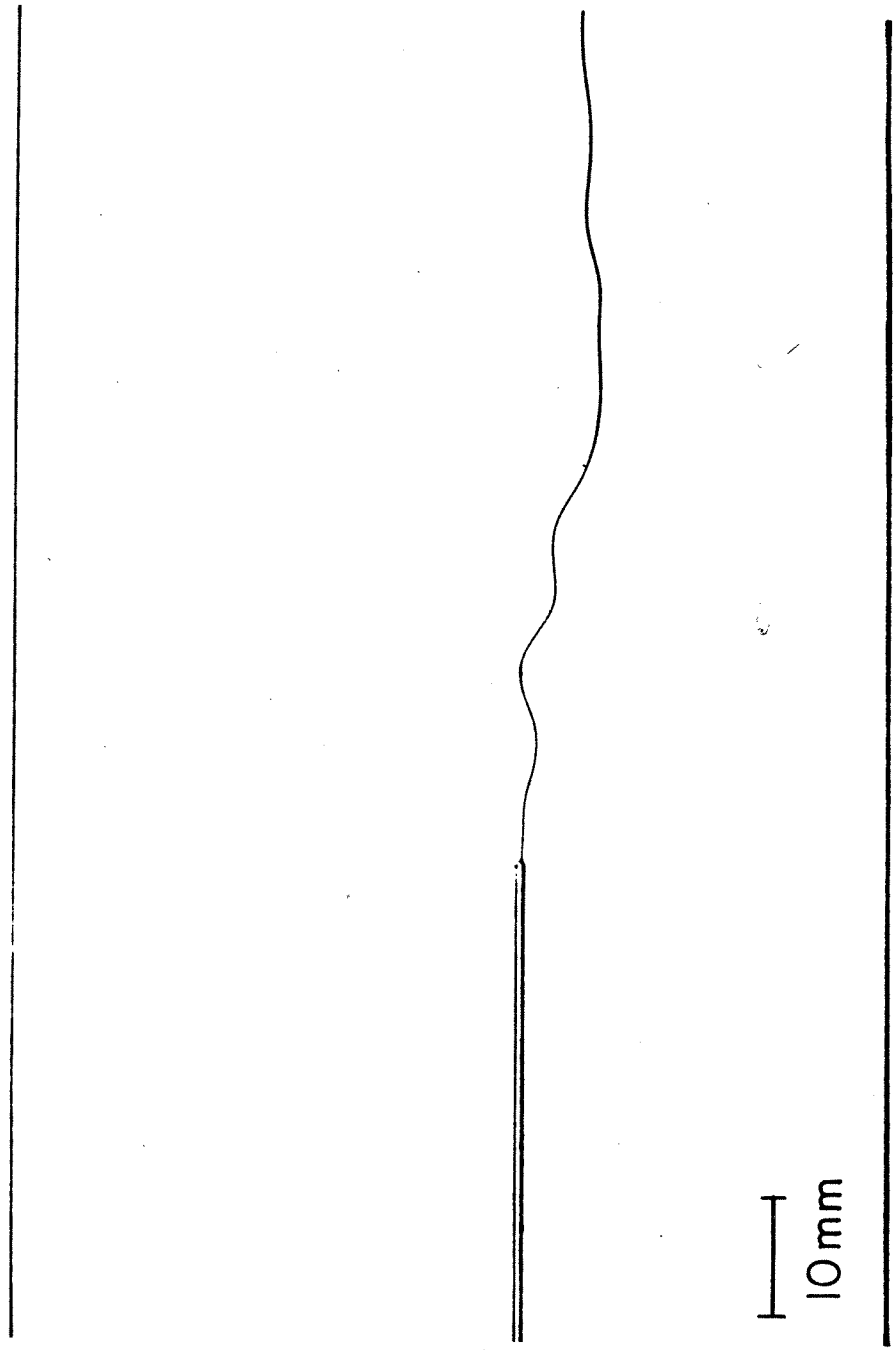

Figure 48. Specimen geometry and the crack path.

reflected from the top boundary arrives which then causes the crack to revert back towards its original direction of propagation,leading to an oscillatory crack path. Thus the interaction of low amplitude stress waves cause changes in the crack path by virtue of the changes in the stress field that these stress waves induce at the crack tip. If the reflected waves from the top and bottom had arrived at the crack tip at the same time, the symmetry at the crack tip would have been preserved and the crack path would have been along the original straight line path.

The second case considered is illustrated in figure 49. The specimen size is the same as in the first case,except that now the bottom boundary is left to rest on an aluminium plate and thus the bottom boundary condition is now different from the one at the top. The transmission coefficient at this boundary is ideally 0.25 and hence the wave that is reflected from this boundary is compressive in nature but certainly has a reduced amplitude. Also, in this case, the amplitude of the applied loading was increased to produce a high stress intensity factor situation. The resulting stress intensity factor history and the crack position history are shown in figure 50. Due to a mechanical quirk in the design of the high speed camera which causes a random loss of eight frames, data from the initial part of the experiment were lost, but the important part of the data was still obtained. In this case, the bottom reflection arrived first and being compressive inhibited the usual increase in the stress intensity factor that would otherwise have been observed. After 25 μsec, the tensile wave reflected from the top boundary arrives at the crack tip and causes the stress intensity factor to increase rapidly. Notice that *the crack velocity remains constant during all of these changes in the stress intensity factor*. The increase in the stress intensity factor finally causes the crack to branch. The stress wave interactions with the propagating crack are denoted on the crack extension

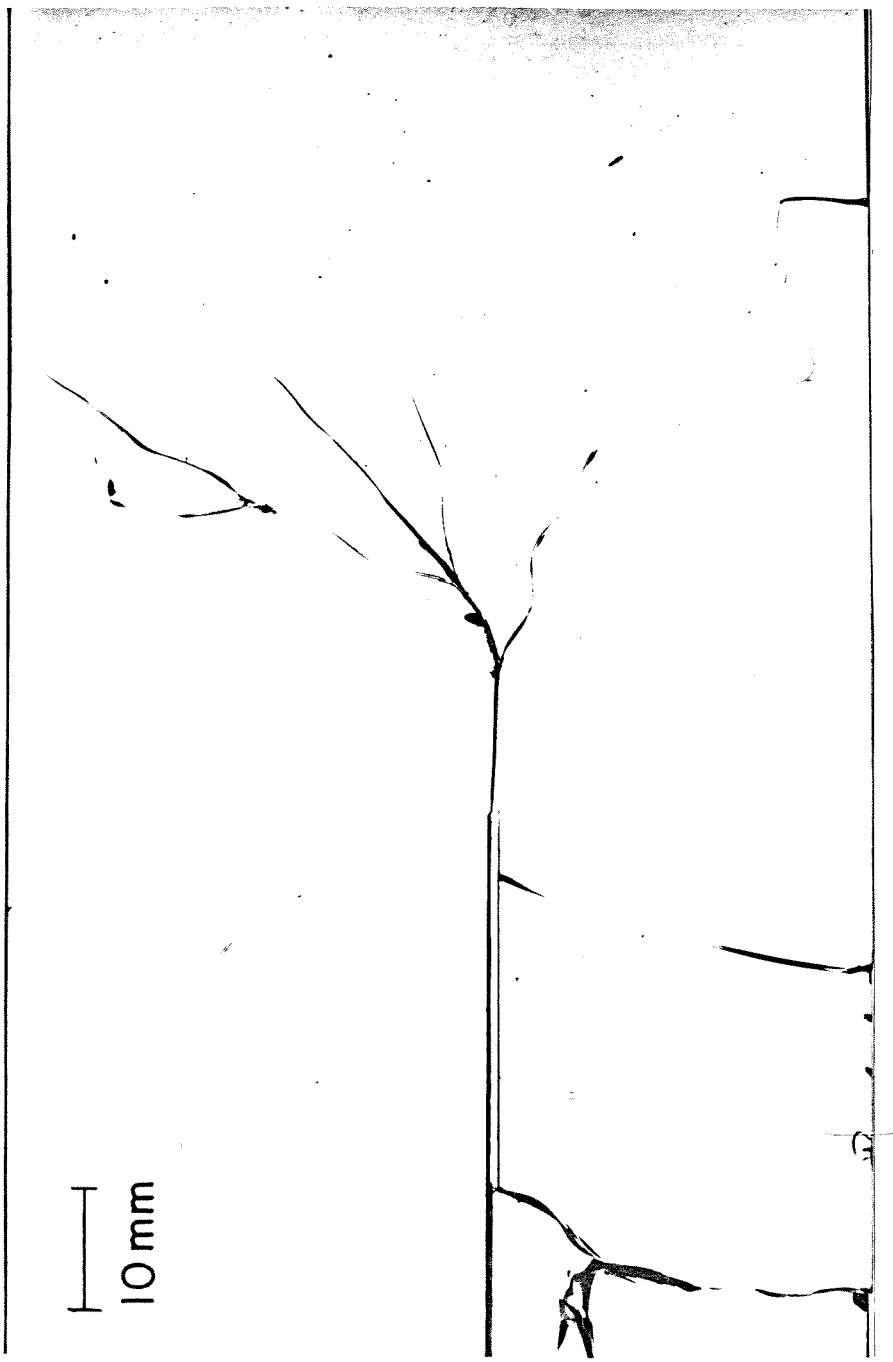

Figure 49. Stress wave induced crack branching.

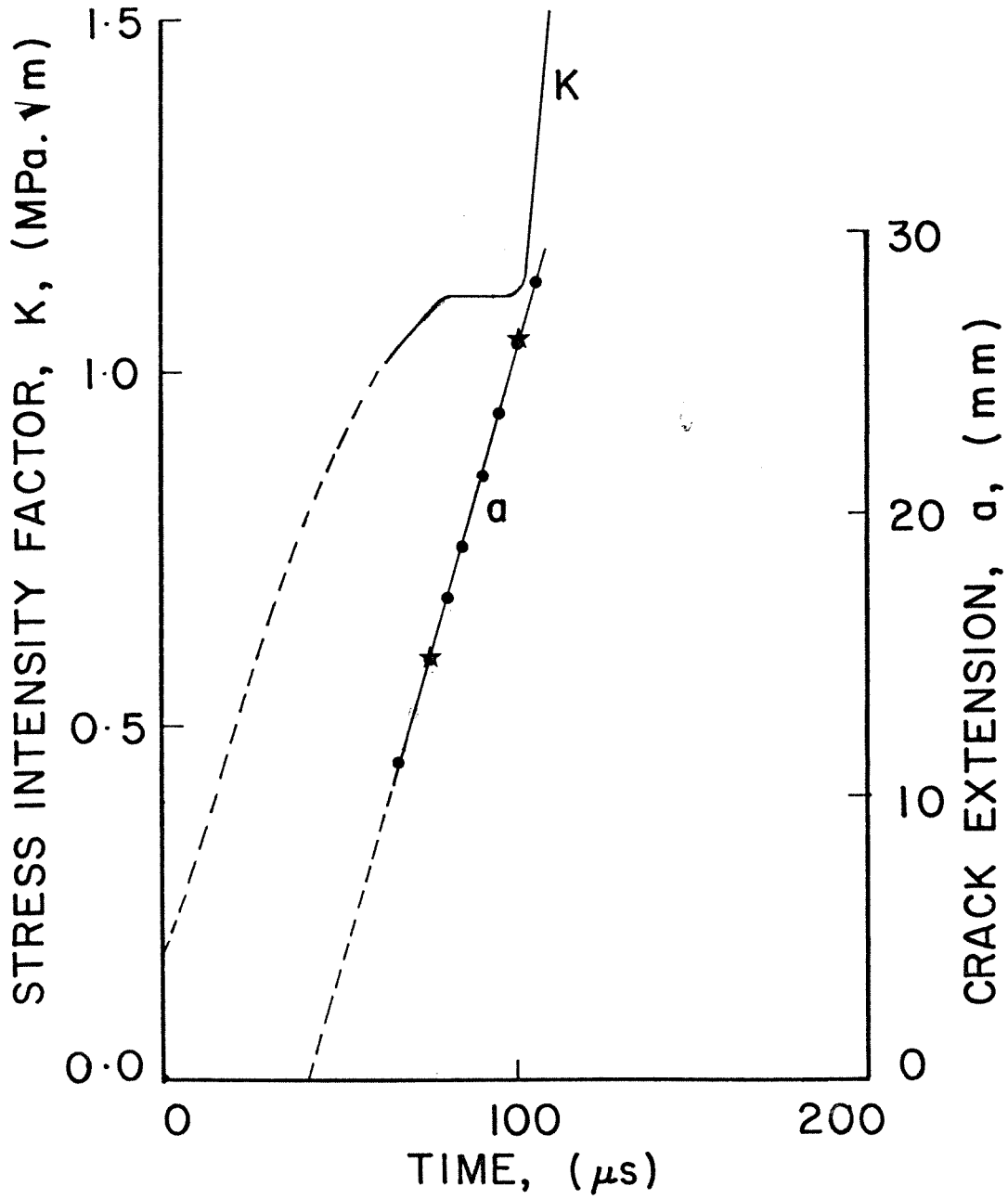

Figure 50. Stress intensity factor and crack extension histories for the case in figure 49.

history plot by asterisks.

We have now shown that stress waves interacting with propagating cracks may on the one hand alter the path of crack propagation, if the stress intensity factor is low or, on the other, induce crack branching if the stress intensity factor is sufficiently high. We investigate next the effect of the various reflections on the branching process. Since we know the pressure level at which the reflected waves have sufficient intensity to induce crack branching, many experiments can be performed at the same pressure level with different specimen sizes in order to have various reflections arrive first at the crack tip. Figures 51, 52 and 53 show the results from three such tests; here the stress wave and crack positions are plotted on $x-t$ diagrams. Since the waves propagate along two dimensions a $y-t$ diagram is also included for each test. In these diagrams, the motion of the wave front points A and B in figure 47 and the motion of the crack tip C are indicated. The interactions of the stress waves with the crack tip are marked by asterisks. From these three cases we see that while the top and bottom reflected waves induce crack branching, the front reflection does not. This is not really surprising in view of the fact that the amplitude of the wave reflected from the front is very small. What is perhaps surprising is the fact that the tensile stress acting *parallel* to the crack tip resulting from the front reflection does not even affect the crack path as one might expect from the crack path stability analysis of Cotterell and Rice.[16]

5.3.2 Second Stress Wave Loading: The second method of generating interacting stress waves is to provide a second loading using another loading device identical to the one described in Chapter 2. Since our main aim in these investigations was to study the effect of stress waves on crack branching, all the stress wave experiments were performed with dynamic compressive stresses parallel to

16. Cotterell, B., and Rice, J.R., *op. cit.*

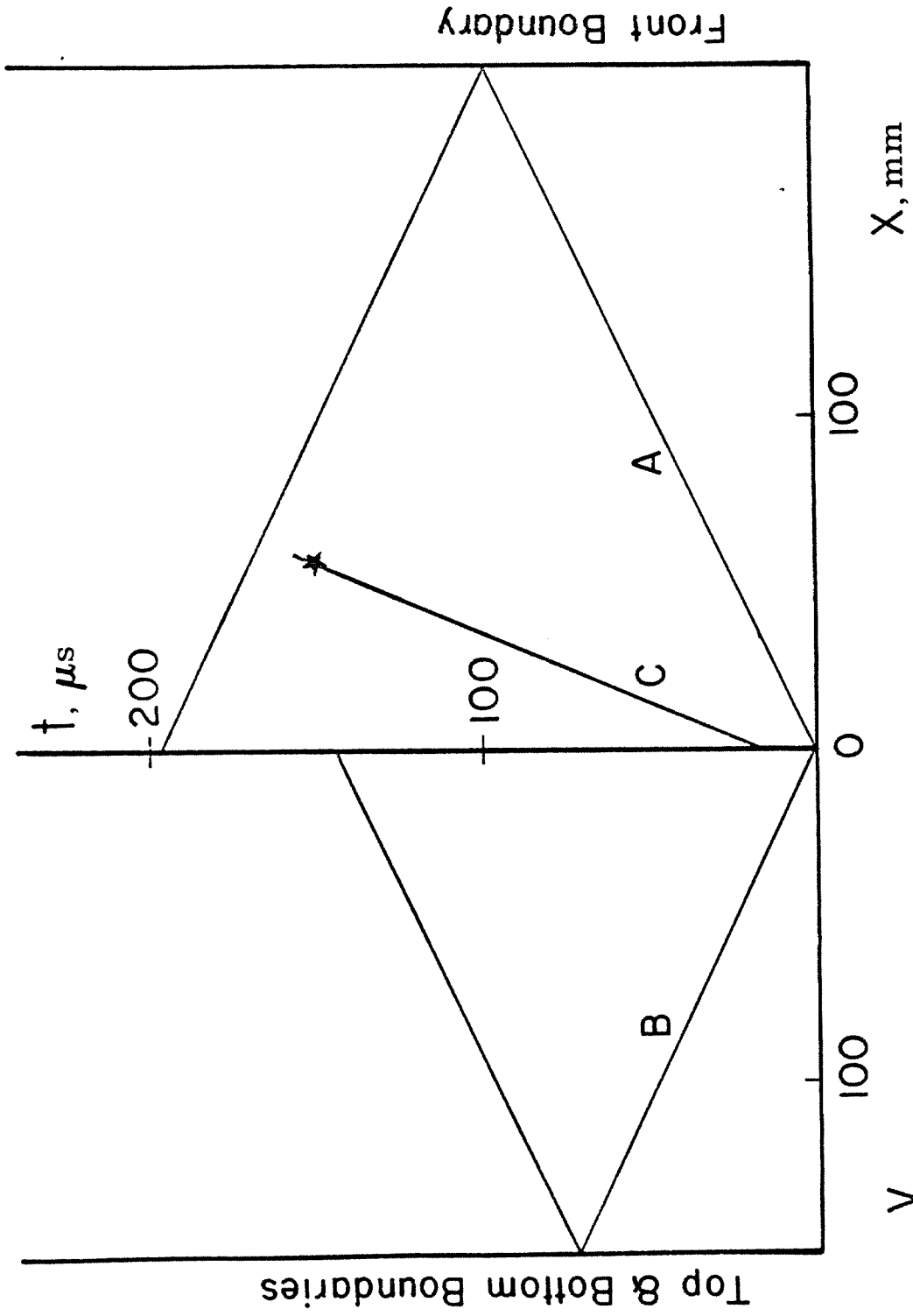

Figure 51. x–t and y–t diagrams for stress wave induced crack branching.

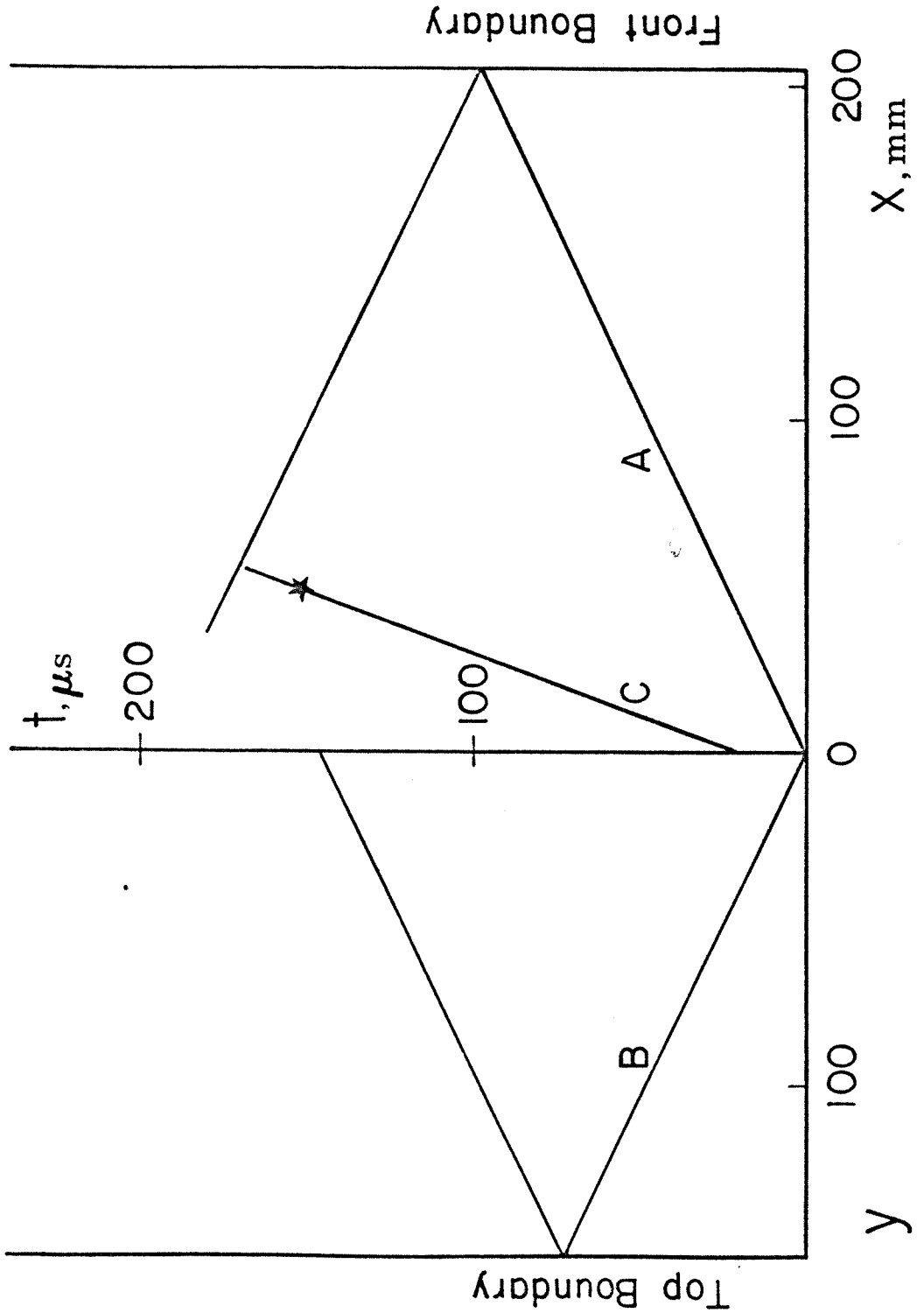

Figure 52. x-t and y-t diagrams for stress wave induced crack branching.

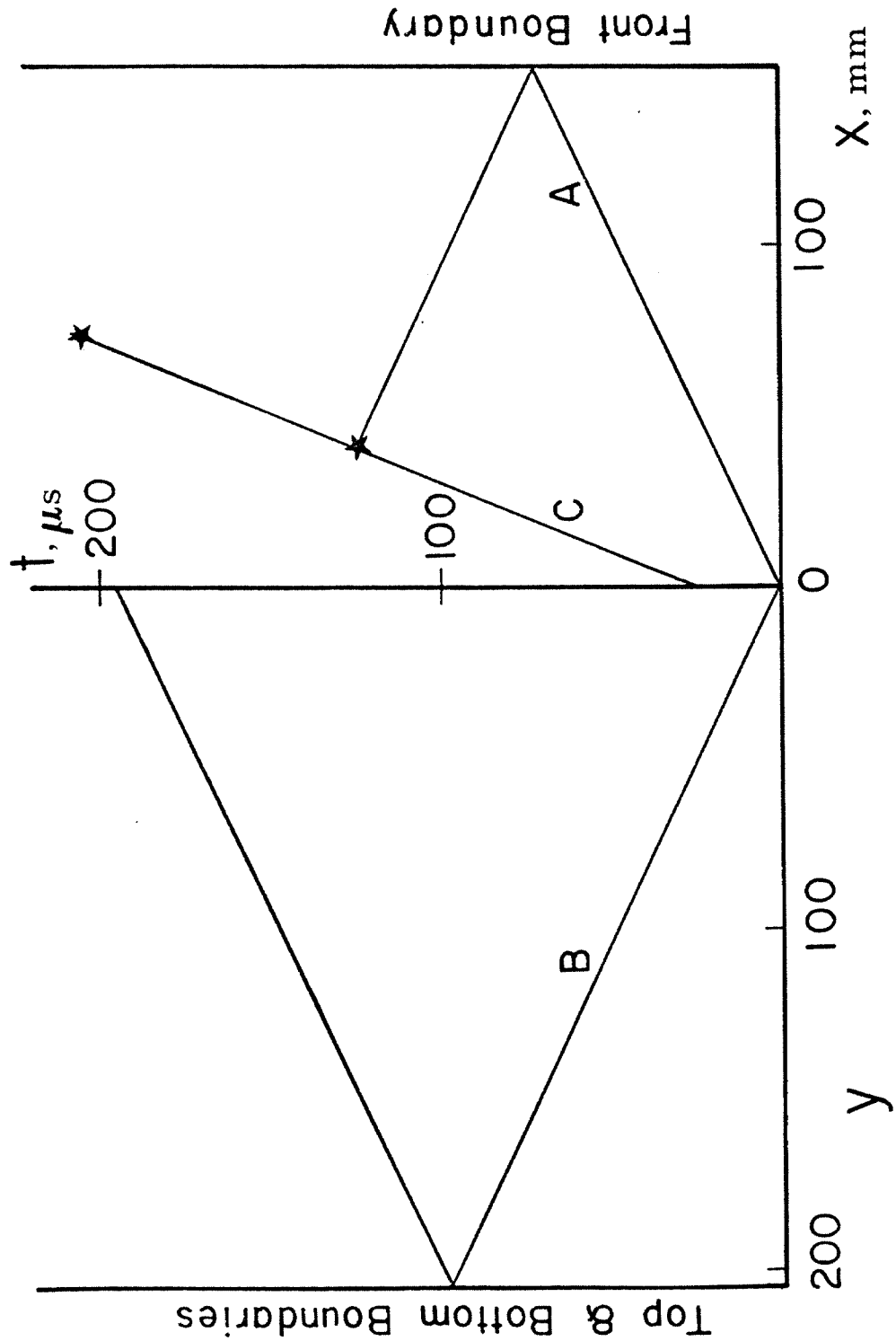

Figure 53. x–t and y–t diagrams for stress wave induced crack branching.

the crack axis, that is, the copper strip was oriented as shown in figure 54. The time of application of the second load was arranged such that it would arrive at the crack tip exactly at the instant of incipient crack branching. The magnitude of the main load (p_1) was maintained constant and the magnitude of the side load (p_2) was changed so as to study the influence of this load on crack branching. It was observed that the effect of the dynamic compressive stress parallel to the crack tip was to

1. suppress crack branching for a duration of time that depends on the magnitude of the side load and
2. affect the angle into which subsequent branches spread.

Assembled plates from two tests are shown in figure 55, showing the delay in branching and also the change in the angle of branching. The marker in the photographs indicates L_{br} for the case $p_2 = 0$. The results of this investigation are shown in figure 56. The velocity of propagation in all the cases was constant at about 400 m/sec. Even the arrival of the second stress wave - which in fact was a biaxial stress field and hence reduced the crack tip stress intensity factor - *did not change the velocity of crack propagation.*

From the microscopic mechanism for branching that was proposed in section 5.2, we can interpret some of this observed behaviour. The stress wave that arrives at the crack tip is really a biaxial stress field and therefore reduces the stress intensity factor. This reduction in the stress intensity factor should lead to a smaller fracture process zone and should also decrease the number of microcracks that are available to interact and induce branching. Furthermore, the compressive stress parallel to the crack propagation direction, would also act unfavourably on any microcracks that deviate away from the main crack plane in that a component of the compressive stress would act in such a way as

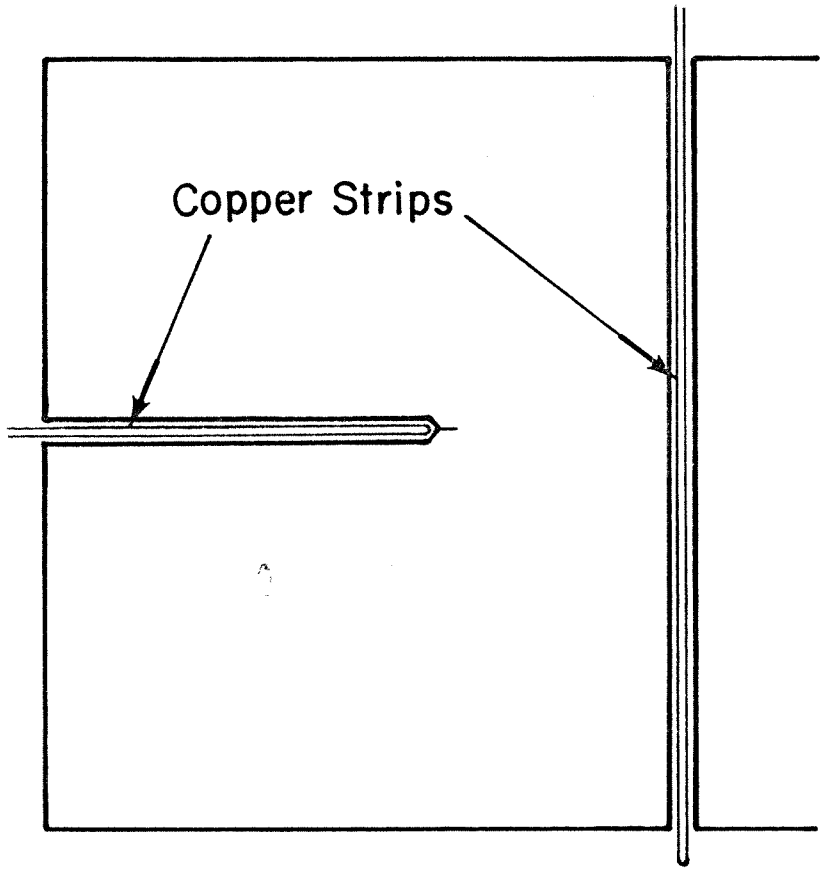

Figure 54. Geometry of the specimen for the second stress pulse.

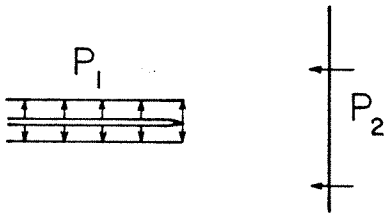

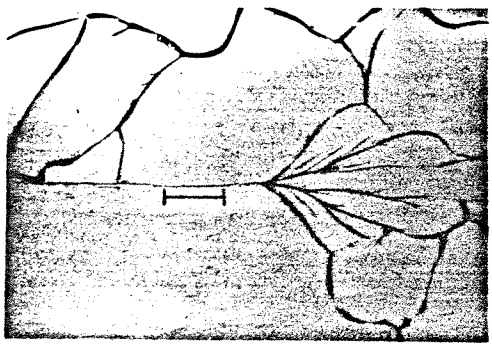

P_1=10.35 MPa; P_2=5.5 MPa

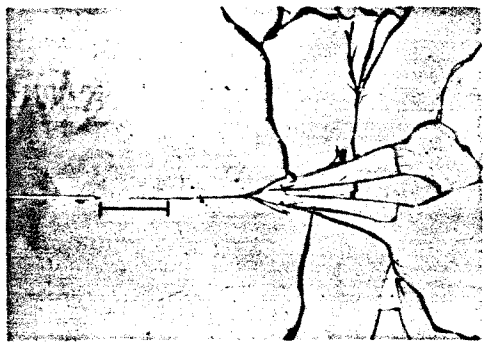

P_1=10.35 MPa; P_2=10.35 MPa

Figure 55. Effect of second stress wave on crack branching

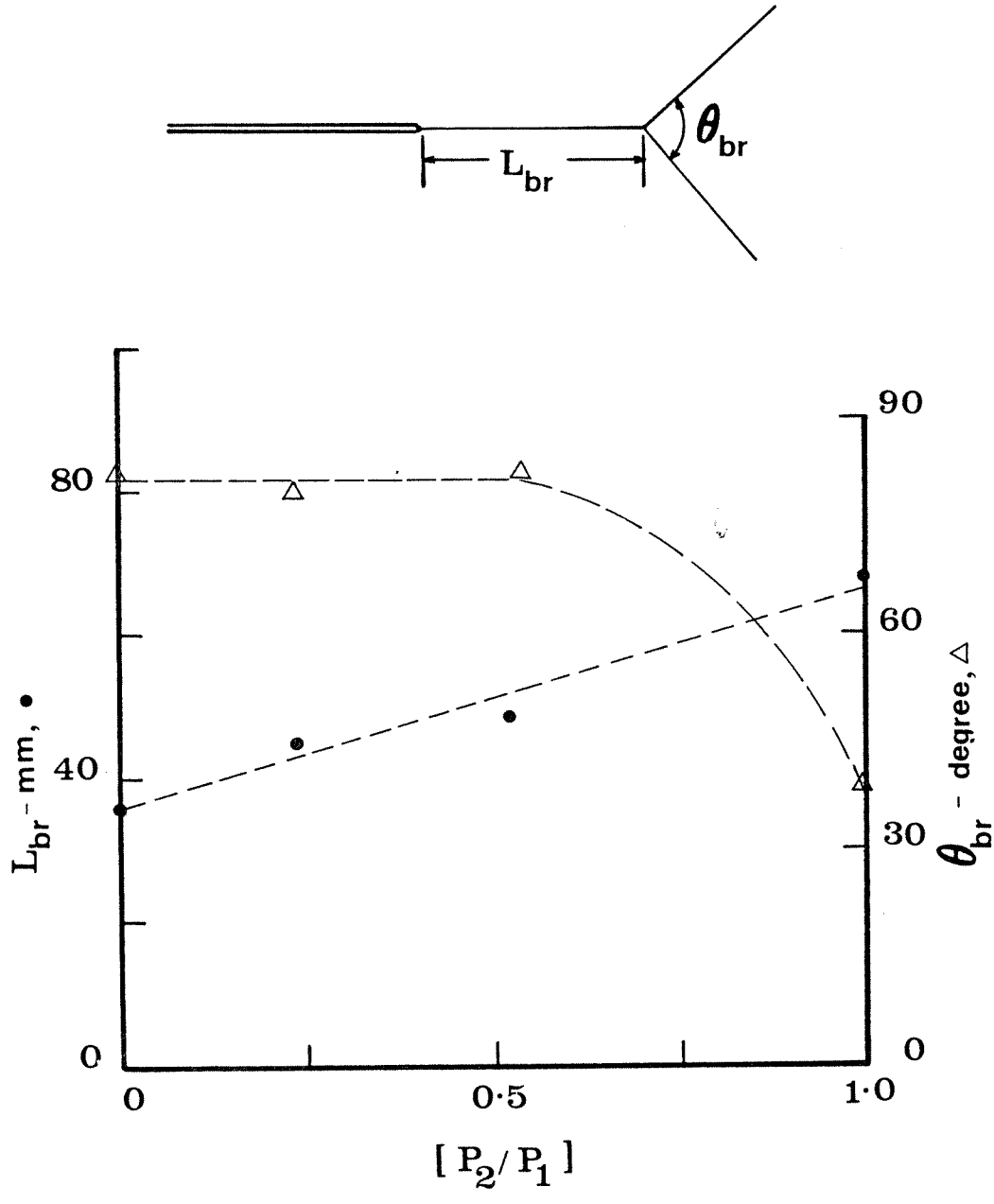

Figure 56. Effect of second stress wave on crack branching.

to close any crack that is formed at an angle to the main crack. One would, therefore, expect the fracture surface to indicate that the process zone is indeed smaller. A direct examination of the fracture surface indicates indeed that upon arrival of the stress wave, the roughness of the fracture surface changes and appears smoother than it had been prior to the arrival of the stress wave. Moreover, the crack velocity remains constant during this entire crack propagation process up to and beyond crack branching. Thus we see that actual observations on new situations seem to agree with microscopy based interpretation of the crack propagation and branching mechanisms.

The generation of a dynamic tensile wave is difficult and was not attempted. Another way to check the effect of tensile load parallel to the crack would be to apply a static tensile load, but this also posed experimental problems except when the tensile load was very small. The sharp crack in the specimen is made with a razor blade that is placed in the machined slit and impacted, This does not always provide a perfectly straight crack and there is usually some asymmetry associated with this initial crack. While a dynamic tensile load would not affect the sharp asymmetric crack, a static load, if sufficiently high, would initiate the crack prior to the actual test. Therefore, it was not possible to obtain the effect of a crack-parallel tensile load on crack propagation and branching. Based on the present mechanism for crack propagation, it would be expected that when a crack parallel tension field exists, branching would be enhanced by this stress and also the angle into which the branches propagate would be increased. Unfortunately, it was not yet possible to carry out this investigation due to the poor adaptability of the loading apparatus to this loading configuration.